



ÓBUDAI EGYETEM
ÓBUDA UNIVERSITY

DOCTORAL (PhD) THESIS

YANG SONG

Biomechanical exploration on long-
distance running forefoot injury
mechanism and implication for footwear
design optimization

Supervisor: Prof. Dr. Bíró István

**DOCTORAL SCHOOL ON SAFETY
AND SECURITY SCIENCES**

2023/03/17

Complex Exam Committee:

President:

Prof. Dr. Zoltán RAJNAI

Members:

Dr. habil. Gusztáv FEKETE

Prof. Dr. József SÁROSI

Public Defence Committee:

President:

Prof. Dr. Zoltán RAJNAI

Secretary:

Dr. István NAGY

Members:

Dr. Endre JÁNOSI

Prof. Dr. József SÁROSI

Dr. habil. Árpád CZIFRA

Reviewers:

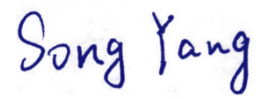
Dr. Ildikó MOLNÁR

Dr. habil. Gusztáv FEKETE

DECLARATION AGAINST PLAGIARISM AND CORRECT REFERENCING

I, Yang SONG, declare that the dissertation entitled: Biomechanical exploration on long-distance running forefoot injury mechanism and implication for footwear design optimization is my original work where the references given in the Reference list are used. All sections, which are transcribed or rewritten from some publications, they are correctly referenced.

Date: 2023.03.17



(Signature)

Content

Motivation of the work	1
Research objectives	4
1. LITERATURE REVIEW.....	5
1.1 The structure and functions of the human foot.....	5
1.1.1 The anatomical structure of the foot	5
1.1.2 The basic functions of the foot movement.....	10
1.2 Long distance running biomechanics.....	11
1.2.1 Running biomechanical analysis.....	11
1.2.2 Long distance running injuries.....	14
1.2.3 Biomechanical analysis used in running injury exploration	18
1.3 Biomechanics of running shoes.....	21
1.3.1 The structure and biomechanical function of running shoes	21
1.3.2 Finite element analysis and its application in running shoe	24
2. MATERIAL AND METHODS	33
2.1 Overview of the experimental and computational workflow.....	33
2.2 Ethics statement	34
2.3 Participants.....	35
2.3.1 Human participants	35
2.3.2 Animal participants	36
2.4 Biomechanical experiments.....	37
2.4.1 Experimental protocol and procedures	37
2.4.2 Experimental instrument and data analysis process.....	38
2.4.3 Statistical analysis	45
2.5 Finite element simulation	46
2.5.1 Model construction	46
2.5.2 Mesh development	49
2.5.3 Material properties	50
2.5.4 Boundary and loading conditions	51

2.5.5	Model validation	54
3	RESULTS.....	55
3.1	Results of biomechanical experiments	55
3.1.1	Foot kinematics	55
3.1.2	Ground reaction forces.....	58
3.1.3	Foot morphology.....	59
3.1.4	Foot skin temperature	60
3.1.5	Subjective-perceived hallux comfort	61
3.1.6	Gap length between the hallux and toebox of the shoe	62
3.2	Results of finite element simulation.....	63
3.2.1	Finite element simulation of the foot-shoe model	63
3.2.2	Finite element simulation of the feline paw model.....	67
4	DISCUSSION	70
4.1	BT and MSF injury mechanism and prevention.....	70
4.2	FE modelling and footwear design optimization.....	76
4.2.1	Finite element analysis of the foot-shoe model	76
4.2.2	Finite element analysis of the feline paw model.....	79
4.3	Limitations.....	82
5	CONCLUSIONS AND FUTURE WORKS	82
5.1	Conclusions.....	82
5.2	Recommendations for future works	84
	NEW SCIENTIFIC THESIS POINTS	86
	LIST OF PUBLICATIONS.....	92
	REFERENCE.....	95
	ABBREVIATION.....	115
	LIST OF TABLES.....	116
	LIST OF FIGURES	117
	ACKNOWLEDGEMENTS	120

Motivation of the work

As one of the convenient and low-cost forms of exercise, running has attracted extensive participation by people of all age groups around the world [1,2]. The possibility of obtaining multiple benefits such as weight loss, improved cardiovascular health, and stress relief makes it no surprise that the number of runners and running events has grown progressively during recent years [1,3,4]. More participants tend to run long distances in order to gain further benefits from a long-term perspective. It has been reported that the number of runners has doubled, and the number of marathon finishers has shown an exponential increase over the past decade [3]. For instance, at least 344,000 marathon runners finished the “New York City Marathon” from 2010 to 2017, which is more than 10 times compared to ~25,000 in 1970–1979 [5]. More recently, the 2021 New York City Marathon has seen 25,020 finishers among 30,000 people ran in this event even under the COVID-19 pandemic [6].

Wide participation in running, especially the prolonged distance, has been found to be associated with a higher injury rate of foot [7–14]. As the only interface that may be responsible for both the contact and propulsive motion during running based on the individual’s strike patterns, the forefoot has been previously demonstrated to be a high injury site due to the large loads and the repetitive nature of running [15]. The most common overuse injuries affecting the forefoot are pain across the metatarsal bones, metatarsal stress reactions and metatarsal stress fractures (MSF) [15]. Meanwhile, among other forefoot injury complaints, dermatologic issues are also frequently encountered particularly over longer distances [9,10,12,13]. Bruised toenail (BT), also known as Jogger’s toe, which appear as a collection of blood below the nail plate of the longest toe, is one of the most common types of forefoot dermatologic injuries that can bedevil runners after a race [16]. These common injuries can lead to significant pain due to the pressure forces that develop at the corresponding area and may cause temporary limitations of activities, which highlights the urgency to reveal the potential development mechanisms of these specific running injuries and propose the prevention strategies [17,18].

Running-related injuries (RRIs) can be caused from multiple aspects. Despite a longstanding interest in the running injury mechanism exploration, there has also been little research investigated more fully the multidimensional foot alterations (kinematics, kinetics, morphology, infrared thermography, etc.) during long-distance running, and subsequently the initial development mechanisms of specific foot injuries. For example, how forefoot kinematics during running might relate to foot structure and how this might further relate to forefoot injury (e.g., MSF) have not been fully analyzed. For the development of injury prevention strategies, a thorough understanding of foot biomechanics before and after running is prerequisite. In addition, to the author's knowledge, there is currently no study conducted quantitative analysis on dermatologic issues partly because of the fact that many of these dermatologic injuries are minor in nature. Most of the prior research were case studies or epidemiological studies based on questionnaires. However, experimental analysis can offer more accurate information in terms of injury mechanisms and protection strategies. Therefore, this dissertation mainly focuses on these undressed questions.

Not only alterations happened on foot might relate to forefoot injuries, but shoes may also play an important role during this process. It was previously demonstrated that wearing inappropriate shoes for a long-time exercise would add the odds and risk for foot injuries [19,20]. For example, the great toe might be more subject to toenail injury (e.g., BT) if the shoe has a shallow toebox [7]. Thus, developing a comprehensive approach to investigate the effects of shoe characteristics on foot variables could not only help to prevent injuries but also promote the optimization of footwear product design. Currently, traditional approaches are limited to investigating the *in vivo* structure of the foot during locomotion. While on the contrary, finite element (FE) methods have been increasingly applied for biomechanics analysis because of their capability of revealing the internal states within bony structures under different loading conditions, which offers an accurate alternative for fast and efficient footwear assessment [21–25]. Meanwhile, it is also worth noting that the animal bionic research has been increasingly conducted and applied for designing footwear or equipment [26–

28]. For instance, the special morphological structure of the feline paw allows it to absorb two to three times of the body weight (BW) while landing from a height, which may provide an inspiration for the footwear cushioning feature. Based on the above findings in terms of forefoot injury mechanisms, this dissertation further aims to propose a completed workflow combining experiments and computational simulation for footwear optimization and forefoot injury prevention.

Research objectives

Based on the work motivation, the main research objectives of this dissertation are as follows.

The first research objective: To quantitatively reveal the intrinsic mechanism of BT injury development and verify the previously proposed injury mechanism of MSF during long-distance running. This aim is to be accomplished by investigating the multidimensional alterations (i.e., subjective comfort, kinematics, kinetics, morphology, thermography) happened to the forefoot segments during 10 km of running, including an interval test after 5km, when compared to the static condition (before running). By identifying these underlying mechanisms, a safer long-distance running guideline can be proposed to reduce the injury risks.

The second research objective: To propose an efficient and accurate approach that can be used to realistically determine the foot-shoe interaction in case of running and further contribute to optimize the design of the shoe toebox in order to reduce the injury risk of BT. This aim is to be accomplished by establishing a fully coupled three-dimensional (3D) foot-running shoe FE model, on which the experimental data (e.g., joint angle, ground reaction force (GRF), and muscle force) will be applied for running simulation.

The third research objective: To explore the buffering characteristics of the feline distal limb during landing and further apply it to optimize the design of the shoe insole in order to reduce the injury risk of MSF. This aim is to be accomplished by establishing a 3D feline paw FE model and investigating the internal stress distribution of the distal joint limb during landing from different jump height (0.6m, 0.8m, and 1.0m) respectively.

1. LITERATURE REVIEW

1.1 The structure and functions of the human foot

1.1.1 The anatomical structure of the foot

The human foot is always considered as one of the most complex anatomical and biomechanical structure of the human body. As the primary interface of the internal dynamic chain that interact with the external environment, the foot acts in coordination with the rest of the body segments during various movements [29–31]. It has been widely demonstrated that the foot would contribute to shock absorption, adapting irregular contact surface and generating momentum for forward propulsion during gait [32,33]. In order to achieve these functions, the foot needs to be stable and supportive, flexible, and energy-efficient, which further highlights the specificity of the foot structure and materials system.

From the anatomical perspective, the human foot is made up of bones, cartilages, muscles, tendons, and ligaments [34,35]. There are twenty six individual bones, thirty three joints, and more than one hundred muscles, tendons, and ligaments. Moreover, it also includes a network of blood vessels, nerves, skin, and soft tissue. Normally, the foot can be transversely divided into three main parts including forefoot, midfoot, and hindfoot. The hindfoot is connected with the midfoot through the talonavicular and calcaneocuboid (midtarsal) joints and the midfoot articulates with the forefoot through the tarsometatarsal joints. All these three parts work together which can provide the human body with sufficient support, balance, and mobility [31,32]. To be specific, the foot supportive function is mainly created by the bones, joints, and ligaments of the midfoot, the central tarsometatarsal joints, and the midtarsal joint. Meanwhile, the plantar aponeurosis and deep transverse intermetatarsal ligaments also play important roles in foot stabilization. The function of adapting irregular contact surface and changing foot shape during heel elevation and propulsion is provided by the flexibility of the subtalar, talonavicular, medial and lateral tarsometatarsal joints. The combination of the stable 2-arched bone structure (transverse arch and longitudinal arch) and the elastic soft tissues allows the foot switch between a stronger more rigid structure and a

softer more flexible one, which further helps it efficiently propel the body forward. Detailed anatomical structures of the bones, tendons, ligaments, and arches system are described below as the background for the main content of this dissertation.

1.1.1.1 Bones of the foot

As shown in Figure 1, the foot skeleton structure begins with the talus, which upward connects with the two bones of the lower leg (tibia and fibula) and come together to form a very stable mortise and tendon joint (ankle joint). Just down from the talus is the calcaneus bone, which is the main back part of the foot and connects with the talus by the subtalar joint. Anterior to the talus and calcaneus are the navicular, cuboid, and cuneiform bones. These bones make up the main part of the midfoot, and they fit together with multiple joints between them. Together with the talus and calcaneus bones, these seven bones make up the tarsus, which represents all short bones of the back half of the foot, and it accounts for about the third of the foot bone. Anterior to the tarsal bones is a group of metatarsal bones, which are the longest bones of the foot. These two bone groups (tarsal and metatarsal bones) are rigidly connected, contributing to less movement at the tarsometatarsal joint. Lastly, the long metatarsal bones are connected to a set of shorter and thinner bones, which are the bones of the toes and is called phalanges. These bones can be further divided into proximal, middle, and distal phalanges based on their relative centripetal position. Together with the metatarsal bones, they make up the main part of the forefoot.

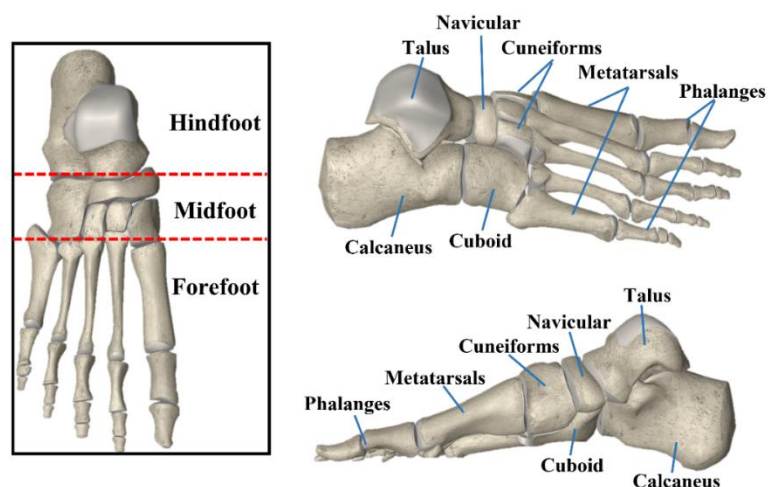


Figure 1 The bone structure of the foot

1.1.1.2 Tendons and ligaments of the foot

Both tendons and ligaments are very important structures in the foot. Basically, a tendon refers to a band of fibrous tissue which attach muscles to bones. When a muscle starts to contract, it pulls on the tendon and consequently moves the connected bones [36,37]. Figure 2A illustrates the main tendons connecting muscles to the bones in the foot. Here in this section one of the most prominent tendons named Achilles tendon (AT) is introduced, which was further applied as the loading condition for the computational simulation in this dissertation. AT is one of the largest and thickest tendon structures in the human body, consisting of the gastrocnemius tendon and the soleus tendon [38]. As shown in Figure 2B, AT is located at the back of the foot just above the heel and attaches the calf muscles of the lower leg to the calcaneus bone. It has been demonstrated that AT plays a crucial role during movements such as walking, running, and jumping since it can transmit force upward through the lower limb joint chain and further consumes energy through the bone and soft tissues [39]. To take running as an example, AT would store energy during the ground contact phase and then release the energy during the push-off phase. Farris et al. [40] found in their study that the contribution rate of the AT to the ankle joint when running was over 50%, which further confirmed the above point.

Generally, ligaments are very similar to tendons, while the main difference between these two structures is that tendons connect muscles to bones but ligaments connect bones to bones. Basically, a ligament presents as a rope-like structure that are bundled together through numerous small fibers (collagen), which indicates that the thickness of fiber bundle would further determine the ligament strength [41]. As shown in Figure 2A, there are various ligaments in the foot which help bound the bone together. They are further classified into several groups according to their locations with respect to the foot bones. One of the longest ligaments is the plantar fascia, which is extended from the toes to the heel (Figure 2C). The complete structure of plantar fascia is formed from three main parts including the central, lateral, and medial, and it has been found that the central portion is the major one. Furthermore, the central part of the plantar fascia

consists of five superficial longitudinal tracts that extend to the five toes from the heel [42]. The main function of the plantar fascia is to maintain the arch height of the foot (which is introduced in the next session) and maintain the correct gait posture. Usually, this tissue would expand and contract to allow the curving and flattening of the arch and consequently provide the necessary balance and strength to the foot when walking or running. In addition, the plantar fascia could provide torque and absorb the reaction force from the ground, acting as a shock absorber during movements [43].

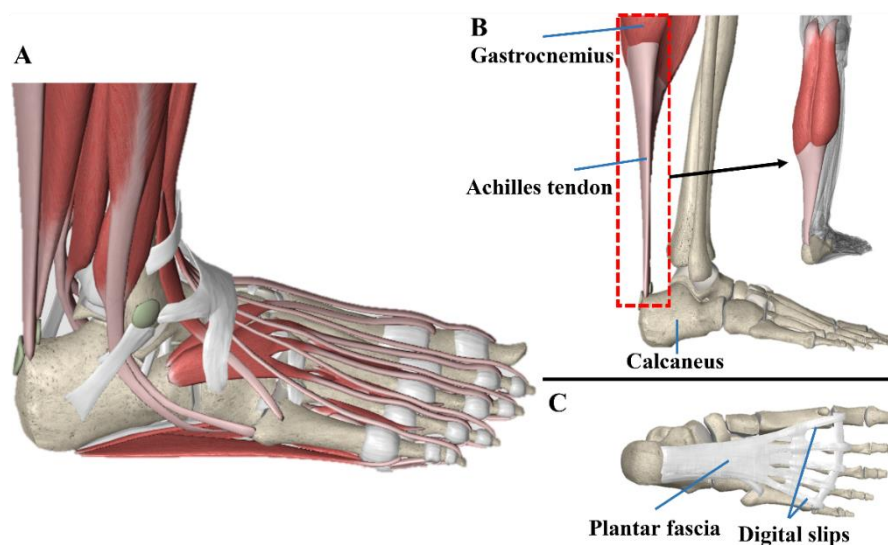


Figure 2 The tendons and ligaments of the foot, A: Overview; B: Achilles tendon; C: Plantar fascia

1.1.1.3 Arches of the foot

As shown in Figure 3, the foot arches are anatomically formed by the metatarsal and tarsal bones and further supported by the tendon and ligament structures. Generally, there are three arches including the transverse arch, the medial longitudinal arch, and the lateral longitudinal arch, of which the latter two (antero-posterior arches) are the main arches of the foot [44,45]. It has been widely demonstrated that the unique structure of the foot arches let the foot act as an adaptive and elastic base to support the human body [46].

The medial longitudinal arch is formed by three metatarsals (the first, second, and third one), three cuneiforms, the navicular, the talus, and the calcaneus. It is the highest

of the three arches and the primary feature of this arch is the elasticity, which plays an important role in shock absorption and foot propulsion during movements [47]. The lateral longitudinal arch is made up by two metatarsals (the fourth and fifth one), the cuboid, and the calcaneus. Compared to the medial longitudinal arch, the height of the lateral longitudinal arch is much lower. Nevertheless, the main dominant characteristic of this arch is the solidity, and it is much closing contact with the foot support surface, which allows it to play an important role in maintaining the erect posture [48]. The transverse arch is composed of the distal of five metatarsals, the cuboid, and three cuneiforms. The most marked function of this arch is its contribution to maintain stability in the midfoot and forefoot through the capsuloligamentous structures [49].

Clinically, arch height refers to the height of the medial longitudinal arch of the foot and it is used to define the foot morphology including normal-arched foot, low-arched foot, and high-arched foot [50]. The normal arch height is 14 to 18 mm, with flat feet below 14 mm and high arched feet above 18 mm. It has been widely demonstrated that the alternation of arch height is highly associated with injury occurrence. To be more specific, the altered arch structure could lead to the redistributed plantar foot pressure and abnormal lower limb biomechanics, which may greatly increase the risk of related injuries, such as plantar fasciitis, ankle sprain, and hallux valgus [51,52].

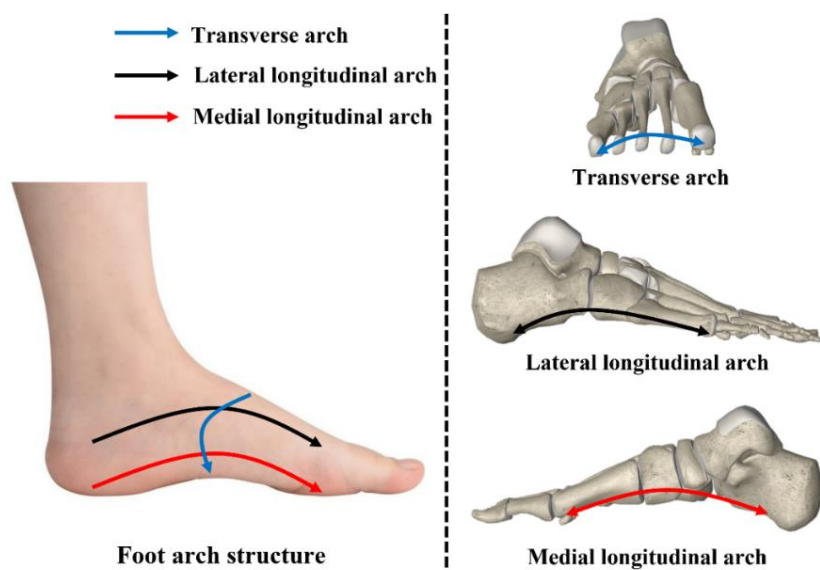


Figure 3 The arches of the foot

1.1.2 The basic functions of the foot movement

Motion refers to the rotation of all related joints about an axis in a plane. The foot would exhibit different types of motion according to different axes and planes. Normally, the foot movement involves six degrees of freedom in three planes, which are defined as dorsiflexion and plantarflexion in the sagittal plane, inversion and eversion in the frontal plane, and adduction and abduction in the transverse plane(Figure 4) [32,53,54].

In terms of dorsiflexion and plantarflexion in the sagittal plane, the foot is considered as plantarflexion when its distal part rotates away from the tibia while it is described as dorsiflexion when its distal part rotates towards the tibia in the sagittal plane.

In terms of inversion and eversion in the frontal plane, the foot is considered as inversion when it is tilted so that the plantar surface faces into the body midline while it is described as eversion when the plantar surface faces away from the body midline in the frontal plane.

In terms of adduction and abduction in the transverse plane, the foot is considered as adduction when its distal part rotates towards the body midline while it is described as abduction when its distal part rotates away from the body midline in the transverse plane. In addition, the combination of these motion in different planes would further contribute to two interdependence motions called foot supination and foot pronation. To be specific, the foot would be described as supination when it presents plantarflexion, inversion, and adduction motion simultaneously while on the other hand it would be considered as pronation when it exhibits dorsiflexion, eversion, and abduction motion simultaneously [35,55].

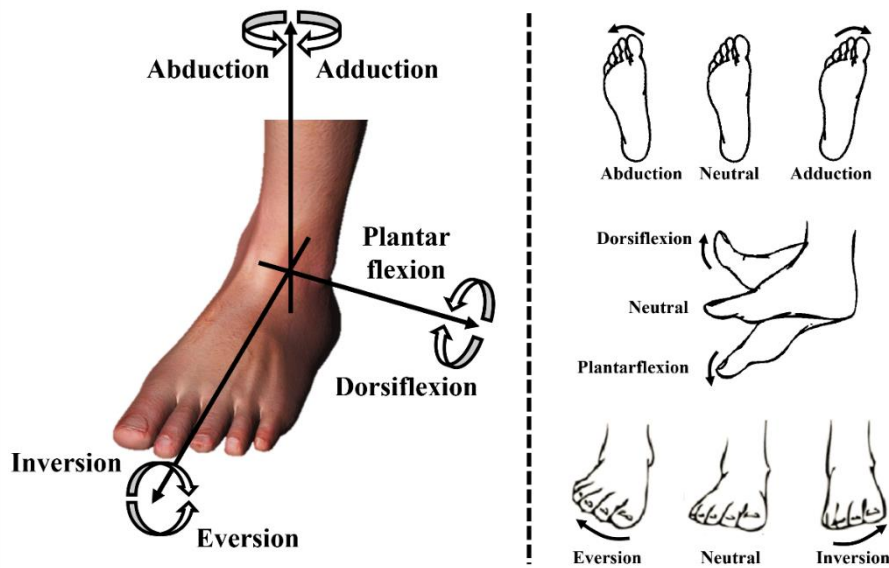


Figure 4 The foot movement in three planes

1.2 Long distance running biomechanics

1.2.1 Running biomechanical analysis

1.2.1.1 The basic biomechanical characteristics of running

Running is the basic movement during human daily life, and it is also a fundamental part of many different sports activities. From the perspective of biomechanics, a completed running gait cycle starts when one foot makes the first contact with the ground, and then finishes when that same foot contacts with the ground again [56–58]. As shown in Figure 5, the gait cycle can be divided into two different phases, including the stance phase and the swing phase. The stance phase refers to the time when the foot is in contact with the ground until the body is over the foot and it can be further subdivided into three phases, initial contact, midstance, and toe off. Initial contact is also named as the heel strike, during which the whole body (mainly the lower limb) starts to absorb the GRF as the foot strikes the ground. It should be noted that there are mainly three different foot strike patterns, hindfoot strike, midfoot strike, and forefoot strike [59–61]. It has been reported that approximately 80% of the long-distance runners are used to hindfoot strike while most of the remainder are found to be midfoot strikers [32]. After initial contact, the body continues to travel over the foot until it reaches the lowest point (which is the highest point for absorbing GRF), letting the foot in a relatively neutral or dorsiflexed and pronated position and prepare to generate

propulsive force. Finally, during the toe off phase, the body travels ahead the foot and the foot plantarflexes greatly in order to propel the body further forward.

The swing phase refers to the time when the foot loses contact with the ground, during which the foot starts to dorsiflex and supinate to get ready for making contact with the ground again. It is worth noting that during the swing phase of running, there is a period of time when both feet are simultaneously not touching the ground, which refers to as the double float phase. The double float phase has been widely clarified as the demarcation between walking and running [56–58].

Generally, the stance phase has been paid more attention for the investigation of running performance and RRIs since it is in this phase when the foot sustains the force from BW and the ground [62]. On the other hand, the swing phase has been proposed as the product of the stance phase and may not be objectively controlled.

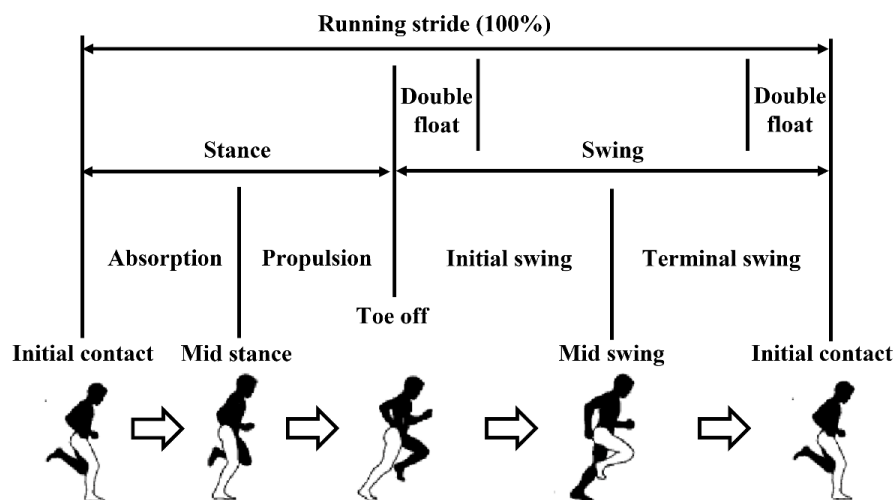


Figure 5 Functional divisions of a running stride [32]

1.2.1.2 The typical gait biomechanical testing systems and applications

Generally, biomechanics refers to the study of the mechanics (kinematics and kinetics) of the musculoskeletal system by assessing forces and their influences on anatomical structures [63,64]. Therefore, the biomechanical analysis of human gait could be defined as the systematic investigation of human movement based on visual measurements. In the field of sports science, biomechanical assessment of human gait

is a fundamental approach that has been applied to improve performance technique, determine injury factors and underlying mechanism, and facilitate injury recovery [65–67]. A various of biomechanical testing methods and systems have been subsequently developed and applied to analyze human gait under different scenarios.

The two-dimensional (2D) image digitization was found to be the most widespread tool for biomechanical gait analysis for decades [68]. Before the advent of digital technology, cine cameras (continuous photos) were usually applied in this field because of their relatively high image quality and fast frequency rates (mostly 100Hz). For example, Procter and Paul analyzed the ankle joint biomechanical characteristics during the stance phase of normal walking by cine cameras and force plate [69]. However, it was soon disregarded because the long processing time, poor accuracy, and slow frequency rates that have limited its further practicality. With the rapid development of more sophisticated technologies, 3D gait analysis systems have emerged for motion analysis research. One of the primary differences between 3D gait analysis and the above 2D methodologies is that, based on multiple optical cameras, which emits infrared light, these optoelectronic systems can automatically deduce and calculate the 3D joint coordinate position through the external marker, substantially reduce the processing time and improve the accuracy [70,71].

Currently, the commonly used 3D gait analysis system usually consists of the following parts. Firstly, as mentioned above, a motion capture system is applied to continuously monitor the 3D movement trajectories of reflective markers. Normally, the motion capture system contains more than six optical cameras, and based on the arrangement of special spatial position, several infrared reflective markers are attached to the corresponding surface of the components (e.g., anatomical landmark of the foot or a shoe) [72]. Then the kinematic data (e.g., joint motions) is collected through the cameras and calculated using the inverse kinematics algorithm [73]. Secondly, a force platform installed in the ground is applied to simultaneously collect the 3D GRF with the motion capture system. The 3D GRF shows the directions and magnitude of external loading directly applied to the foot and lower limb structures during movements (e.g.,

running), and they could be further used to calculate the reaction moment of joints (e.g., hip, knee, ankle, and metatarsal) [74]. These two systems are generally integrated via the specific computer software (e.g., Vicon Nexus software) to maintain consistency during data collection process. Thirdly, despite the force platform can provide the GRF during locomotion, it cannot offer further information that corresponds with the specific foot anatomical locations. On the contrary, pressure distribution devices such as the in-shoe pressure measurement system, are useful tools that can provide plantar pressure of the specific foot anatomical locations during locomotion since they are placed beneath the moving foot [75]. Moreover, based on the experiment setup, the surface electromyography (EMG) system is also commonly used in biomechanical tests. By attaching the electrode slices to the skin surface, the muscle EMG signals during dynamic movements can be recorded for further analysis [76]. Through these measurement techniques, the basic biomechanical characteristics during locomotion (e.g., the spatial-temporal, kinematic, kinetic parameters) can be calculated, which could provide important information on foot movement and further make some guidance for the clinical intervention and injury prevention.

1.2.2 Long distance running injuries

1.2.2.1 Overview of long distance running injuries

As one of the convenient and low-cost forms of exercise, running has attracted extensive participation by people of all age groups around the world [1,2]. The possibility of obtaining multiple benefits such as weight loss, improved cardiovascular health, and stress relief makes it no surprise that the number of runners and running events has grown progressively during recent years [1,3,4]. More participants tend to run long distances in order to gain further benefits from a long-term perspective. By investigating the associations of running with death risks in 55,137 adults, Lee et al. reported a markedly reduced risk of all-cause (30%) and cardiovascular (45%) mortality contributed by leisure-time running [77]. Nevertheless, wide participation in running, especially the prolonged distance, is also associated with a high risk of injuries, which may in return offset the positives of this activity.

Over the past few decades, the increasing popularity and extensive participation of running have inspired many scientific investigations on RRIs. Several systematic reviews and meta-analyses have attempted to summarize the incidence and risk factors for long-distance running [78–84]. In general, the incidence rate of RRIs ranges from 2.5 to 33.0 injuries per 1000h running [79]. To be specific, the injury incidence proportion is 3.5% for professional runners, 7.7% for recreational runners, and 17.8% for novice runners [85,86]. Meanwhile, for recreational runners who have a steady and periodical long-distance run experience, it has been found that 37% to 56% of these runners may suffer a RRI per year [87]. In addition, the running injury incidence rate is also reported different between different running distance of runners. Van der Worp et al. summarized that, short distance runners present an incidence rate of 14.3% to 44.7% while their long distance counterparts seem to suffer more injuries with the incidence ranged from 16.7% to 79.3% [88]. For some special types of runners such as cross-country runners, Kluitenberg et al. found that the pain-related injury incidence even reached up to 94.4% over a lifetime recall period [89]. A retrospective study focused on the lifetime prevalence of previous running injury of adolescent runners demonstrated that the injury incidence is markedly associated with longer distance and faster performance (68% for girls and 59% for boys) [90].

In terms of the common site of RRIs, it has been demonstrated that lower limbs which mainly include joints (hip, knee, and ankle), lower leg, and foot are much more vulnerable during running and consequently vast majority of injuries happen among these areas [79,80]. Specifically, a previous systematic review investigating the lower extremity injuries in long-distance runners found that the overall incidence of leg injuries ranges from 19.4% to 79.3%, with the predominant injury sites including the knee joint (7.2%-50%), lower leg (9%-32.2%), foot (5.7%-39.3%), and upper leg (3.4%-38.1%) while the less common locations involving the ankle and the hip joints (3.9%-16.6% and 3.3%-11.5%, respectively) [79]. Regarding the types of RRIs, it can be roughly divided into the following several specific groups, including skeletal (e.g., stress fractures), musculotendinous (e.g., tendinosis) and vascular injuries. However,

no previous reviews have explicitly made a summary on this topic. Currently, it has been well demonstrated that one of the most common types of generalized RRI is over stress or over use, which accounts for about 80% of all injuries and especially common for lower limb and foot [78,91,92]. On the other hand, among all these RRIs, dermatologic issues are also more frequently encountered. For example, in a review of post-marathon injuries, Mailler-Savage et al. reported that at least 20% of injuries sustained by marathon runners are related to the skin [9]. Despite the fact that many of these dermatologic injuries are minor in nature, few were found to have a great impact on physical activity or even become life-threatening, such as subungual hematoma [10,13].

Despite all these results in terms of the prevalence and incidence of RRIs, it should be mentioned that there may be different injury definitions and running types involved in these studies, thus the incidence of RRIs varies considerably and should take with caution. Nevertheless, these findings indicated that most of the runners have a high risk of getting injured, especially for the lower extremity.

1.2.2.2 Forefoot injury during long-distance running

As the primary interface of the lower limb with the external environment during running, the foot has been previously demonstrated to be a common injury site. According to the previous results presented in the above session, the foot is the third common injury sites among the six locations, contributing to 5.7% to 39.3% of the injury incidence rate [79]. There are various types of injuries related to the bone and soft tissues of the foot, such as heel pad pain, plantar fasciitis, and tendinopathies. Meanwhile, the foot injuries can be further divided into those that involve the hindfoot, midfoot, or forefoot. From the biomechanical perspective, the forefoot needs to sustain the entire body load during the propulsive phase of gait (toe-off). Therefore, as the only interface that may be responsible for both the contact and propulsive motion during running based on the individual's strike patterns, the forefoot injuries contribute to a significant portion of the problems that affect runners, especially during long distance

running, when considering the great loads on the forefoot during running (four to five times of a runner's BW) and the repetitive nature of this activity [93–96].

As shown in section 1.1.1, the metatarsals are the longest and relatively slender bones in the foot that connect the tarsal bone and the phalanges. These bones usually act as a unit to form the main plantar surface of the forefoot for balancing and load holding and also play an important role in supporting and propulsion of the ankle and the foot during locomotion. It has been documented that the most common injuries affecting the forefoot is the MSF [97,98]. Anatomically speaking, bone stress injuries in the forefoot are very common because there is very limited soft tissue that can protect this area [99]. The second to the third metatarsals account for 90% of this fracture since these two parts are the longest while the narrowest metatarsal bones, while on the other hand the first metatarsal contributes to 7-8%, and the fourth and fifth account for 3% [100]. In addition, among other forefoot injury complaints, dermatologic issues are also frequently encountered particularly over longer distances [9,10,12,13]. Subungual hematomas, which appear as a collection of blood below the nail plate, are one of the most common types of dermatologic injuries that can bedevil runners after a race [17,18]. Despite the fact that many of these dermatologic injuries are minor in nature, few were found to have a great impact on physical activity or even become life-threatening. It has been found that the above forefoot injuries can lead to significant pain due to the pressure forces that develop at the nail bed and may cause temporary limitations of activities. In some cases they could further result in long-term complications such as secondary fungal infections and nail plate deformities [17,18].

As a conclusion of this session, long distance running results in extremely high forces on the foot, especially the forefoot since it plays a very important role during the running propulsive phase, causing pain or injuries that impact the forefoot functions. For this reason, it is always of great importance to reveal the underlying injury mechanism in order to reduce their morbidity during running.

1.2.3 Biomechanical analysis used in running injury exploration

With the increasing popularity of long distance running, RRIs of the foot are very commonly happened and could further lead to significant morbidity if the inaccurate diagnosis results in incorrect body management. For this reason, more emphasis on the underlying mechanisms and the treatment of some specific running related injuries has surfaced over the past few decades. Currently, several risk factors of RRIs have been found. According to the previous reviews, these determinants can be further divided into several categories, which include systemic (personal) factors (e.g., age, weight, and height), lifestyle factors (e.g., smoking and drinking alcohol), health factors (e.g., injury history), and running related factors (e.g., training frequency, distance, and shoe use), etc [78,88,101]. The injury history was reported to be the most crucial risk factor for both short- and long-distance runners. The use of shoe orthotic insoles and lower limb muscle weakness are reported to increase the running injury risk as well. Inconsistent results were reported for other determinants, such as age [102,103], body mass index [104,105], and training factors [106,107]. Nevertheless, despite that these above factors would result in a large portion of running injuries, none of them have been confirmed as the cause of any particular running injuries. Observational or epidemiologic studies can offer some useful information for RRIs but it may also be fraught with error and uncertainty.

Nowadays, it has been widely demonstrated that gait analysis is the most accurate and effective mean to quantitatively investigate the risk of RRIs. Running is a dynamic and repetitive process, thus any small but significant changes may further cause the increase risk of RRIs. Biomechanical factors, such as foot posture, muscle strength, and lower limb kinematics, was found to contribute to 40% of running injuries [80]. For example, altered morphology leading to altered biomechanics, such as hallux valgus, may lead to a predisposition toward the development of foot injuries during running [108]. Therefore, a dynamic gait analysis would help observe the biomechanical changes in foot motion during running, allow for identification of biomechanical

determinants for some specific injuries that may not be obvious with other examinations, and hence provide direct strategy to decrease the corresponding injury risk.

Currently, numerous studies have been conducted to reveal the biomechanical changes during long-distance running and also their association with RRIs [7,109]. In these studies, participants were normally required to run for a given distance on a treadmill or track, and the biomechanical and injury factors were collected before, during and immediately at the time when they finished the running. A previous systematic review conducted by Kim et al. summarized the current state of knowledge about the biomechanical alternations in response to long-distance running, and some of their findings further reveal the potential injury development mechanisms during running [110]. For instance, regarding the forefoot injuries, it was found that the loss of toe control function while increased load under the medial forefoot region are highly associated with MSF.

In terms of dermatologic issues, previous research have deduced that the changed foot morphology may create an environment where the potential friction between foot and shoe interface would increase and consequently lead to some skin injuries [109]. However, due to the limitation of experimental setup, the speculation has not been further confirmed. It is worth noting that a multi-segment foot model, such as the Oxford foot model, can be used for in-depth foot kinematics analysis since it divides the foot into several rigid segments, which could help further observe the foot motion and detect any tiny changes that may related to running-relate injuries. It has shown robust reliability on inter-segmental angles through the gait cycle and been extensively applied to explore the biomechanical properties of the foot during different movement tasks, such as walking, running, and jumping [111,112].

In summary, dynamic analysis has been widely applied to the investigation of running injury development mechanisms. However, concerning the specific forefoot RRIs, the following problems still exist.

1. Currently, previous research often set the focus on the investigation of injury mechanisms on the lower limb large joints, with the knee being the most common one. However, the application of multi-segment foot model and gait parameters in the exploration of running foot-related injuries is relatively limited.
2. RRIs can be caused from multiple aspects. Despite a longstanding interest in the running injury mechanism exploration, there has also been little research investigated more fully the multidimensional foot alterations during long-distance running, and subsequently the initial development mechanisms of specific foot injuries. For example, how forefoot kinematics during running might relate to foot structure and how this might further relate to forefoot injury have not been fully analyzed.
3. Although it has been widely documented that the repetitive contact between the nail bed and toebox of the shoe is responsible for developing subungual hematomas, there is currently no study conducted quantitative analysis on dermatologic issues partly because of the fact that many of these dermatologic injuries are minor in nature. Most of the prior research were case studies or epidemiological studies based on questionnaires. Experimental analysis that can offer more accurate information in terms of injury mechanisms and protection strategies are much warranted.

1.3 Biomechanics of running shoes

1.3.1 The structure and biomechanical function of running shoes

As the direct protective equipment for the foot, the main role of a shoe is to protect it from hard and rough terrain or any external intrusion during daily locomotion [113]. Meanwhile, the rapid advance of the structural and material engineering over the past few decades has let the shoe, especially the running shoe, experience tremendous changes and further given them more functionality. Running shoes with various functionality (e.g., cushioning, energy return, and arch support) were introduced, which serves to improve performance and decrease the risk of unexpected injuries during running [114]. A prominent trend is that the running shoe structure shifts from minimal to highly supportive one, and then to minimal and finally back to highly cushioned structure [115]. Currently, Nike Vaporfly 4% has been demonstrated as one of the ‘super shoe’ to significantly improve running economy up to 6% because of the thicker midsole and curved carbon fibre plate which may contribute to a “teeter-totter effect” and further strengthen the energy return function [116]. The thicker midsole was also previously found to be able to reduce the impact forces from the ground and may further contribute to decrease the lower limb injury risks during running [117]. However, on the other hand, emerging evidence has reported that the injury rate of running has not remarkably decreased with iterative updates of running shoes [118]. Meanwhile, it was also clarified that wearing inappropriate sports shoes for a long-time exercise would add the odds for foot injuries. Plantar fasciitis, foot fractures, and heel pain were all found to be associated with abnormal plantar pressure concentration and overload during exercise, while the structure and material property of footwear play crucial roles in this process [115]. Therefore, decreasing the RRI risks and improving performance through the innovative design of running shoes’ structure and material are continuously to be a focus in both industrial and academic fields.

In order to identify the appropriate functionality for running shoes, numerous studies have been conducted to examine the influences of different shoe constructions on running performance and injuries [114,115]. Technically, running shoes are usually

made up of four main parts, including shoe upper, insert (insole), midsole, and outsole. It has been widely demonstrated that the core technology of sports shoes is mainly reflected in the sole design, especially for the insole and midsole parts [100,114,115]. On the contrary, the main functions of shoe upper are to hold the shoe together while the outsole which normally made of rubber mainly contribute to traction and wear resistance.



Figure 6 The basic structure of a running shoe

There is limited information available regarding the effects of shoe upper and outsole on running performance and injury risks. However, with the continuous deepening and refinement of relevant research, many scholars also began to pay attention to the impact of shoe upper on running characteristics. These studies investigated the effects of different shoe upper constructions on performance and injuries-related variables in running, and it was demonstrated that shoe upper has a high association with the fit and comfort and a structured shoe upper would contribute to greater maneuverability and a uniformly distributed plantar pressure because of a better coupling between the foot and footwear [119,120]. Additionally, some studies also speculated that the shoe upper may alter the kinematic strategies of the foot during running. The shaped and shallow toebox may limit the flexion-extension movement of a flexible toes, causing the toenails jam into the upper, which is more subject to toenail injuries (e.g., hematomas under the nails) [7]. Nevertheless, there is still limited evidence that directly prove these speculations from a biomechanical perspective.

In terms of the midsole, it has been widely recognized that the functions of this part play a very important role for a running shoe to control foot motion (e.g., excessive pronation), provide cushioning and energy return, and limit shock impact [100]. Numerous of studies have been conducted to investigate the effects of midsole hardness, thickness, material properties, and specific structures on the lower limb biomechanics that is associated with running injuries and performance [115,117]. Currently, one of the major research trends of the midsole is the imbedded stiff plates that aims to increase the longitudinal bending stiffness (LBS) of this part. According to the findings of a recent meta-analysis, increasing the footwear LBS help improve running economy up to 3.15% when the mass of the footwear is controlled [121]. From a biomechanical perspective, the increased footwear LBS would decrease the amount of mechanical energy lost, mostly concentrate on metatarsophalangeal (MTP) joint, by reducing the dorsiflexion motion of this joint, which has been demonstrated to be one of the reasons for running economy enhancement. In the meantime, it is also demonstrated that imbedding the stiff plates in the midsole contributes to even the plantar pressure, especially for the metatarsal region, which could potentially reduce the injury risks [121]. Alongside these proposed benefits of the increased LBS for running, however, it must be noted that there may be a certain benefit limitation with regarding to running distance and running speed. In addition, there are still several controversies in terms of running performance and related injuries [122].

Lastly, with regarding to the insole, the main functions of this part are demonstrated to help support the arch structure and dissipate heat and sweat away from the foot [100]. Besides that, there are currently more and more studies further indicated the positive effects of the custom-molded insoles on reducing the peak plantar pressure. For example, Bus et al. found in their study that the custom-molded insoles were significantly greater to decrease the region-focused peak pressure than that of the normal insoles [123]. It must be noted, however, that most of these structured insoles are widely applied on correcting the foot posture and treating the foot morphological and physiological diseases, while the relatively flat insoles (non-structured one) are still

used in sports shoes (e.g., running shoe). A good insole design, such as the metatarsal pad, may contribute to spread the impact force more evenly and dissipate the peak one, which could help reduce the injury risks during running.

To conclude, despite a longstanding interest in the effect of shoe design on running performance and injuries, there also still plenty of space that worth further consideration. In addition, some advanced and mature engineering technologies (e.g., FE method) present an exciting prospect in fast and efficient footwear assessment. Meanwhile, the animal bionic research has been increasingly conducted and applied for designing footwear or equipment. These two aspects will be discussed further in the following subsequent sections. In general, all these aspects would further promote the prosperity of the footwear industry and footwear biomechanics.

1.3.2 Finite element analysis and its application in running shoe

1.3.2.1 Introduction to the finite element method

Generally, as stated in session 1.2.1.2, sports biomechanics normally involves the using of the motion capture system, force platform, pressure measurement system, and also EMG system based on experimental setup to record different variables related to human movements. Then these collected data were inputted into analysis systems (e.g., Visual 3D, Vicon Nexus) to determine the kinematics and kinetics characteristics of each joint of interest during locomotion. However, it has been gradually realized by the experts and scholars that the traditional motion analysis method has several deficits in revealing the internal biomechanical alternation of human body, especially for the foot structure. To be specific, despite that the direct experiment does increase the biomechanics knowledge of foot-footwear interactions, changes of the internal stress and strain of the foot structures (e.g., bony, ligament, and soft tissue) during the interaction is unmeasurable, which has prompted the researchers to find an alternative for in-depth exploration.

With the rapid development of computer engineering technology in 1970s, the FE method was introduced into the biomechanical analysis of human musculoskeletal

system. Basically, FE analysis refers to the simulation of real physical systems (geometry and loading conditions) using mathematical approximations. By using simple but interacting elements, a finite number of unknowns can be used to approximate a real system with infinite unknowns (Figure 7) [124]. The fundamental advantage of FE analysis is its capability of modelling complicated geometry, diversified material properties, and complex boundary and loading conditions. Combining with the experimental approach, it can reveal the internal states within bony structures under different scenarios [25,125]. FE analysis has been widely conducted to give new insights for the industry and clinical applications over the past decades. Two main FE application fields are currently associated with human sports biomechanics, one is the FE modelling for human skeleton and the other is the application of FE modelling for implant or sports equipment design [100]. Accordingly, a large number of foot and footwear models were continually established for various biomechanical investigations, including pathology analysis, prosthetic/sports equipment designs, and rehabilitation evaluation [25,125]. In terms of the foot-shoe FE model, it is worth noting that FE analysis can provide efficient and fast parametric assessment for footwear shape modifications and function update without the prerequisite of fabricated footwear, which can also simultaneously reduce the corresponding production batches and costs. However, there are still a lot of gaps to be filled in the computational exploration of the foot-shoe coupled models at present when compared to the foot FE simulation.

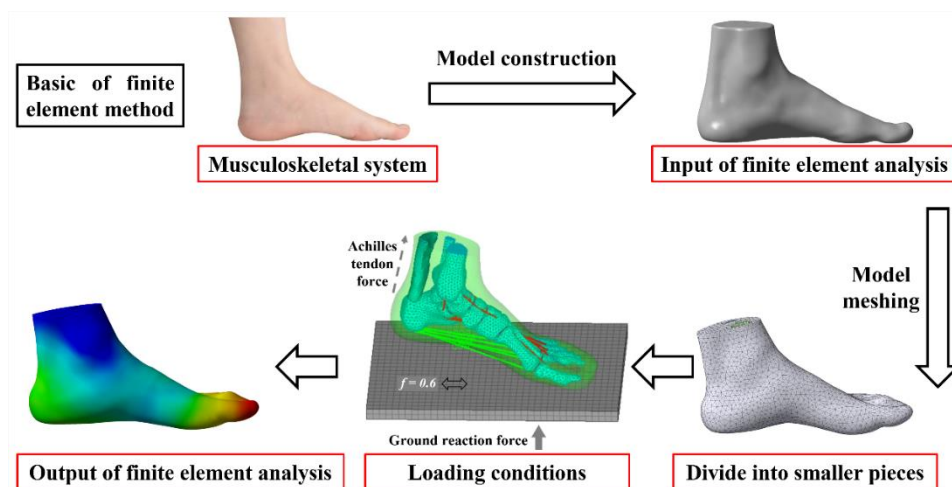


Figure 7 Basic of the FE method

1.3.2.2 Finite element modelling of the foot-shoe complex

Running shoe manufacturing is a relatively complex activity that would involve many experts from different departments of a company, with the main goal is to achieve the best footwear function while ensure the cost-optimized manufacturing of these products. The current digital revolution has been reported to have a big influence on shoe industry, letting the computational engineering tools be used to explore the best footwear design for performance enhancement and injury reduction through virtual FE models. With the rapid advancement of computational techniques, the coupled foot and shoe FE models were developed from 2D to 3D, from partial structures to the representation of most complicated structure characteristics, aiming for a more delicate exploration of the foot-shoe interactions and shoe optimization [25,125,126].

Normally, the operation steps for the foot-shoe coupled FE analysis include model reconstruction, material property assignment, boundary and loading condition, and model validation. The foot models were mainly reconstructed from high-resolution magnetic resonance images (MRI), while depending on the research emphasis they could also be built using a 3D laser scanner or computer aided design (CAD) software. Meanwhile, the geometry of the footwear was built using the CAD software or 3D laser, which could replicate the fundamental contours of the shoe segments, as shown in Figure 8. MRI segmentation can be conducted using the medical image segmentation software (e.g., Mimics), and some components may be further fused or omitted. For surface smoothing and solid model creation, the reconstructed foot and shoe geometries can be imported into reverse engineering software (e.g., Geomagic, Solidworks). Within the reverse engineering environment, some other basic structures such as cartilages can be further created based on the different levels of analytical definition. The foot connective components such as plantar fascia and ligaments were usually built by connecting the anatomical origins and terminations through the 2D tension-only truss, instead of reconstructing the 3D solid geometries. In addition, the coupled models can be established by directly aligning and assembling the foot and footwear structure or through the specified shoe fitting process using FE software such as ABAQUS. Then,

in terms of the material data, most of the material properties were acquired from existing literature while some material properties of the footwear were obtained through experiments using mechanical testing machines. Most components were idealized to be homogeneous, isotropic, and linearly elastic, except for soft tissue and outsole, which were commonly assumed hyper elastic in current models.

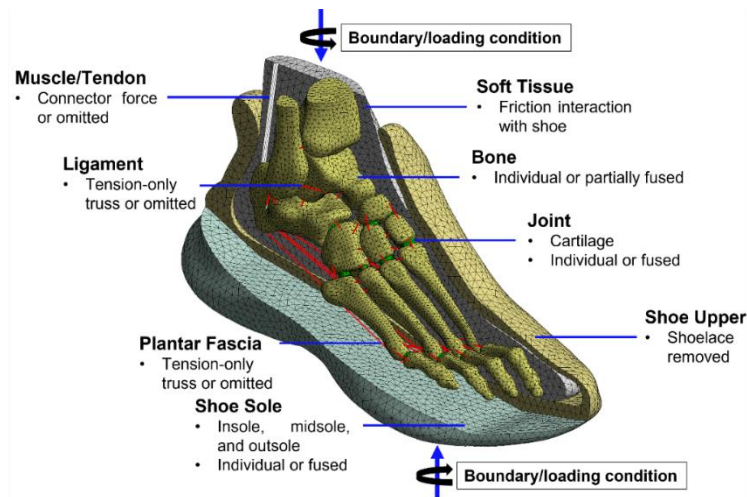


Figure 8 The main components of the coupled foot-shoe FE model and basic modelling methods

The boundary and loading conditions were determined experimentally for most of the simulations [125,126]. For instance, the foot-plate system approach was commonly used to simulate the interaction between the foot, shoe, and ground. In this scenario, the proximal surfaces of the soft tissue, tibia, and fibula components or the underneath of the support plate were fixed, and the muscle forces and GRF were estimated from BW of the subject (e.g., 50% BW for GRF and 50% GRF for the AT force). For some dynamic movements, the subject-specific boundary and loading conditions were obtained from 3D motion analysis, including kinematics and kinetics variables, more accurately representing the conditions. The foot intrinsic and extrinsic muscle forces were further calculated from EMG and respective physiological cross-sectional areas. For the interactions between the foot, shoe, ground plate etc., the connection types were commonly defined as the frictional contact surface with a coefficient of 0.5 to 0.6. Implicit or explicit formulations (quasi-static/dynamic simulation) were then applied to obtain the FE solution depending on the analysis setup. Lastly, model validation

determines the accuracy of the model that can be used to represent the reality situation. Normally, the loading response of the foot, footwear, or other components such as plantar and outsole pressure were used for model validation. Meanwhile, statistical analysis such as the measure of correlation and also Bland-Altman plot could be conducted for validation. Here in the following sessions, the current research status, the corresponding challenges of existing foot-shoe FE models, and the possible advancements of each operation step would be explained as a background for this dissertation.

1) Model construction

Based on previous studies, it is obvious that MRI is currently the most used imaging modality that can provide high-resolution images for accurate reconstruction of soft tissue and bony structures. Besides that, the 3D foot laser scanner has also been applied to support foot modelling [25,125,126]. However, although this surface topography method can offer a relatively quick and accurate geometry reconstruction of the foot external surfaces, the limitation is that it cannot provide any information about the foot internal structure, and this restricts its further usage for modelling purposes. On the other hand, CAD software design appears to be the dominant option for the reconstruction of shoe geometries. The virtual shoe models were either made based on the structure of their realistic counterparts or the contour of the foot models. However, two issues may arise during the shoe modelling process. First, since the shoe models were built separately, an extra shoe fitting simulation is needed to resolve the surface overclosure between the dorsal foot and shoe upper. Second, the accuracy and reliability of the shoe models, especially the shoe upper, need further verification if they were designed based on the profile of the foot and ankle. It is proposed that using MRI or computed tomography (CT) to obtain the shod medical image could be a more effective alternative for reliable foot and shoe modelling.

Footwear can reshape foot biomechanics. Therefore, a geometrically detailed FE model involving all major foot and shoe structures is necessary for realistic evaluation of the foot-shoe biomechanics and footwear optimization [125,126]. However, only the

major ligaments were included in many of the existing models, and some that fused distal bones were also considered [100, 113]. Besides that, many non-structural shoe features such as shoelaces were often removed during the shoe modelling process. The ignorance of these structures would lead to the inaccurate representation of model integrity, which may further affect the simulation accuracy and limit its further usage. Recent barefoot FE simulations have focused on developing realistic structural modellings such as tendons, skin, and fat tissue of the foot, which indicates that there is potential for further improvement of the existing foot-shoe FE models [127,128].

The above drawback also brings another critical challenge in terms of model design, which is the balance between accurate details and computational cost. Regardless of the analysis complexity, it is generally assumed that the computational time increases with the model size, which in turn is associated with the types and the total number of the model elements [25,125]. Thus, it is obvious that a detailed foot-shoe FE model will include a greater number of model elements and consequently the computational cost would significantly increase. However, it should be re-iterated that model accuracy is crucial, especially for special-shaped footwear analyses and for clinical applicability. Future research on this topic should focus on methods that could help achieve the minimum simulation cost with industrial and/or clinically satisfied model accuracy.

2) *Material property assignment*

For now, the main issue on material property assignment is that most of the previous studies assumed linearly elasticity for both foot and footwear structures based on previous literature, which is certainly an approximated situation for biological tissue [25,125,126]. Normally, all biological tissues present complex nonlinear behavior. Several existing models have considered nonlinear material for the soft tissue of the foot and the shoe outsole to increase accuracy [100, 113]. However, it is currently not practical to build a foot-shoe FE model assuming all components are nonlinear, as this would make the simulation significantly difficult and time-consuming. Besides that, it is also worth mentioning that in some studies the bone structures were further simplified or even not included [129,130]. In these cases, the material properties of the model

should be further calculated since the ignorance of bone structures may in turn have significant influences on the model stiffness. To achieve that, a combination of mechanical measurements and sensitivity tests of material property is proposed.

3) Boundary and loading condition

The main direct step for implementing accurate FE analyses is defining a realistic boundary and loading condition. For some FE analyses such as balanced standing, a certain number of existing models considered only the GRF or vertical concentrated forces estimated from the BW, with all foot muscle forces ignored or only the simplified AT force included [25,125,126]. Moreover, it was found that the boundary and loading conditions were not always determined from the same model subjects. According to the literature, it may be acceptable in some cases where subject-specified characteristics were restricted or not the study focus, while on the other hand obtaining relevant loading data through biomechanical and computational tests on the involved subjects is critical, especially for clinical-related scenario where model accuracy is the prerequisite [25].

Currently, human motion analysis and musculoskeletal modelling have been widely used in barefoot and foot-insole FE simulations to accurately determine the subject-specific boundary and loading conditions for motions like walking and running. However, only a limited number of existing foot-shoe models have incorporated the above methods to improve accuracy, and in these studies foot muscle forces were estimated by EMG data and physiological cross-sectional areas. It has been previously clarified that musculoskeletal analysis may be a more computationally efficient approach in muscle force estimation compared to the EMG approach [125]. More attempts for foot-shoe analysis, including motion analysis and multi-body models, could add further verifications.

4) Model validation

The validation of a FE model is a direct step that is highly associated with the model practicality. Currently, existing foot-shoe FE models are mainly validated against the

distribution and peak values of experiment-measured plantar pressure data [25,125,126]. However, it is proposed that comparing the pressure characteristics of the specific anatomical sites and the shoe outsole are also necessary for further model validation. In addition, for some specific footwear types, such as high-heel shoes, the pressure validation of the dorsal surface of the foot should also be conducted since the foot would experience large deformation during high-heeled motions [113]. Moreover, some experimental validations were performed by comparing the GRF-time curves during the movement [131,132]. In these cases, using statistical analyses such as Goodness of Fit could further help to evaluate the method consistency. Lastly, since contact modelling was generally applied on all the bony segments and foot-shoe interfaces, internal joint movements, soft tissue deformations, as well as relative movements between foot and shoe could all be experimentally validated by dual-plane fluoroscopy and MRI-based measurements [125,126].

1.3.2.3 Biomimetic implication for running shoe design

During the process of mammalian evolution, limb morphology and posture have evolved to improve aspects of performance such as running speed. These developments include changes in the digitigrade posture with metapodial elevation associated with cursoriality. As the proportion in the distal segment of the limb increases, digitigrade provides the advantage of a longer effective limb length to increase stride/step lengths or maintain duration at higher speeds [133].

As the typical digitigrade mammals, felines have the carpus, and proximal ends of the metapodials elevated off the ground, in conjunction with a plantarflexing wrist joint. The metapodial head and 2–4 proximal phalanges remain in contact with the substrate in a dorsiflexed metacarpophalangeal (MCP) joint. Additionally, the phalanx portion is the main body component that contacts with the ground in activities such as standing, walking, and running [134]. This special morphological structure allows felines to absorb two to three times their BW while resting on their small distal joint. The foot distal structure, such as the MTP joint in humans, serves as the base of support once propulsion begins. When the heel is raised off the ground, the ankle carries out plantar

flexion while MTP dorsiflexion also increases. It should be reiterated that the MTP joint as the main support segment during human running, is often exposed to instability, pain, or luxation. However, this condition rarely seems to occur in felines even though their entire BW rests on the MCP and distal interphalangeal joint during their daily movement patterns [134,135].

Accordingly, several studies explored the impact-resistant biomechanism of cat's paw pad using micromechanical FE methods, which could offer some new insights for the improvement of the cushioning and shock absorption characteristics of the footwear [26–28]. Nevertheless, it should be mentioned that the distal limb joint which comprises multiple segments may together play a crucial role in landing cushioning and ground force-transmission, not just the paw pad alone. Caliebe et al. previously found that force transmission in this distal multi-joint had been optimized and simplified by a rigid connection between the elbow and MCP joints. The rigid junction had been created in conjunction with muscular action and tight ligaments, which crossed the joints to stabilize different distal limb joints during the stance phase [134]. However, how the forces transmit along the distal joint in a feline limb, which finally transfers the bodyweight to the ground, has not been systematic investigated through FE methods. Information on stress distribution of the internal structure could further enhance the knowledge on felines distal limb biomechanics while providing new insights into human MTP joint injury prevention by inspiring the design of health-care products, footwear insoles, and foot functional aids.

1.3.2.4 Summary

To summarize, although numerical modelling of the entire foot-shoe complex has received less attention than other conditions, it has shown essential contributions to further understanding the foot and footwear biomechanics. This is specifically the case where the FE model was applied for identifying mechanical properties of the foot in casual or athletic footwear and for optimizing footwear design to enhance its functional performance. Nevertheless, this dissertation highlights the need for improvement in several aspects, including geometry, material, boundary and loading properties, and

validation of the foot and footwear. Meanwhile, the animal bionic research has been increasingly conducted and applied for designing footwear or equipment. For instance, the special morphological structure of the feline paw allows it to absorb two to three times of BW while landing from a height, which may provide an inspiration for the footwear cushioning feature.

2. MATERIAL AND METHODS

2.1 Overview of the experimental and computational workflow

This work combined experimental test and FE simulation to reveal the intrinsic mechanism of forefoot injury development (BT and MSF) during long-distance running and further contribute to optimize the design of the running shoe in order to reduce the corresponding forefoot injury risk.

The dissertation began with the experimental measurement to describe the multidimensional alterations of the foot before and immediately after 5 km and 10 km of running. An eight-camera Vicon motion capture system (Oxford Metrics Ltd., Oxford, United Kingdom) was used to capture the marker trajectory data through Oxford foot model, an in-ground AMTI force platform (AMTI, Watertown, MA, United States) was used to record the GRF data, a 3D foot scanner (Easy-Foot-Scan, OrthoBaltic, Kaunas, Lithuania) was used to collect the foot morphology data, an infrared camera (Magnity Electronics Co. Ltd., Shanghai, P.R. China) was used to measure the foot skin temperature data, the visual analogue scale (VAS) was used to calculate the subjective-perceived comfort, and a high-speed digital camera (Fastcam SA3, Photron, Japan) was used to collect the gap length between the hallux and toebox of the shoe. The same researcher conducted all procedures and data analyses to ensure consistency.

Regarding to the computational simulation, the reverse engineering technology was used to acquire geometrical data of foot, footwear, and distal forelimb structures of the cat and establish the corresponding 3D models. Firstly, the foot-shoe and distal limb

geometries were reconstructed from the high-resolution CT image using Mimic (Materialise, Leuven, Belgium). Secondly, for surface smoothing and solid model creation, the reconstructed geometries were imported into reverse engineering software (Geomagic (3D Systems, South Carolina, United States) and Solidworks (Dassault Systèmes, Massachusetts, United States)). Within the reverse engineering environment, some other basic structures such as cartilages, plantar fascia and ligaments were further created based on the anatomical structure. Lastly, the coupled models were established by aligning and assembling the corresponding structures.

Moreover, the FE analysis through ANSYS (ANSYS, Pennsylvania, United States) was utilized to simulate the foot-shoe interaction and evaluate the biomechanical response of feline distal limb under landing condition. The boundary and loading conditions were determined by the data inputs from the experimental part, and the simulated pressure distribution of the foot, footwear, and forelimb was compared to the corresponding experimental data measured by Novel pressure measurement systems (Novel GmbH, Munich, Germany) for model validation.

The details about the experimental test and FE simulation are listed in 2.2-2.3 sessions. Based on these results, a generalized methodology workflow that considers both the human musculoskeletal and shoe structures, together with the bionic analysis, was introduced for the quantitative exploration of forefoot injury mechanism and the fast evaluation and optimization of footwear.

2.2 Ethics statement

This dissertation was performed in compliance with the declaration of Helsinki and was approved by the Institutional Ethics Committee of Ningbo University. Before taking part in this study, all human subjects and the animal owners were informed of the corresponding experiment and simulation content as well as the potential risks and then they gave the consent to participate, as shown in Figure 9.

A

Research Academy of Grand Health, Ningbo University

Human Informed Consent Form

Instructions to the Student Researcher(s): An informed consent/assent/permission form should be developed in consultation with the Adult Sponsor, Designated Supervisor or Qualified Scientist. This form is used to provide information to the research participant (or parent/guardian) and to document written informed consent, minor assent, and/or parental permission.

- When written documentation is required, the researcher keeps the original, signed form.
- Students may use this sample form or may copy ALL elements of it into a new document.

If the form is serving to document parental permission, a copy of any survey or questionnaire must be attached.

Student Researcher(s): _____
 Title of Project: _____

I am asking for your voluntary participation in my science fair project. Please read the following information about the project. If you would like to participate, please sign in the appropriate area below.

Purpose of the project: _____

If you participate, you will be asked to:

Time required for participation: _____

Potential Risks of Study: _____

Benefits: _____

How confidentiality will be maintained: _____

If you have any questions about this study, feel free to contact:

Adult Sponsor/SGDS: _____ Phone/email: _____

Voluntary Participation:
 Participation in this study is completely voluntary. If you decide not to participate there will not be any negative consequences. Please be aware that if you decide to participate, you may stop participating at any time and you may decide not to answer any specific question.
 By signing this form I am attesting that I have read and understand the information above and I freely give my consent/assent to participate or permission for my child to participate.

Adult Informed Consent or Minor Assent Date Reviewed & Signed: _____

Research Participant Printed Name: _____ Signature: _____

Parent/Guardian Permission (if applicable) Date Reviewed & Signed: _____

Parent/Guardian Printed Name: _____ Signature: _____

B

Research Academy of Grand Health, Ningbo University

Animal Owner Informed Consent Form

Instructions to the Student Researcher(s): An informed consent/assent/permission form should be developed in consultation with the Adult Sponsor, Designated Supervisor or Qualified Scientist. This form is used to provide information to the owner of animal(s) participated in project and to document written informed consent.

- When written documentation is required, the researcher keeps the original, signed form.
- Students may use this sample form or may copy ALL elements of it into a new document.

Student Researcher(s): _____
 Title of Project: _____

As the owner or duty authorized agent for the owner you have been asked to have your animal(s) participate in my science fair project. Your informed consent is required prior to this use. Please read the following information about the project and feel free to ask any questions you might have. If you would like to have your animal(s) participate, please sign in the appropriate area below.

Purposes and benefits of the project: _____

Location where animal participation/project occurs: _____

Duration of animal participation: _____

Description of animal procedures to be carried out: _____

Possible discomfort, risks and complications and steps taken to minimize risks: _____

Possible benefits to the animal: _____

How confidentiality will be maintained: _____

If you have any questions about this project, feel free to contact:

Adult Sponsor/SGDS: _____ Phone/email: _____

Voluntary Participation:
 The participation of your animal(s) is completely voluntary, and you may withdraw your animal(s) for any reason at any time. If you do not wish to participate you do not have to provide any reason for your decision. Refusal to participate or withdrawal will in no way affect the care to which animal participants are otherwise entitled.
 By signing this form I am attesting that I have read and understand the information above and I freely give my consent/assent for my animal(s) to participate.

Consenting Owner/Authorized Agent Printed Name: _____

Signature: _____ Date: _____

Owner/Agent Contact details Phone/email: _____

Address: _____

Figure 9 A: Human informed consent form; B: Animal informed consent form

2.3 Participants

2.3.1 Human participants

The recreational runner was defined based on regular running practice (frequency: ≥ 3 times/week, distance: ≥ 20 km/week) and the World Masters Association age grading performance tables (age-graded score $< 60\%$), for more details about age-graded score see the previous study [136]. Accordingly, a total of ten male recreational runners (age: 25.63 ± 2.88 years, height: 1.72 ± 0.04 m, weight: 64.73 ± 5.68 kg, BMI: 21.99 ± 2.75 kg/m²) were recruited from the university and local running clubs to participate in the experimental test. Among them, one of the runners (age: 27 years, height: 175 cm, mass: 70 kg) was further involved in the FE simulation test. All participants have regularly joined in the half or full marathon race within 3 years, and they were confirmed as right leg-dominant, habitual rearfoot strikers and reported no prior history of lower limb injuries or foot abnormalities and neither any orthopedic surgeries at least six months before the experiment.

In terms of the running shoe, the same one with EVA midsole, rubber outsole, and 8 mm heel-to-toe drop was used in this study (Figure 10). All participants preferred the same shoe size of 41 (Europe) and were required to wear the experimental shoe while performing daily exercise for one week before the test.



Figure 10 Illustration of basic information of the running shoe

2.3.2 Animal participants

One British shorthair cat (neutered male, age: 2 years, weight: 4.7 kg, Figure 11) was recruited to provided data for this study. A full clinical examination was conducted to ensure the cat had no health issues or musculoskeletal injury in any of his limbs that could impact the result of this study.

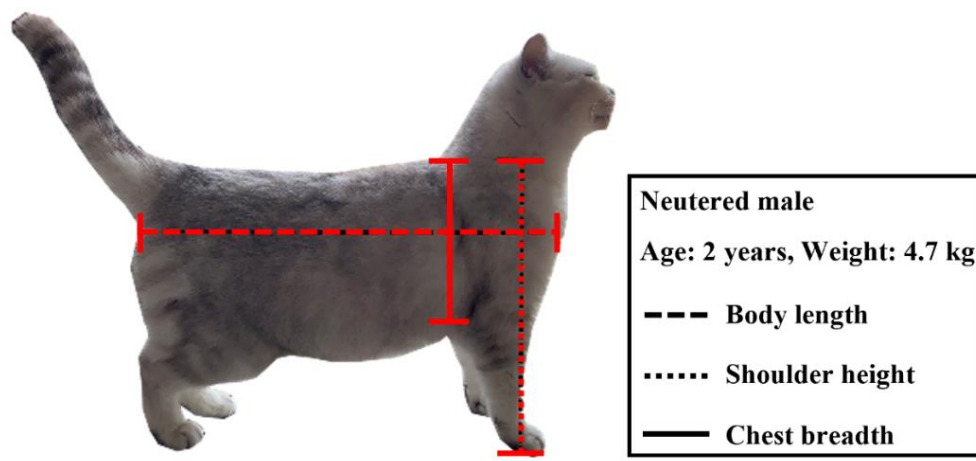


Figure 11 Illustration of basic information of the cat

2.4 Biomechanical experiments

2.4.1 Experimental protocol and procedures

2.4.1.1 Long-distance running test

Prior to the test, participants were required to wear the sports pants and experiment shoes and run on the treadmill at a speed of 8km/h for 10 minutes as a warm-up. The foot kinematics and kinetics, foot morphology, foot skin temperature, subjective-perceived hallux comfort, and gap length between the hallux and toebox were then collected for static condition (baseline data). After that, participants were asked to run on the treadmill with a speed of 12km/h and a 0% slope for 10km in total. This running protocol was chosen because a running distance of 10 km is long enough to initiate changes, and 12 km/h corresponds to the average moderate running speed for recreational runners [110]. The variables mentioned above were again measured immediately after 5 km of running. After the interval test, participants kept running for another 5 km and did the final 10-km test.

2.4.1.2 Feline landing test

This test was conducted in a quiet room with only the researchers and the owners present. To ensure the success of the experiment, owners were required to bring the cat to the laboratory in advance in order to get them familiar with the test environment, which lasts until the cat can be enticed by food, toys and/or encouragement of the owners to accurately jump and land on the specific region [137,138]. During the formal test, the cat was firstly encouraged to relax and maintain a natural standing position on the measurement instrument in order to collect the baseline static data. After that, it was moved to a height-adjustable table and encouraged to sit in a squat position at the table edge, from where it would jump onto the instrument with its forelimbs landing first (Figure 12). The table height was adjusted to three specific values (0.6m, 0.8m, and 1.0m) for this experiment and 1-min interval after each landing task was given to avoid any influences of fatigue on data collection. The trial was considered successful if there was no apparent tilt of the cat's body and it landed correctly and continued to walk forward.

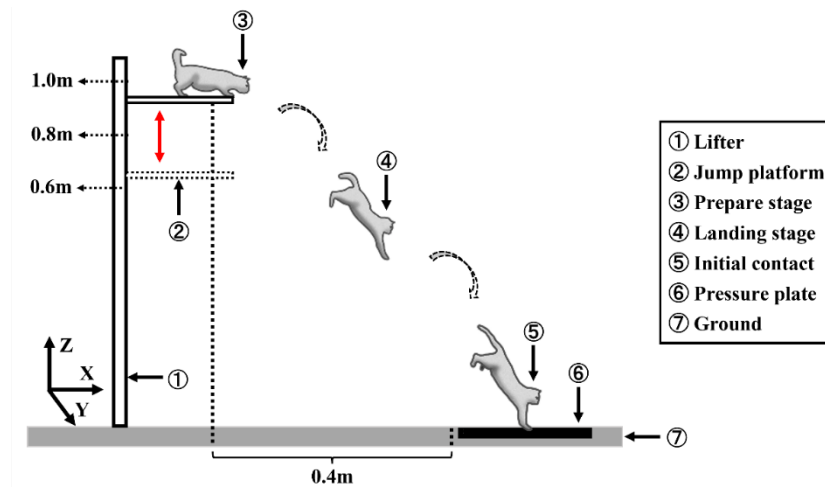


Figure 12 Illustration of cat landing procedure

2.4.2 Experimental instrument and data analysis process

2.4.2.1 Foot kinematics and kinetics

A Vicon motion capture system (Oxford Metrics Ltd., Oxford, United Kingdom) with 8 infrared cameras was applied to collect the foot kinematics during running at 200 Hz (Figure 13). Prior to data collection, the motion capture system was calibrated according to the manufacturer's instructions. A total of 30 spherical reflective markers with 9 mm in diameter were attached to the corresponding bony landmarks through the hole cut in the shoes based on a previously established protocol, and 3 markers were removed after the static calibration trials (Figure 14) [139]. In addition, a 0.6 m×0.8 m AMTI force platform (AMTI, Watertown, MA, United States) embedded in the middle of the 20 m indoor walkway was utilized to determine GRF data and gait cycle at a frequency of 1000Hz (Figure 13). The Vicon Nexus software package (Version 1.8.5, Oxford Metrics Ltd., Oxford, United Kingdom) was used to record the marker trajectories and GRF data synchronously. During the test, participants were asked to run on the 20-m indoor track at the same speed of the 10 km treadmill running and land on the force plate with their dominate leg, with the above motion capture system and force platform used to record data. The Brower timing gates (Brower Timing System, Draper, UT, United States) were set 2 m apart on the middle of the force platform to monitor the running velocity (Figure 13). Each participant performed eight successful trials of running and at least 30-second rest were allowed after one trial.

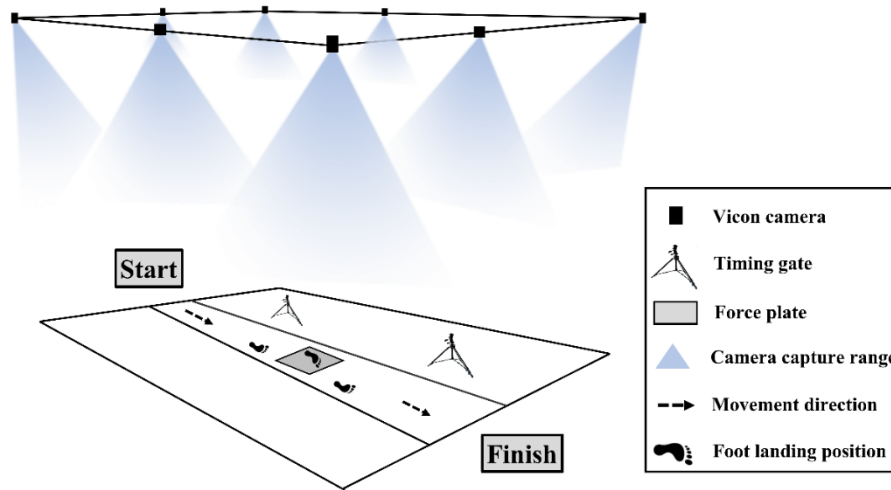


Figure 13 Illustration of experimental setup for foot kinematics and kinetics

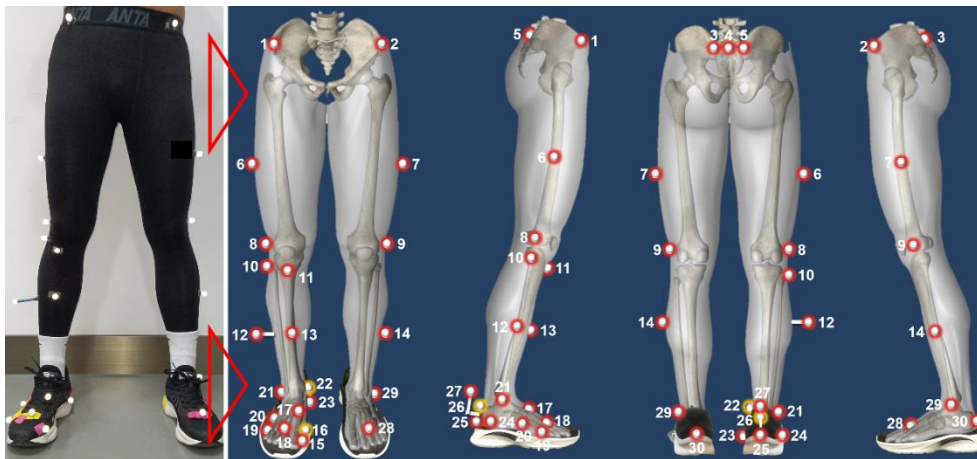


Figure 14 Illustration of Oxford foot model marker placement

Note: 1, right anterior superior iliac spine; 2, left anterior superior iliac spine; 3, left posterior superior iliac spine; 4, Sacral marker; 5, right posterior superior iliac spine; 6, right thigh marker; 7, left thigh marker; 8, right lateral knee; 9, left lateral knee; 10, right lateral head of fibula; 11, right tibial tuberosity; 12, right tibial marker; 13, right anterior aspect of the shin; 14, left tibial marker; 15, right hallux; 16, right 1st metatarsal, distal medial; 17, right 1st metatarsal, proximal dorsal; 18, right toe; 19, right 5th metatarsal, distal lateral; 20, right 5th metatarsal, proximal lateral; 21, right ankle; 22, right medial malleoli; 23, right sustentaculum tali; 24, right lateral calcaneus; 25, right heel; 26, right posterior calcaneus proximal; 27, right peg marker; 28, left toe; 29, left ankle; 30, left heel; The yellow markers were removed after static calibration.

The Vicon Nexus software was used to perform the preliminary processing of the data. Firstly, the gait data were labelled and run in this system, and an experienced technician further checked the traces and removed all the inconsistent trials. Five gait cycles of the dominant foot were selected out of eight trials for each participant. Afterwards, the marker trajectories and GRF were filtered using the low-pass, fourth-order, zero-lag Butterworth filter with a frequency of 8 Hz and extracted as CSV files for further analysis.

The Oxford foot model divides the foot structure into three parts, including hallux, forefoot, and hindfoot. Therefore, in this dissertation the dominant foot inter-segment kinematics from the entire stance phase, including forefoot with respect to hindfoot angles (FFHFA) in the sagittal, frontal, and transverse planes, as well as hallux with respect to forefoot angle (HXFFA) in the sagittal plane, were determined. In addition, angle values at initial contact and toe-off, as well as the peak values and range of motion (ROM) during the stance phase, were also derived. Stance phase was defined as the period of time when the vertical GRF value surpassed 20 N while initial contact and toe-off represent the starting and ending points of this period respectively. ROM refers to the difference between the maximum and minimum joint angles during the stance phase.

For the GRF data of interest, the 1st and 2nd vertical GRFs, peak propulsive and braking GRFs in the stance phase, together with the 1st and 2nd vertical average loading rate (VALR), were extracted. The peak propulsive and braking GRFs refer to the peak positive and negative GRFs in X-axis (anteroposterior direction), and VALR was calculated according to the following established equation, where the $F_{n\%}$ and $t_{n\%}$ represent the percentage of force magnitude and time till the corresponding peak values [140]. All kinetic parameters were normalized to BW for further analysis.

$$VALR = [F_{80\%} - F_{20\%}] / [t_{80\%} - t_{20\%}] \quad (1)$$

2.4.2.2 Foot morphology

The foot morphology data were collected using a 3D foot scanner (Easy-Foot-Scan, OrthoBaltic, Kaunas, Lithuania) with an accuracy of 0.3 mm and the scanner volume of 400 (length)*200(width)*200(height) mm³(Figure 15). During the test, participants had their dominant foot scanned while standing with legs separated at the shoulder width [109].

Twelve foot dimensions were measured according to the previously established protocol (Table 1), which includes foot length ①, arch length ②, heel to fifth toe length ③, mid-ball to heel length ④, ball width ⑤, maximal heel width ⑥, maximal heel location ⑦, dorsal height ⑧, arch height ⑨, ball girth ⑩, instep girth ⑪, and short heel girth ⑫ [141].

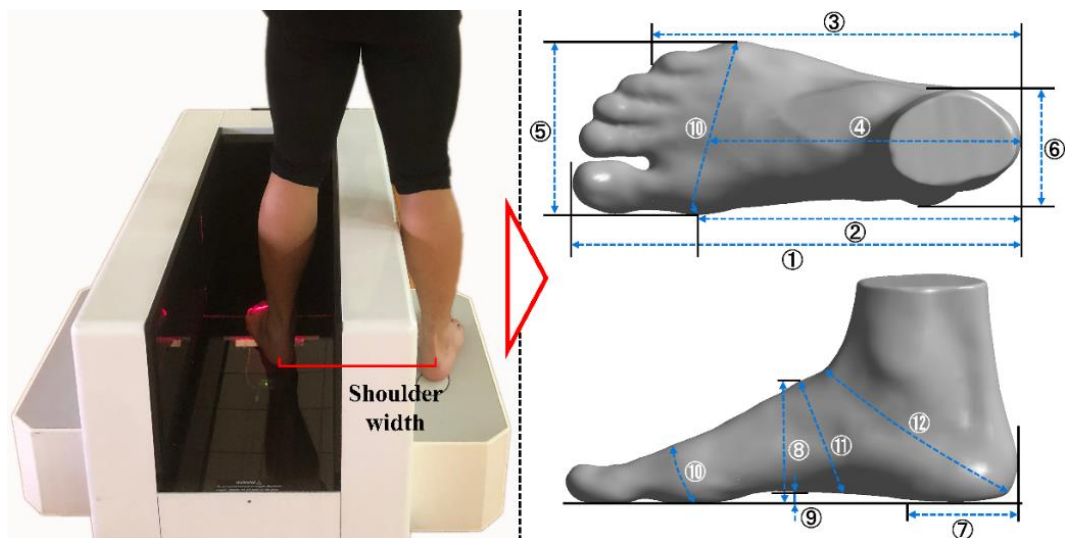
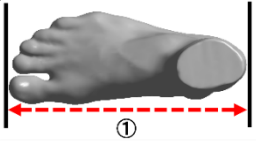
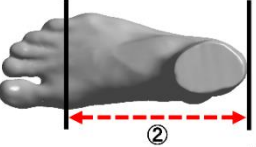
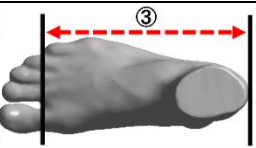
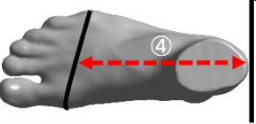

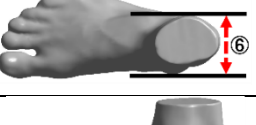


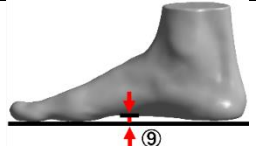
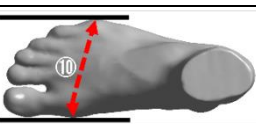
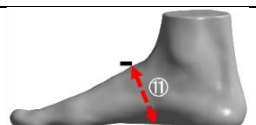
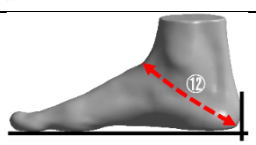


Figure 15 Illustration of foot morphology measurement

Note: foot length ①, arch length ②, heel to fifth toe length ③, mid-ball to heel length ④, ball width ⑤, maximal heel width ⑥, maximal heel location ⑦, dorsal height ⑧, arch height ⑨, ball girth ⑩, instep girth ⑪, and short heel girth ⑫.

Table 1 Foot morphology definitions [141]

Foot dimensions	Definition	Image
Foot length	Distance between pternion and the tip of the longest toe in X-direction.	
Arch length	Distance between pternion and the medially prominent point of the first metatarsal head in X-direction.	
Heel to fifth toe length	Distance between pternion and the tip of the fifth toe in X-direction.	
Mid-ball-to heel length	Distance between pternion and the middle point of the metatarsal ball in X-direction.	
Ball width	Distance between the prominent point of the first and the fifth metatarsal heads in Y-direction.	
Maximal heel width	Distance between the prominent point of the medial and lateral malleolus in Y-direction.	
Maximal heel location	Distance between pternion and the prominent point of the medial malleolus in X-direction.	
Dorsal height	Height of the vertical cross-section at 50% of foot length from the pternion in Z-direction.	
Arch height	Height between the lower edge of the navicular and the vertical line from the base of the first metatarsal head to the heel in Z-direction.	
Ball girth	Girth from the lateral margin of the first metatarsal head to the lateral margin of the fifth metatarsal head.	
Instep girth	Minimum girth over the middle prominence of the cuneiform.	
Short heel girth	Minimum girth around back heel point and dorsal foot surface.	

2.4.2.3 *Foot skin temperature*

The foot skin temperature was recorded by an infrared camera (Magnity Electronics Co. Ltd., Shanghai, P.R. China) with a resolution of 384×288 pixels. As shown in Figure 16, for the plantar region, participants sat down with their legs in a horizontal position and perpendicular to the infrared camera at a distance of 1m. An anti-reflection panel was placed behind the feet to minimize the effect of the reflected temperature from the surroundings, and to remove the other parts of the body from the image [142]. For the dorsal region, participants stood on the panel and the infrared camera was placed 1m above the ground for measurement. The indoor temperature was controlled at 20°C using an air conditioner, and participants were required to remain barefoot for 10 minutes to adapt to the room temperature before the thermographic measurement for the static condition [142].

A thermographic software (ThermoScope v1.2, Magnity Electronics Co. Ltd., Shanghai, P.R. China) was used to obtain the mean temperature of the foot regions at the skin emissivity factor of 0.98. Based on the foot anatomical model, 8 regions of interest were defined to obtain the mean temperature, including hallux (H), other toes (OT), medial metatarsal (MM), central metatarsal (CM), lateral metatarsal (LM), dorsal hallux (DH), dorsal other toes (DOT), and dorsal metatarsal (DM) (Figure 16). The proportion criteria for the delimitation of the regions of interest are as follows. First, the hallux and other toes regions were delimited, and from which the rest of the sole was divided into three equal longitudinal regions, named forefoot, midfoot, and hindfoot. Next, the width of the hallux and the delimitation between the third and fourth toes were taken as the references to divide the medial, central, and lateral metatarsal regions respectively. Lastly, the dorsal region was further delimited according to the above criteria [143].

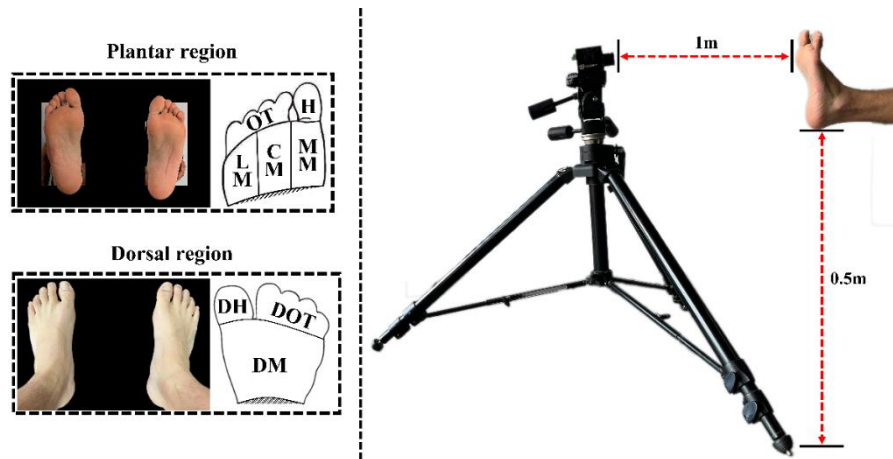


Figure 16 Illustration of foot skin temperature measurement

2.4.2.4 Subjective-perceived hallux comfort

The subjective-perceived comfort of hallux was measured using the VAS form, which is a popular instrument for pain measurement. It usually consists of a straight line of 100 mm, with anchor descriptors such as “no pain” at the left end (0mm) while “worst pain imaginable” at the right end (100mm), as shown in Figure 17. Based on a previous literature review, we considered VAS to be reported in centimeters (i.e., 0-10cm) for easier data processing in this study [144]. During the test, participants were required to make a mark which can reflect his perception about hallux comfort. Afterwards, the distance between the left end point and the mark is calculated in mm, representing as the VAS score.

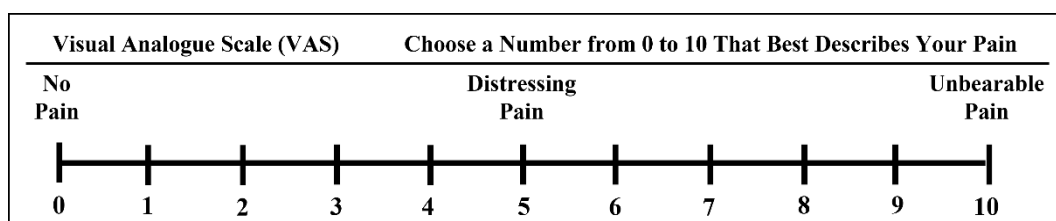


Figure 17 Illustration of VAS

2.4.2.5 Gap length between the hallux and toebox of the shoe

The gap length between the hallux and toebox of the shoe, defined as the vertical distance between the phalangeal joint of the hallux and toe cap in the sagittal plane, was collected with a high-speed digital camera (Fastcam SA3, Photron, Japan) at a frequency of 1000Hz. As shown in Figure 18, the camera was positioned on a portable

tripod placed 0.3m above the floor and 1m away from the treadmill. A triangle-shaped hole was cut in the shoe upper and a reflective point (1.5mm) was attached to the phalangeal joint of the hallux to allow the camera to capture the hallux motion. During the test, participants were instructed to switch the shoe and continue to run on the treadmill at 12km/h until 5 complete gait cycles were recorded during each condition.

Single-stride video clips at three stance instants (initial contact, midstance, and toe-off) were first created from the captured videos and then the gap length was quantified visually in a subjective way using a video analysis software (Photron FASTCAM Viewer Ver.3620, Photron, Japan). Initial contact in the videos was defined as the moment when the shoe makes first contact with the treadmill belt, midstance in the videos was defined as the moment when the knee of the swing lower limb was adjacent to the knee of the stance one, and toe-off in the videos was defined as the moment when the shoe makes the last contact with the treadmill belt [145].



Figure 18 Illustration of gap length measurement

2.4.3 Statistical analysis

All statistical analyses were performed with the SPSS 22 (IBM SPSS inc., Chicago, IL, USA). Prior to analysis, the Shapiro-Wilk test was applied to check the normality of data distribution and Levene's test for homogeneity of variances was used for homogeneity assessment. All data were presented as mean \pm SD (standard deviation). One-way repeated-measures analysis of variance (ANOVA) with Bonferroni post-hoc

comparison was conducted to determine the differences in the above-mentioned five aspects among static, 5km, and 10km conditions. Moreover, one-way repeated-measures ANOVA of one-dimensional statistical parametric mapping (SPM1d) was also conducted to further observe foot kinematics changes over the stance phase by using MATLAB 2019b software (The MathWorks, Natick, MA, USA). The significance level was set at $p < 0.05$.

2.5 Finite element simulation

2.5.1 Model construction

The medical CT images (Optima CT540, GE Healthcare, Chicago, United States) of the foot and sports shoe were collected through scanning the participant's right leg (shod), which was fixed by an ankle-foot orthosis to the neutral position (Figure 19) [128]. The DICOM images were segmented by Mimic 21.0 (Materialise, Leuven, Belgium) to obtain the boundaries of bones, soft tissues, and shoe and build the 3D geometry model. The noise pixels between soft tissue and shoe cavity were manually deleted while keeping the shoe contour and thicknesses as same as the real one. To reduce the computation, the second to fifth intermediate and distal phalanges were fused to one bony structure, the sock structure was considered but not separated from the soft tissue, and the shoe model was divided into two parts which stand for the shoe upper and the shoe sole, respectively. These geometries were smoothed using Geomagic Wrap 2017 (3D Systems, South Carolina, United States) and then imported into Solidworks 2020 (Dassault Systèmes, Massachusetts, United States) to form solid parts (Figure 20 and Figure 21).

Twenty cartilaginous structures were modelled for articulations between 20 bones considered in this model (distal parts of tibia and fibula, talus, calcaneus, cuboid, navicular, 3 cuneiforms, 5 metatarsals, and 6 phalanges) to allow the connection and relative movements, and the encapsulated soft tissue was further obtained by subtracting all the bony and cartilaginous structures from the full soft tissue volume. A total of 66 ligaments and 5 plantar fasciae were created using tension-only link elements based on the anatomical locations on corresponding bones. As shown in Figure 22, the

foot model was finally assembled with the shoe model to achieve the coupled foot-sports shoe complex.



Figure 19 Illustration of CT imaging for the participant

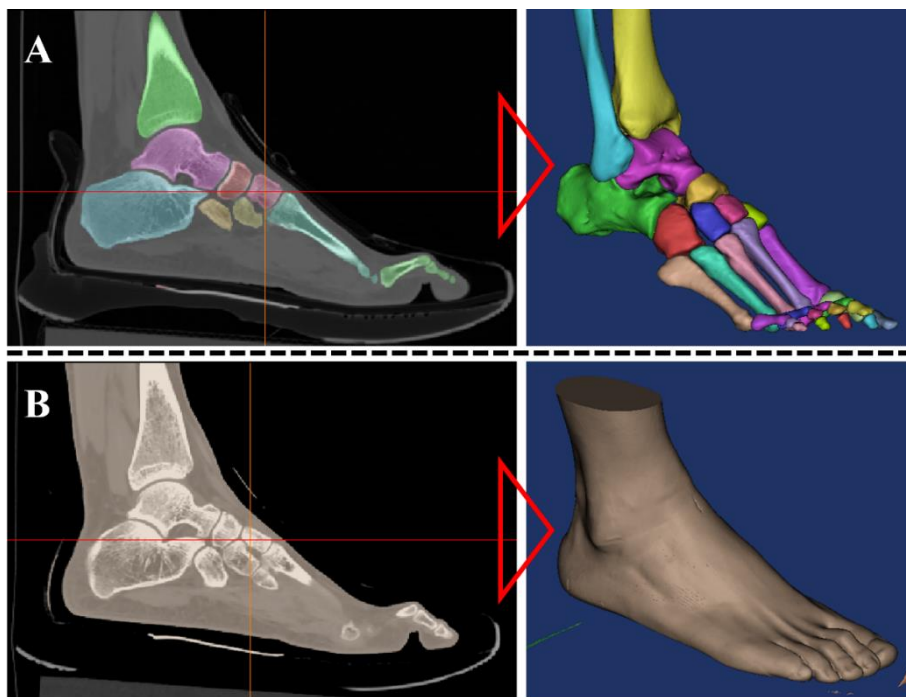


Figure 20 Illustration of CT imaging and 3D geometries of the bone (A) and soft tissue (B)

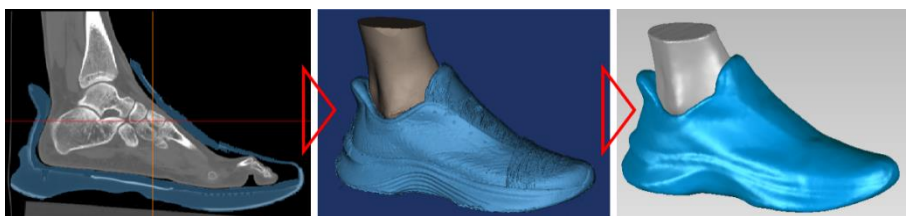


Figure 21 Illustration of CT imaging and 3D geometry of the foot and shoe and smoothing process

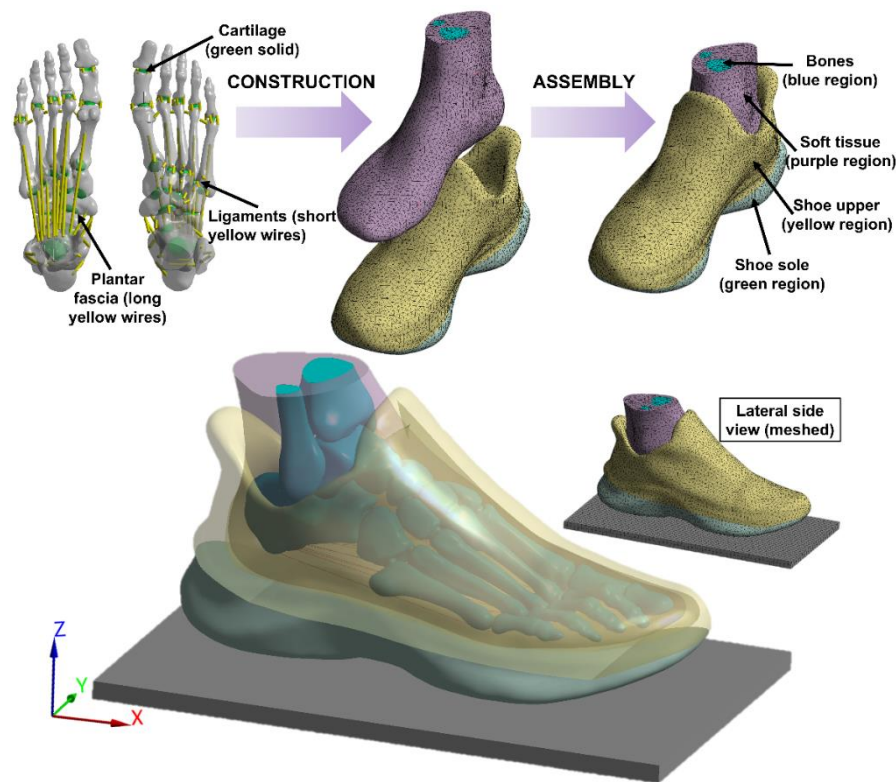


Figure 22 Illustration of 3D FE model of the foot and sports shoe complex

Regarding the feline paw model, similar image acquisition and segmentation were applied. As shown in Figure 23, the CT images of the cat's whole body were collected in the unloaded position, while only the left forelimb paw was analyzed in this study. The body of the cat was oriented in the scanner in a specific way to mimic the posture when the fore paws of the cat are naturally placed on the ground. This position was easy to manipulate because the cat was anesthetized by a veterinarian. The structures of 23 bones, which included 1 radius, 1 ulna, 7 carpus, 5 metatarsals, and 9 components of the phalanges together with the encapsulated volume were segmented, smoothed, and then form into solid parts. To simulate the real situation of the cat's paw, the solid volume of the articular cartilaginous structure was shaped. Thus, 18 cartilages were created according to the feline paw anatomical structure [146]. In addition, the ligaments were then generated based on anatomical characteristics and the encapsulated soft tissue was built by subtracting all bones and cartilages and converting them into a solid format. Eventually, the paw model consists of 23 bones, 18 cartilages, 30 ligaments, and an encapsulated soft tissue.

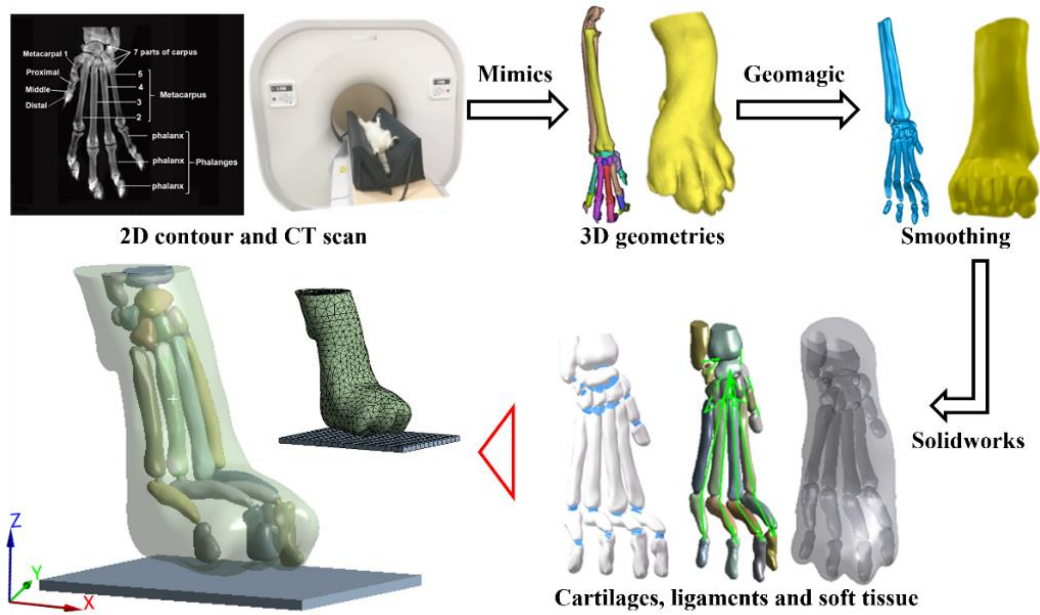


Figure 23 Illustration of the process of reconstructing the paw model

2.5.2 Mesh development

The mesh for each part of the foot-shoe model and paw model was created by HyperMesh 16.0 (Altair, Michigan, USA). During the process, 4-node linear tetrahedral elements were used on the irregular geometries such as bones, cartilage, and encapsulated tissue. A convergence analysis was applied to both ensure the model accuracy and the optimum requirement on computational resources in the preliminary phase. In this process, the mesh density was gradually decreased until the difference in predicted peak stress values between two meshes were within 3% [147].

Finally, except for the ground plate, which was meshed with hexahedrons, all other components meshed with tetrahedral solid elements. For the foot-shoe model, the mesh size was 5.0mm for the soft tissue, shoe upper, shoe sole, and plate, 3.5mm for the bones, and 2.0mm for the cartilage, and in total, there are 358,322 nodes and 208,225 elements for the whole model. In terms of the paw model, the mesh size was set to 0.2 mm for the bony component, 0.1 mm for cartilaginous parts, and 0.2 mm for encapsulated soft tissue. The total number of tetrahedral elements in solid bones, cartilage, and encapsulated parts was 19986.

2.5.3 Material properties

All the materials assigned in this FE analysis were idealized to be homogeneous, isotropic, and linearly elastic except the encapsulated soft tissue of the paw model. Two material constants (i.e., Young's modulus (E) and Poisson's ratio (ν)) were used to define the elasticity. For the foot-shoe model, a further material property sensitivity analysis of shoe sole stiffness was conducted since this part was considered as a whole component in this simulation. To be specific, Young's modulus (E) of shoe sole was adjusted by $\pm 10\%$ and $\pm 20\%$ from the baseline value (2.490MPa), which was obtained from previous literature [131,132,148].

In terms of the paw model, the published data regarding feline bone is limited, therefore the material properties of canine bone are referenced here due to certain similar aspects of mammalian anatomy and function [26]. The cartilage and ligament comprise the same material as human foot. In a recently published research paper, which examined the biomechanics of paw pad of cats, the pad was described as a nonlinear, viscoelastic property similar to polymers [27]. Thus, a hyperelastic material model, with a second-order polynomial strain energy potential, was used to mimic the cat's paw encapsulated soft tissue.

Values for the paws soft tissue were calculated by ANSYS Workbench 2021 (ANSYS, Pennsylvania, USA) based on uniaxial stress-strain data, acquired from published research, under three loading frequencies (0.11 Hz, 1.1 Hz, and 11Hz) [27]. This was done as hyperelastic material behavior is typically characterized by uniaxial tests, biaxial tests, and shears tests. The engineering stress-strain data were directly imported into the processor of ANSYS Workbench 2021. Finally, the plate was created and assigned with an elastic property to simulate concrete ground support. The details of the material properties are listed in Table 2.

Table 2 Material properties assigned to each component in the FE model

Component	Element type	Young's modulus E (MPa)	Poisson's ratio ν	Cross-section area (mm ²)
Foot-shoe model				
Shoe upper	Tetrahedral solid	11.76	0.35	-
Shoe sole (baseline)	Tetrahedral solid	2.49	0.35	-
Bone	Tetrahedral solid	7300	0.30	-
Cartilage	Tetrahedral solid	1	0.40	-
Ligament	Tension-only truss	260	0.40	18.4
Plantar fascia	Tension-only truss	350	0.40	58.6
Soft tissue	Tetrahedral solid	1.15	0.49	-
Paw model				
Bone	Tetrahedral solid	15000	0.30	-
Cartilage	Tetrahedral solid	1	0.40	-
Ligament	Tension-only truss	260	0.40	18.4
Other models				
Ground plate	Hexahedral solid	17000	0.10	-

2.5.4 Boundary and loading conditions

The boundary and loading conditions were determined through the experimental measurements of the same subject used for CT scans and FE model construction. For the foot-shoe model, 3D gait analysis was carried out using the Vicon motion capture system and AMTI force platform synchronously, and a total of 48 reflective markers were attached to the corresponding bony landmarks according to the previously established protocol (Figure 24A) [149]. Firstly, the balanced standing trial was conducted when the subject stood on the force plate with his right leg. The vertical GRF was derived, and the heading angles of foot in sagittal and coronal plane were further calculated based on the Euler angles of foot rigid body coordinate system with respect to the global coordinate system since the plantar pressures were reported to be highly associated with the foot orientation during simulation [150]. The foot-plate system approach, which is a commonly employed method during biomechanical modeling of the human foot in previous studies, was used to simulate the balance standing between

the foot, shoe, and ground (Figure 24B). First, a 3D solid plate that was allowed to move only in the vertical direction was used to model the supporting ground, and the proximal surfaces of the soft tissue, tibia, and fibula components were fixed. Moreover, two additional forces were assigned to the model. One is the vertical GRF, which was applied at the inferior surface of the ground plate (343.00N). The other is the AT force, which is commonly estimated as 50% of the force applying on the foot while balanced standing in previous research [147, 148], was applied at the superior surface of the calcaneus (171.50N).

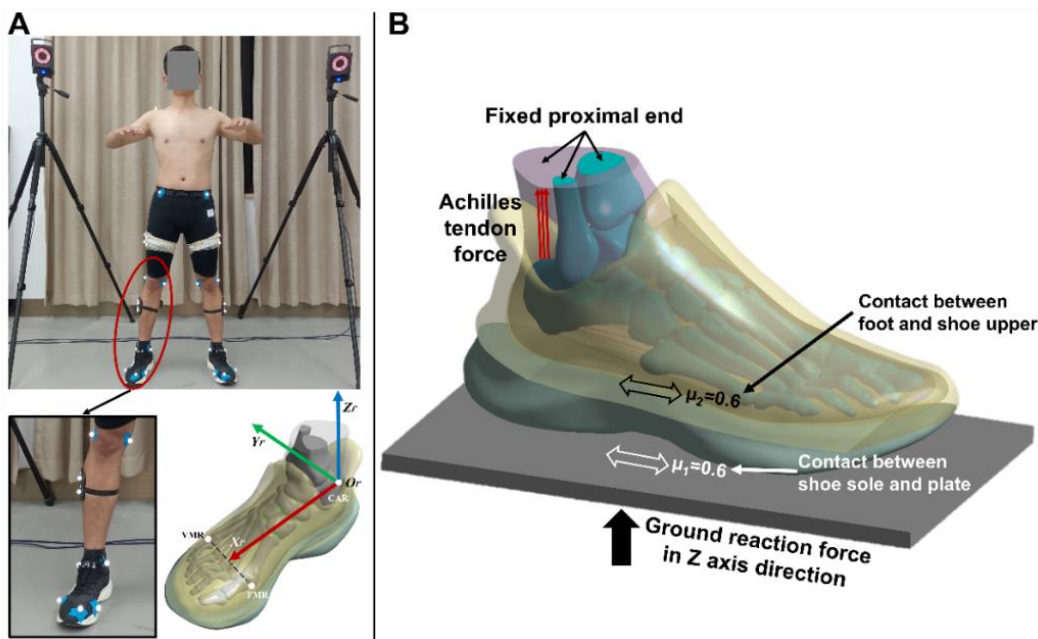


Figure 24 Illustration of markers setting and foot heading angles (A) and boundary and loading conditions for balanced standing (B)

After that, the running trial was performed on the same subject with the running speed of 12km/h using the above equipment. In this study, the foot-shoe dynamic interaction during the last stance phase was simulated as an example to demonstrate the validity and accuracy of the role of the proposed model in fast evaluation and optimization of footwear (Figure 25).

The foot kinematic data during this period of time were calculated as the boundary and loading conditions to drive the running motion. To be specific, the 3D solid plate was fixed in all directions while the displacement load (coordinate position change of

the ankle joint center point) and rotation angle load (alteration of the foot heading angle) were applied to a total of 1968 nodes of the talus, heel, navicular, dice, cuneus and five metatarsals under the global coordinate system. The coordinate position of the center point of the ankle joint was calculated based on the coordinate data of the lateral and medial malleolus, and the alteration of the foot heading angle referred to the total change in foot heading angle over time. In addition, the duration from the midstance to toe-off phases were also measured as the time load for the foot-shoe dynamic simulation. In terms of the interaction between the foot, shoe, and ground plate, both the connection types were defined as the frictional contact with a coefficient of 0.6 [131, 132].

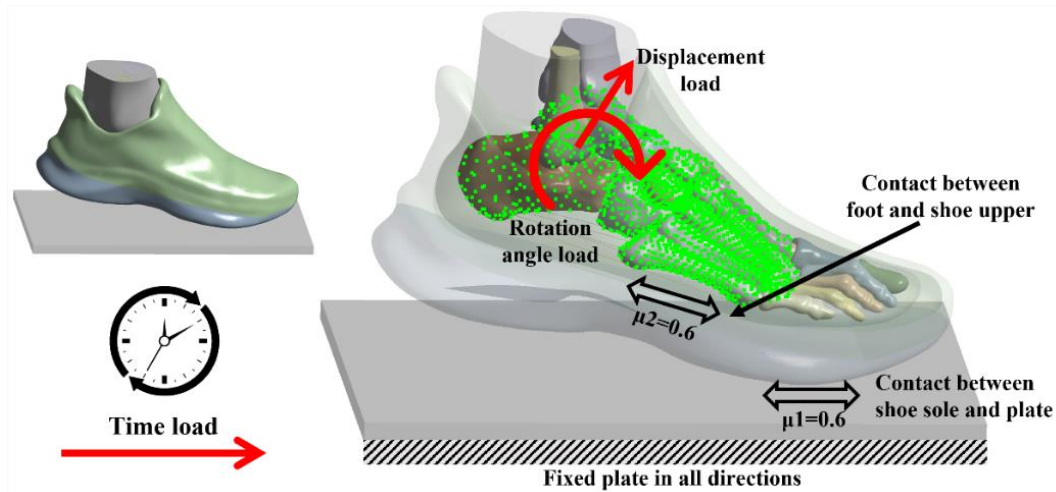


Figure 25 Illustration of boundary and loading conditions for running

In terms of the paw model, the foot-plate system approach was applied for both standing and landing simulation (Figure 26). The superior surface of the encapsulated solid part, distal tibia, and distal fibula was fixed while the plate was allowed to move freely only in a vertical direction. The vertical GRF was collected using the AMTI force platform with the cat standing still or landing from different height and then applied underneath the plate, which created a frictional contact ($\mu=0.6$) with the paw.

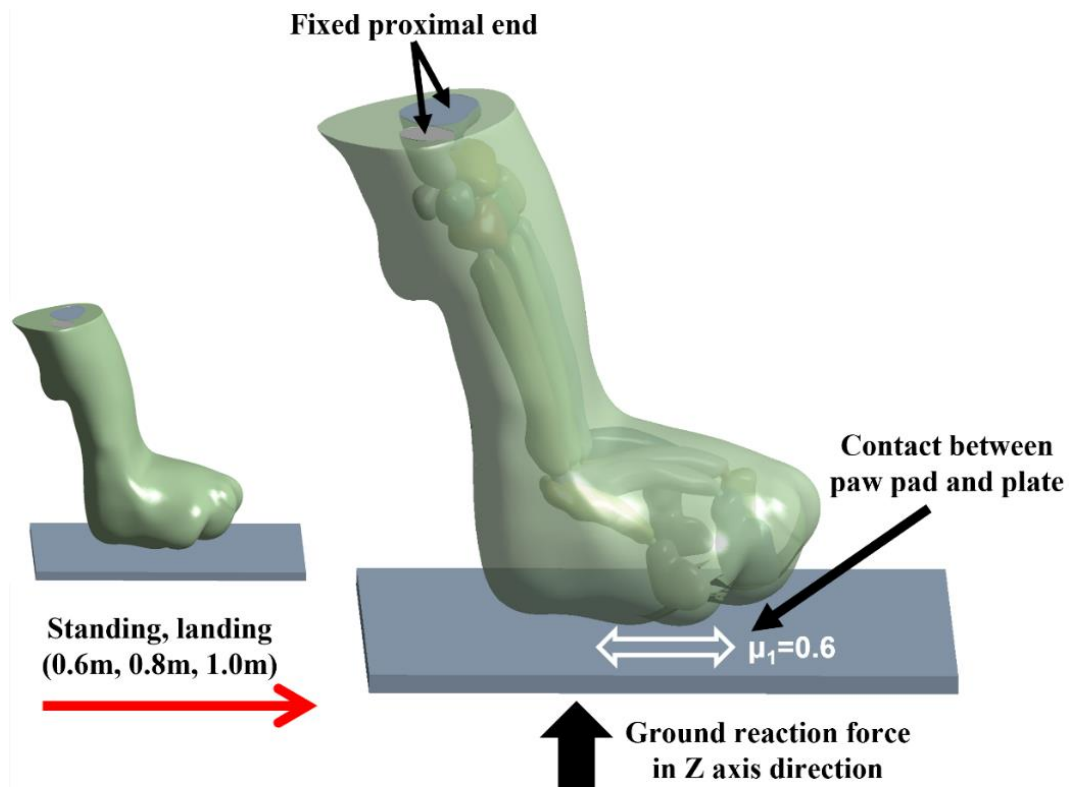


Figure 26 Illustration of boundary and loading conditions for standing and landing

2.5.5 Model validation

To validate the coupled foot-shoe model, the plantar and sole pressure from the computational simulation were compared with the experimental data collected from the same participant using the Novel Pedar-X insole pressure measurement system and Novel Emed force plate measurement system (Novel GmbH, Munich, Germany) at a frequency of 100 Hz, respectively (Figure 27). Both the plantar and sole areas were further divided into four specific regions, including medial forefoot (MFF), lateral forefoot (LFF), midfoot (MF), and hindfoot (HF) for foot model, medial fore-sole (MFS), lateral fore-sole (LFS), medial hind-sole (MHS), and lateral hind-sole (LHS) for shoe model. During the test, the same participant was required to stand still and had his dominant foot on the pressure plate. The pressure distribution and peak pressure of all eight regions were collected to validate against the corresponding predicted pressure. Moreover, the Bland-Altman method was further performed to calculate the difference and mean of the pressure data obtained from experiment and model simulation through MedCalc 19.0.4 (MedCalc Software, Ostend, Belgium). The two approaches would be

considered as good consistency if the difference was within the 95% limits of agreement (LOA).

Regarding the feline paw model, the pressure data under the conditions of static standing were extracted from the Novel Emed force plate measurement system (Novel GmbH, Munich, Germany) with a frequency of 100 Hz for comparison with simulated results.

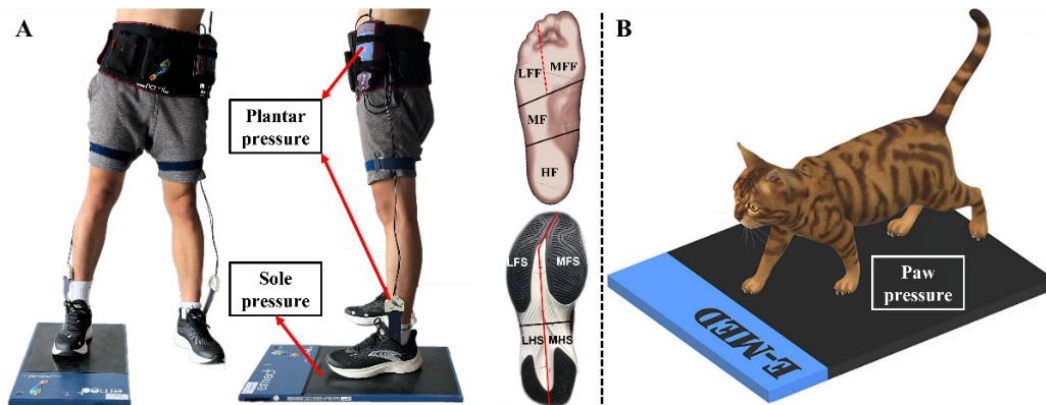


Figure 27 Illustration of pressure measurement for foot-shoe model validation (A) for paw model validation (B)

3 RESULTS

3.1 Results of biomechanical experiments

3.1.1 Foot kinematics

The time-series data of foot inter-segment kinematics and the corresponding SPM1d analysis during the stance phase among three conditions are shown in Figure 28. Table 3-4 exhibits test statistics for all kinematic parameters at critical points.

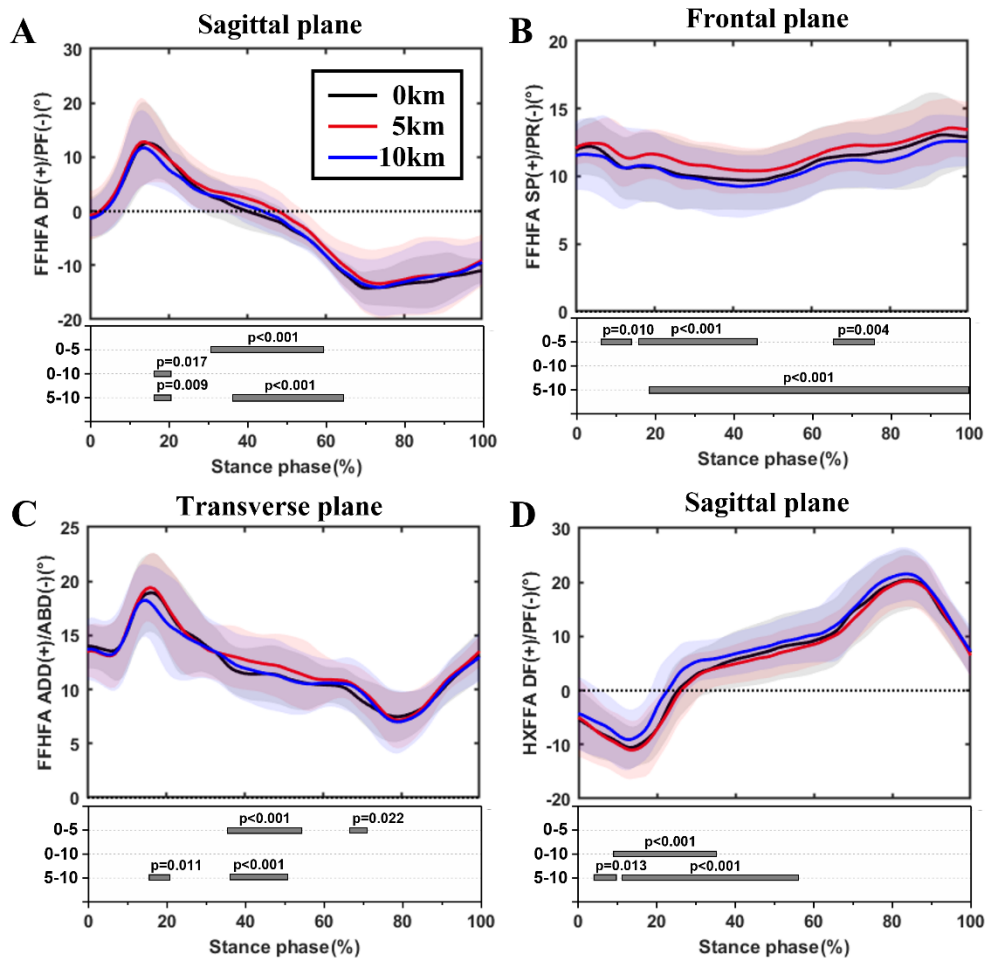


Figure 28 The time-series data and SPM1d analysis of foot inter-segment kinematics during stance phase under static condition and after 5km and 10km of running, A: forefoot with respect to hindfoot motion in sagittal plane; B: forefoot with respect to hindfoot motion in frontal plane; C: forefoot with respect to hindfoot motion in transverse plane; D: hallux with respect to forefoot motion in sagittal plane

3.1.1.1 Forefoot with respect to hindfoot motion

Through the SPM1d analysis, it was found that FFHFA was significantly different after 5 km compared to baseline and 10 km (Figure 28A-C). The larger dorsiflexion and adduction angles during the mid-stance phase and the larger supination throughout the stance phase were found at 5 km ($p < 0.05$). In addition, 10 km running resulted in relatively smaller dorsiflexion at the early stance phase compared to baseline and 5 km ($p < 0.05$). The critical point differences among conditions can be found in Table 3. In the sagittal plane, significantly less plantarflexion was also found after 5 km and 10 km

running by comparing the angles at toe-off with baseline ($p=0.007$ and $p=0.013$). There were no significant differences in the frontal plane after 5 km and 10 km of running when compared with baseline ($p>0.05$). However, supination angle at toe-off and its peak value during stance were significantly reduced after 10 km running compared to 5 km running ($p=0.001$ and $p<0.001$). In terms of the transverse plane, peak adduction ($p=0.049$ and $p=0.002$) and ROM ($p=0.001$ and $p=0.007$) were found to be significantly lower both at baseline and 10 km.

Table 3 Forefoot with respect to hindfoot motion kinematics under static condition and after 5km and 10km of running

Variables	Running distance			One-Way Repeated Measures ANOVA		
	Baseline	5 km	10 km	F-value	η_p^2	p-value
	Mean (SD)	Mean (SD)	Mean (SD)			
FFHFA (°)						
X						
Initial contact	-1.30(3.88)	-0.77(4.63)	-1.29(3.47)	1.50	0.03	0.23
Toe-off	-10.55(2.53)	-8.11(4.83)	-8.54(3.94)	8.16	0.14	0.001
Dorsiflexion(max)	13.98(6.44)	14.14(6.79)	13.42(5.45)	1.62	0.03	0.20
Plantarflexion(max)	-16.35(2.65)	-14.96(6.21)	-15.46(5.10)	3.66	0.07	0.05
ROM	30.33(6.30)	29.10(7.45)	28.88(6.03)	3.08	0.06	0.05
Y						
Initial contact	11.95(1.84)	12.07(1.28)	11.52(2.55)	2.13	0.04	0.13
Toe-off	12.92(2.26)	13.38(2.16)	12.56(1.74)	6.01	0.11	0.003
Supination(max)	13.93(2.93)	14.41(2.21)	13.46(2.17)	10.75	0.18	<0.001
ROM	4.61(1.12)	4.64(1.25)	4.66(0.82)	0.03	0.001	0.97
Z						
Initial contact	14.01(2.07)	13.52(2.37)	13.70(2.85)	2.38	0.05	0.10
Toe-off	14.04(2.26)	14.40(1.68)	13.89(2.42)	2.82	0.05	0.06
Adduction(max)	20.00(3.60)	20.66(3.20)	19.57(3.54)	6.03	0.11	0.003
ROM	13.02(2.16)	14.04(1.81)	12.96(1.92)	6.34	0.12	0.003

3.1.1.2 Hallux with respect to forefoot motion

Through the SPM1d analysis, smaller plantarflexion angles were found to be presented during the early to midstance phase (Figure 28D) at 10 km for HXFFA in the sagittal plane ($p<0.05$). In terms of the critical point differences among conditions, a

significant difference was shown between 5 km and 10 km, with the peak value of plantarflexion decreased after 10 km running ($p=0.006$, Table 4).

Table 4 Hallux with respect to forefoot motion kinematics under static condition and after 5km and 10km of running

Variables	Running distance			One-Way Repeated Measures ANOVA		
	Baseline	5 km	10 km	F-value	η_p^2	p-value
	Mean (SD)	Mean (SD)	Mean (SD)			
HXFFA (°)						
X						
Initial contact	-5.41(5.37)	-4.99(7.34)	-4.22(6.78)	2.58	0.05	0.08
Toe-off	3.37(4.81)	2.28(4.69)	3.77(5.12)	2.26	0.04	0.11
Dorsiflexion(max)	21.39(5.52)	21.02(4.37)	22.28(4.74)	2.70	0.05	0.07
Plantarflexion(max)	-10.87(4.03)	-11.40(5.42)	-9.79(5.40)	6.05	0.11	0.003
ROM	32.25(5.02)	32.42(3.84)	32.06(4.20)	0.29	0.006	0.75

3.1.2 Ground reaction forces

The group average and statistics of GRFs during the stance phase are presented in Table 5. No significant differences were found among conditions except peak propulsive, with its value decreasing significantly after 10 km compared to 5 km of running ($p=0.005$).

Table 5 GRF under static condition and after 5km and 10km of running

Variables	Running distance			One-Way Repeated Measures ANOVA		
	Baseline	5 km	10 km	F-value	η_p^2	p-value
	Mean (SD)	Mean (SD)	Mean (SD)			
GRFs						
First peak vertical (BW)	1.95(0.28)	1.99(0.29)	2.03(0.26)	1.64	0.03	0.20
Second peak vertical (BW)	2.67(0.18)	2.66(0.21)	2.60(0.27)	2.84	0.06	0.06
First VALR (BW/s)	45.64(15.69)	48.11(14.04)	47.58(11.04)	0.70	0.014	0.50
Second VALR (BW/s)	27.14(4.59)	28.14(3.29)	27.85(4.53)	0.98	0.02	0.38
Peak braking (BW)	-0.17(0.05)	-0.18(0.07)	-0.18(0.08)	0.26	0.01	0.77
Peak propulsive (BW)	0.14(0.07)	0.14(0.08)	0.12(0.07)	4.07	0.08	0.02

3.1.3 Foot morphology

In terms of foot morphology, only arch height and ball width altered significantly throughout the running test (Table 6). As shown in Figure 29, after 10km of running, arch height was reduced significantly when compared to 5km and static ($p=0.001$, $p=0.002$) conditions, and ball width was also decreased in statistics versus static condition ($p=0.039$).

Table 6 Foot morphology under static condition and after 5km and 10km of running

Variables	Running distance			One-Way Repeated Measures ANOVA		
	Static	5km	10km	F-value	η_p^2	p-value
	Mean (SD)	Mean (SD)	Mean (SD)			
Morphology (mm)						
①Foot length	249.04(7.13)	250.64(8.12)	250.97(7.05)	0.88	0.09	0.39
②Arch length	176.46(5.33)	178.54(7.00)	177.84(7.75)	0.53	0.06	0.60
③Heel to fifth toe length	200.80(8.39)	200.82(10.53)	201.23(11.35)	0.03	0.01	0.97
④Mid-ball to heel length	209.87(6.28)	210.73(7.16)	210.90(7.18)	0.23	0.03	0.80
⑤Ball width	59.13(1.82)	59.52(1.78)	58.51(2.67)	1.48	0.14	0.26
⑥Maximal heel width	61.58(5.61)	61.76(5.56)	60.94(4.78)	0.39	0.04	0.68
⑦Maximal heel location	57.09(3.81)	57.65(3.10)	57.18(2.81)	0.44	0.05	0.55
⑧Dorsal height	241.43(8.84)	242.68(9.20)	243.27(8.31)	1.01	0.10	0.38
⑨Arch height	320.36(6.29)	321.10(7.82)	319.28(9.83)	0.73	0.08	0.43
⑩Ball girth	107.82(6.63)	106.77(6.68)	106.39(6.55)	8.30	0.48	0.02
⑪Instep girth	13.12(2.58)	12.88(2.47)	12.20(2.34)	26.11	0.74	<0.001
⑫Short heel girth	233.16(6.60)	232.26(6.08)	231.01(6.25)	1.89	0.17	0.20

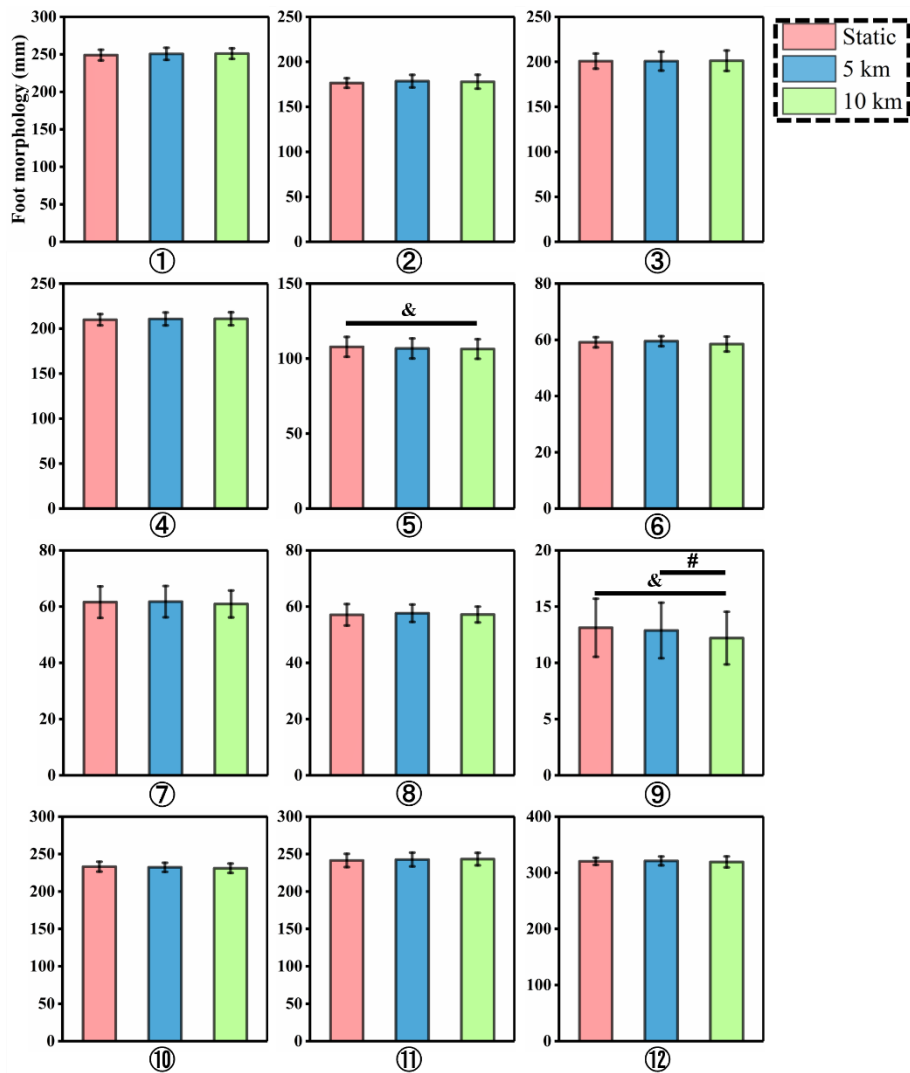


Figure 29 Column chart of the Bonferroni comparisons for foot morphology under static condition and after 5km and 10km of running

Note: ①, foot length; ②, arch length; ③, heel to fifth toe length; ④, mid-ball to heel length; ⑤, ball width; ⑥, maximal heel width; ⑦, maximal heel location; ⑧, dorsal height; ⑨, arch height; ⑩, ball girth; ⑪, instep girth; ⑫, short heel girth

3.1.4 Foot skin temperature

For all the forefoot anatomical regions, foot skin temperature exhibited statistical differences among the three conditions (Table 7). Compared with baseline, it was found that running (5km and 10km) led to significantly higher skin temperature ($p < 0.001$, Figure 30). Moreover, the temperature of DH, DM, and MM regions after 10km running were also significantly greater than the 5km ($p = 0.04$, $p = 0.043$, and $p = 0.014$, Figure 30).

Table 7 Foot temperature under static condition and after 5km and 10km of running

Variables	Running distance			One-Way Repeated Measures ANOVA		
	Static	5km	10km	F-value	η_p^2	p-value
	Mean (SD)	Mean (SD)	Mean (SD)			
Temperature (°C)						
H	22.66(1.00)	33.47(1.54)	32.53(1.52)	271.36	0.97	<0.001
OT	22.69(1.08)	34.62(1.99)	34.24(2.59)	343.49	0.97	<0.001
MM	26.46(1.14)	35.24(1.18)	37.26(1.34)	166.40	0.95	<0.001
CM	26.74(0.75)	36.17(1.24)	37.24(1.57)	195.96	0.96	<0.001
LM	25.34(1.29)	34.73(1.24)	34.81(2.75)	135.81	0.94	<0.001
DH	22.72(1.04)	33.84(1.85)	35.12(1.46)	415.15	0.98	<0.001
DOT	22.48(1.54)	34.34(2.54)	34.27(2.24)	371.92	0.98	<0.001
DM	25.27(1.48)	34.24(1.13)	35.92(1.59)	199.67	0.96	<0.001

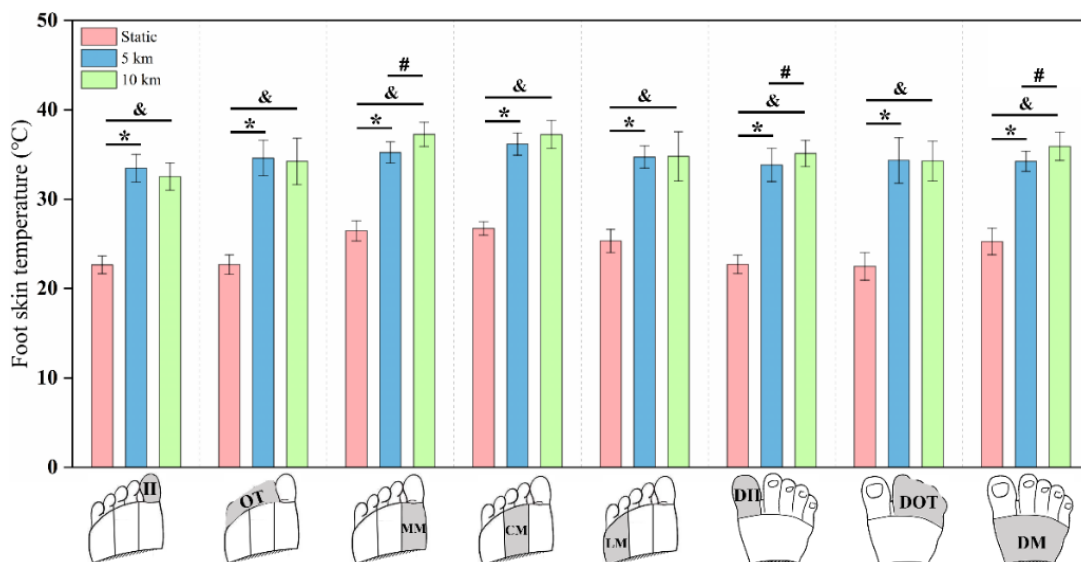


Figure 30 Column chart of the Bonferroni comparisons for foot temperature under static condition and after 5km and 10km of running

3.1.5 Subjective-perceived hallux comfort

ANOVA analysis showed that the VAS scores were statistically different among the three conditions (Table 8). Compared with the static condition, both 5km and 10km significantly increased the hallux VAS levels ($p=0.001$ and $p<0.001$). However, no significant difference was presented between 5km and 10km ($p>0.05$).

Table 8 Perceived VAS scores under static condition and after 5km and 10km of running

Variables	Running distance			One-Way Repeated Measures ANOVA		
	Static	5km	10km	F-value	η_p^2	p-value
	Mean (SD)	Mean (SD)	Mean (SD)			
VAS Hallux	0.00(0.00)	1.60(0.84)	2.10(0.99)	29.81	0.77	<0.001

3.1.6 Gap length between the hallux and toebox of the shoe

The calculated gap length between the hallux and toebox of the shoe showed significant differences both in one stance cycle and throughout the running test (Table 9). As shown in Figure 31A, during the stance phase, gap length at midstance instant reduced significantly when compared to initial contact and toe-off in all conditions ($p < 0.001$). It was also found that gap length at the toe-off instant showed a statistical decrease compared to initial contact at 10km ($p < 0.001$). On the other hand, after 10km of running (Figure 31B), gap length at initial contact instant showed a significant increase compared to 5km ($p = 0.018$), while gap length at midstance instant reduced with significance versus both static and 5km conditions ($p < 0.001$).

Table 9 Gap length analysis under static condition and after 5km and 10km of running

Variables	Running distance			One-Way Repeated Measures ANOVA		
	Static	5km	10km	F-value	η_p^2	p-value
	Mean (SD)	Mean (SD)	Mean (SD)			
Gap length (mm) (Running distance)						
Initial contact	38.58(5.90)	38.34(5.27)	39.56(6.45)	4.81	0.09	0.01
Midstance	31.32(7.46)	31.44(6.82)	29.28(6.81)	17.84	0.27	<0.001
Toe-off	38.23(5.67)	37.97(4.78)	38.17(5.81)	0.22	0.01	0.80
Gap length (mm) (Stance phase)	Initial contact	Midstance	Toe-off			
Static	38.58(5.90)	31.32(7.46)	38.23(5.67)	175.07	0.78	<0.001
5km	38.34(5.27)	31.44(6.82)	37.97(4.78)	253.52	0.84	<0.001
10km	39.56(6.45)	29.28(6.81)	38.17(5.81)	396.624	0.89	<0.001

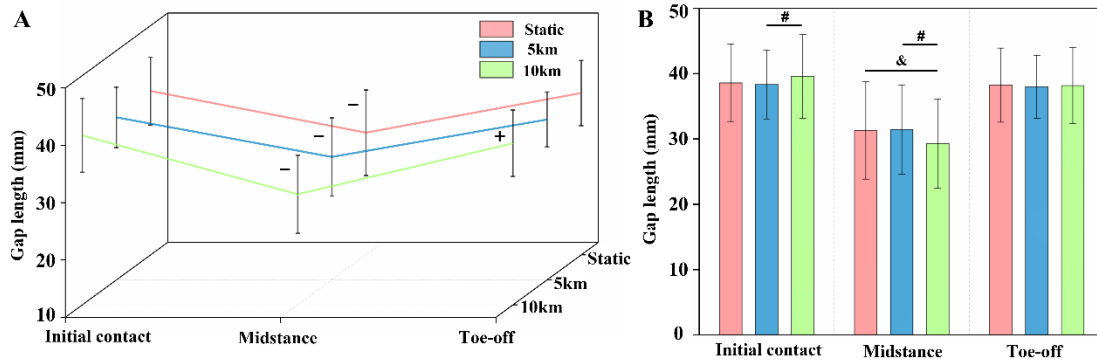


Figure 31 Column chart of the Bonferroni comparisons for gap length under static condition and after 5km and 10km of running, gap length comparisons in one stance phase (A), and gap length comparisons throughout the running test (B)

3.2 Results of finite element simulation

3.2.1 Finite element simulation of the foot-shoe model

3.2.1.1 Foot-shoe model validation

In terms of the plantar pressure validation, Figure 32 shows the subdivided plantar regions and the comparison between predicted plantar pressure distribution and corresponding measured insole pressure data during balanced standing. The highest plantar pressure was located at the HF region and followed by MFF, LFF, and MF region, which presented a good consistency with the experimental pressure data.

The predicted and measured plantar pressure data, the corresponding relative error, and the total average error are given in Table 10. The peak pressure relative errors were less than 10% both in MF and HF regions (8.51% for MF; 1.77% for HF) while it raised to 29.07% and 32.21% in MFF and LFF regions, respectively, and that further led to an average error of 17.89%.

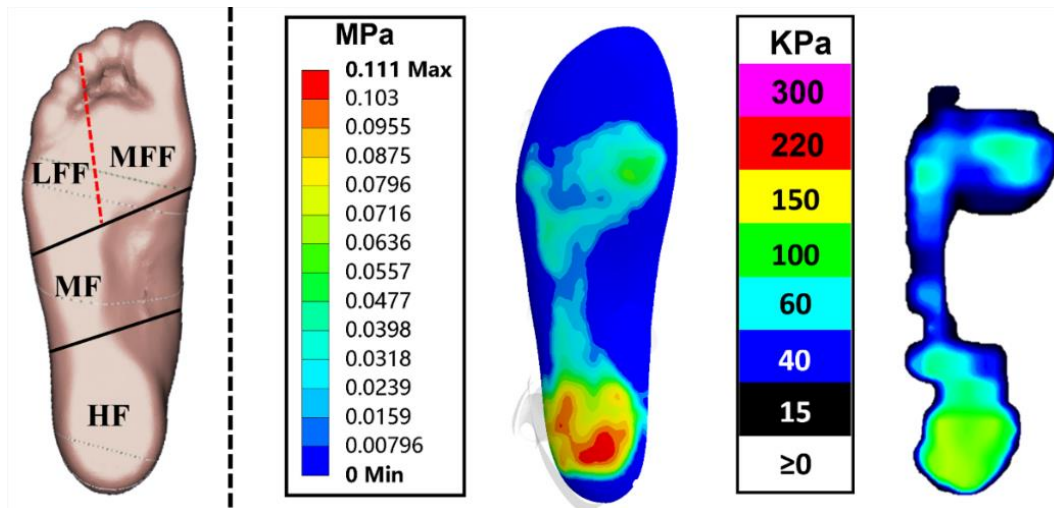


Figure 32 The subdivided plantar regions and comparison between predicted pressure distribution and experimental pressure data

Table 10 Comparison of predicted peak plantar pressures and experimental pressure insole data in 4 plantar regions during balanced standing

Plantar region	Peak plantar pressure (MPa)		
	Experiment	Simulation	Relative error (%)
MFF	0.086	0.061	-29.07
LFF	0.065	0.044	-32.21
MF	0.047	0.043	-8.51
HF	0.113	0.111	-1.77
Average error (%)			$\sum_{n=1}^4 P_i = 17.89$

In terms of the sole pressure validation, Figure 33 shows the subdivided shoe sole regions and the comparison between predicted sole pressure distribution and corresponding measured plate pressure data during balanced standing. The peak pressure was mainly concentrated on the medial regions of the shoe sole (i.e., MFS and MHS regions) and followed by LFS and LHS regions, which was consistent with the measured data. The predicted and measured sole pressure values, the relative and total average error, and the sensitivity analysis results for shoe sole material properties are listed in Table 11. The peak pressure relative errors were all below 10% in the 4 shoe sole regions with the baseline material property (2.20% for the MFS; -6.67% for the LFS; -8.47% for the MHS; -7.79% for the LHS).

Regarding the sensitivity analysis, distinct changes were exhibited in peak pressure when shoe sole material properties changed (Table 11). Specifically, the peak pressure greatly increased with the hardened shoe sole and decreased with the softened shoe sole. The shoe sole material with a 10% increased Young's modulus (E) presented a consistent relative error with baseline when compared to experimental data, while other cases resulted in percentage changes over 10% (13.74% for MFS with (baseline+20%) material property; -12.70% and -11.69% for MHS and LHS, respectively, with (baseline-10%) material property; -13.33%, -16.93%, and -14.94% for LFS, MHS, and LHS, respectively, with (baseline-20%) material property). All the average errors were less than 10%, with only one exception (13.49% with (baseline-20%) material property). In summary, shoe sole with Young's modulus of 2.739MPa (baseline+10%) presented the greatest consistency with the experimental pressure data.

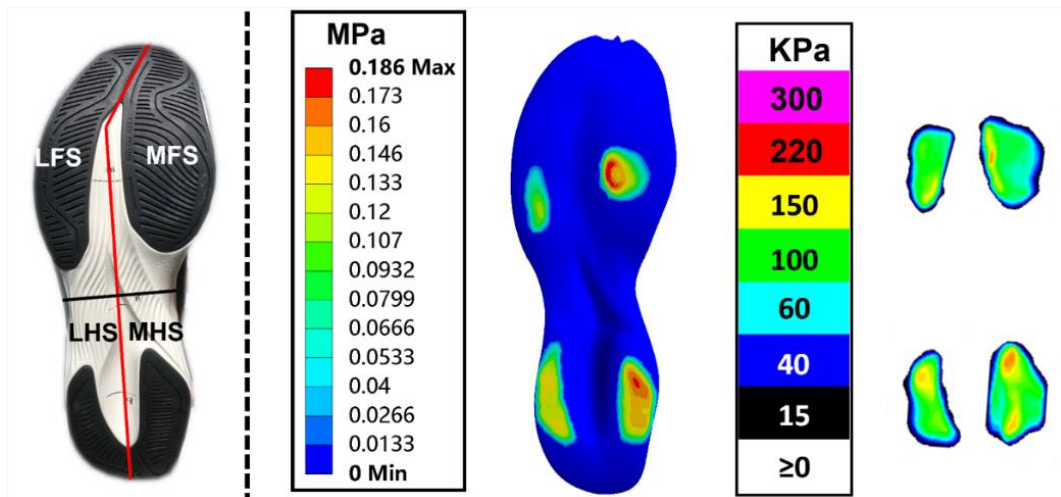


Figure 33 The subdivided sole regions and comparison between predicted pressure distribution and experimental pressure data

Table 11 Comparison of predicted peak sole pressures and experimental pressure plate data in 4 sole regions during balanced standing

Sole region	Peak sole pressure (MPa)										
	Experiment	Simulation (baseline)		Simulation (baseline+10%)		Simulation (baseline+20%)		Simulation (baseline-10%)		Simulation (baseline-20%)	
	Value	Value	Relative error %	Value	Relative error %	Value	Relative error %	Value	Relative error %	Value	Relative error %
MFS	0.182	0.186	2.20	0.198	8.79	0.207	13.74	0.176	-3.30	0.166	-8.79
LFS	0.120	0.112	-6.67	0.117	-2.50	0.120	0.00	0.108	-10.00	0.104	-13.33
MHS	0.189	0.173	-8.47	0.182	-3.70	0.190	0.53	0.165	-12.70	0.157	-16.93
LHS	0.154	0.142	-7.79	0.150	-2.60	0.155	0.65	0.136	-11.69	0.131	-14.94
Average error (%)		$\sum_{n=1}^4 Pi =6.28$		$\sum_{n=1}^4 Pi =4.39$		$\sum_{n=1}^4 Pi =3.73$		$\sum_{n=1}^4 Pi =9.42$		$\sum_{n=1}^4 Pi =13.49$	

As it is shown in Figure 34, the Bland-Altman plot presented the mean difference and 95% LOA between the experimental and simulated pressure data. The mean difference (+0.008) is very close to 0, as indicated by the solid line. Moreover, most of the points (23/24, 96%) are scattered between $\pm 1.96SD$ (red dashed line), which indicates that the two approaches are in relatively great agreement.

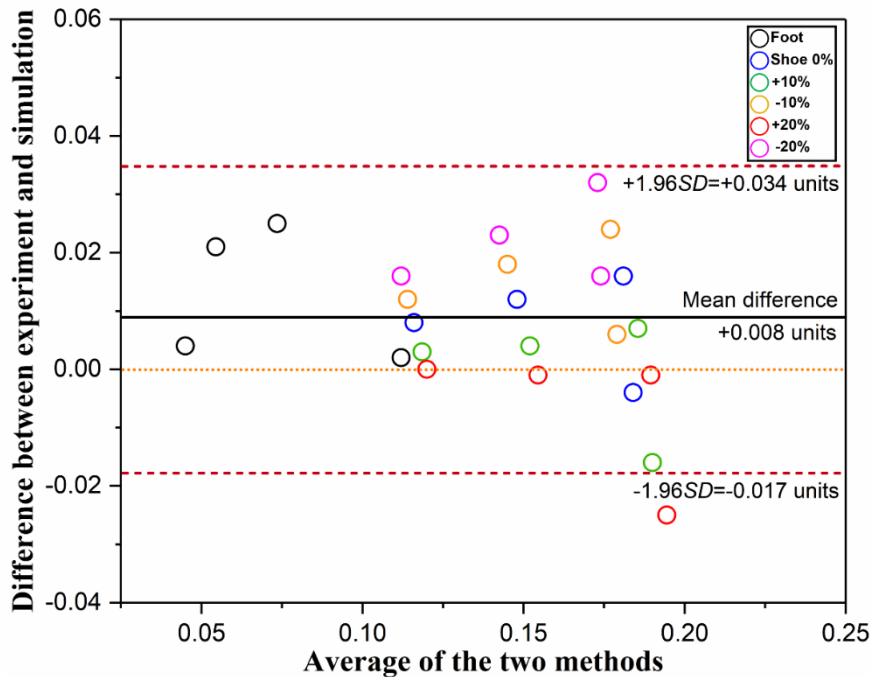


Figure 34 Bland-Altman plot of experimental and simulated pressure data

3.2.1.2 Running simulation of the foot-shoe model

Figure 35 showed the simulation outcome of running dynamics in this study. The gap length difference between midstance and toe off phase was predicted to demonstrate the validity and accuracy of the role of the proposed model in fast evaluation and optimization of footwear. The predicted and measured gap length difference data, the corresponding relative error, and the total average error are given in Table 12. The relative errors of the gap length difference were less than 10% both at baseline and 5km of running (8.83% for baseline; 3.52% for 5km of running) while it raised to 29.13% at 10km of running, which further led to an average error of 13.83%. In general, the results from the running simulation presented a relatively good consistency with the experimental data.

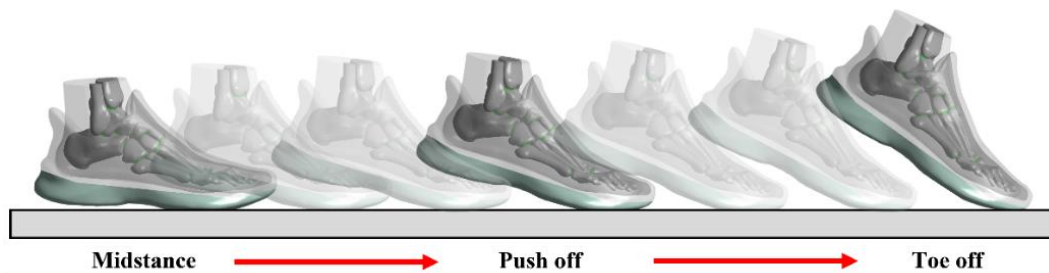


Figure 35 Dynamic simulation of running from the midstance to toe-off phase

Table 12 Comparison of predicted gap length difference and experimental data between midstance and toe off phase during running

Running distance	Gap length difference between midstance and toe off phase (mm)		
	Experiment	Simulation	Relative error (%)
Baseline	6.91	6.30	-8.83
5km	6.53	6.30	-3.52
10km	8.89	6.30	-29.13
Average error (%)	$\sum_{n=1}^4 P_i = 13.83$		

3.2.2 Finite element simulation of the feline paw model

3.2.2.1 Feline paw model validation

For the validation of the feline paw model, the numerically predicted and the experimentally obtained paw pressure distributions were compared. Figure 36 shows the comparison between predicted paw pressure distribution and corresponding

measured pressure data during balanced standing. The paw pressure concentrated mainly on the metapodial pad, which presented a good consistency with the experimental pressure data. The paw model predicted a peak pressure of 0.214 MPa while the experimental result, measured by the pressure platform, was 0.2 MPa, contributing to a relative error of 6.5% (less than 10%).

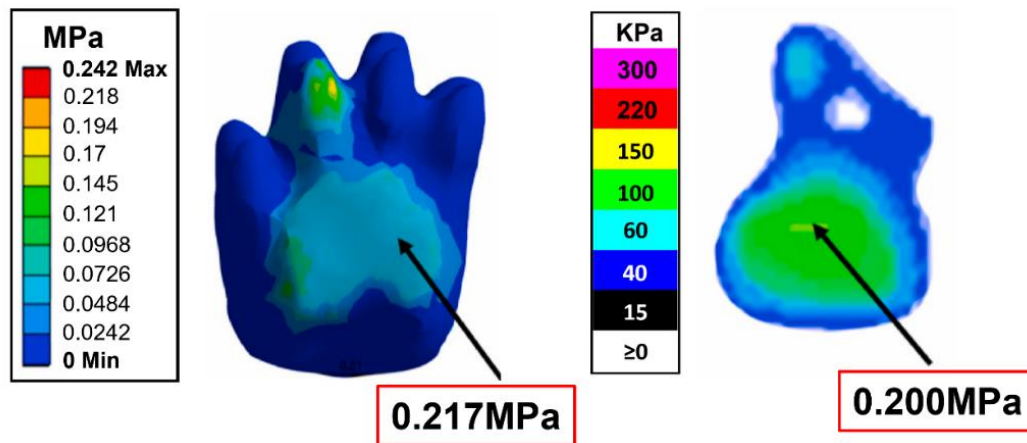


Figure 36 The comparison between predicted pressure distribution and experimental pressure data of the feline paw model

3.2.2.2 Landing simulation of the feline paw model

In this part, we found that the maximum von Mises stress was mainly concentrated on the metacarpal (MP) segments and it increased with the landing heights. As shown in Table 13, the highest von Mises stress was predicted at MP3 in all simulated conditions (0.771MPa for balanced standing, 5.895MPa, 7.036Mpa, and 9.262MPa for three landing height, respectively). The stress distribution of the other MP parts varied with conditions, but it is generally high in the medial and middle parts (MP2 and MP4) and low on the sides (MP5). The lowest stress was in the MP1 due to a relatively higher position compared to the other parts in the MP segments. In addition, it must be noted that stress was also found relatively higher in the proximal phalanx (PP) segments when compared to the corresponding ones at the middle or distal portion. The similar stress distribution with the MP segments was also found, with the highest von Mises stress was predicted at PP3 (0.195MPa for balanced standing, 3.016MPa, 3.532MPa, and

4.532MPa for three landing height, respectively), followed by the second, fourth, and fifth proximal phalanges in all simulated conditions.

Table 13 The von Mises stresses in MP and PP segment under different landing height

Landing height (m)	Von-Mises stress (MPa)							
	MP2	PP2	MP3	PP3	MP4	PP4	MP5	PP5
0.0m (Balanced standing)	0.547	0.165	0.771	0.195	0.518	0.130	0.227	0.118
0.6m	4.755	2.399	5.895	3.016	5.306	1.320	4.676	1.063
0.8m	5.761	2.873	7.036	3.532	6.324	1.549	5.635	1.271
1.0m	7.802	3.904	9.262	4.532	8.666	2.135	7.872	1.822

Regarding the Von-Mises stress growth rate of the MP and PP segments (Figure 37), it was found that the stress growth rate increased faster from 0.8m to 1.0m than from 0.6m to 0.8m of landing heights. In addition, the stress growth rates of the MP segments were higher than the rates of the corresponding PP segments, ranging from 2 to 4 times larger. Moreover, the growth rates of the MP3 were found to increase faster from 0.6m to 0.8m while the growth rates of the MP4 increased faster from 0.8m to 1.0m of landing heights when compared to other parts.

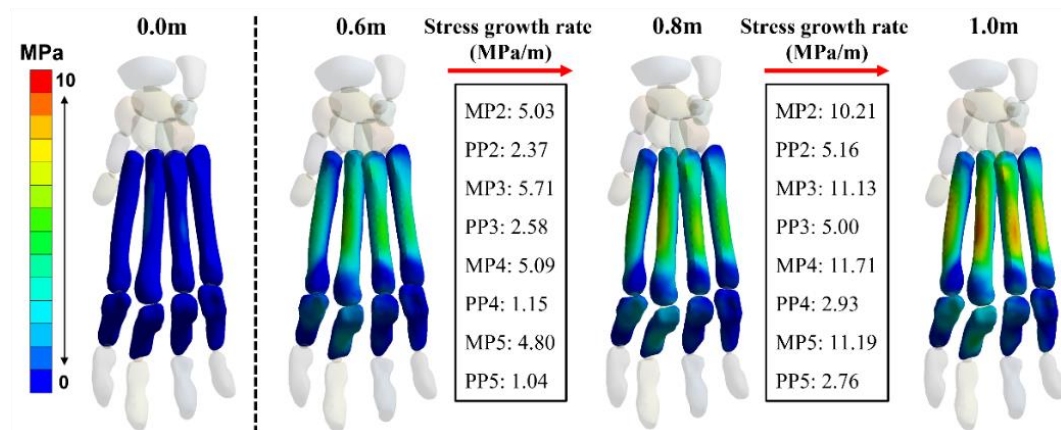


Figure 37 Illustration of the maximum values of MP and PP stress growth rate and stress distribution of cat during landing from different height

4 DISCUSSION

4.1 BT and MSF injury mechanism and prevention

This dissertation integrated several experimental measurements to describe the multidimensional alterations in the foot before and immediately after 5 km and 10 km of running. In this session, the intrinsic mechanism of forefoot injury development (BT and MSF) would be further discussed.

By collecting the inter-segment foot kinematics before and after long-distance running, it is possible to gain further insight into the forefoot dynamic changes during this process. In this work, the FFHFA and HXFFA during the stance phase were derived. For FFHFA, it was found that the plantarflexion angle at toe-off significantly decreased both after 5 km and 10 km of running. Although the differences seem relatively small at first glance (2.45° between baseline and 5 km, 2.01° between baseline and 5 km), several previous studies have revealed that the intricate foot inter-segment movement could have a significant effect on the plantar fascia function [151–153]. For instance, a tiny distance change between the forefoot and rearfoot ($<1\text{mm}$) would contribute to a 34.8% change of plantar fascia strain [152]. Also, a change of 1° in arch angle can lead to a plantar fascia tension change of 0.4 to 0.7 times of BW during the early stance phase [153]. Thus, it was speculated that the decreased forefoot plantarflexion motion during the stance phase may result in the increased stress and strain of plantar aponeurosis and consequently higher injury risks. On the other hand, stress fracture of the metatarsals has been reported in patients with plantar fasciitis. Therefore, it is reasonable to speculate that the reduced forefoot plantarflexion could be one of the potential influencing factors for long-distance running MSF injuries [110].

In a review of long-distance running biomechanics, Kim et al. reported that runners might tended to change their landing techniques from a heel-toe to midfoot landing strategy after long-distance running because of compensating for local muscle fatigue [110]. Consistent with their findings, smaller forefoot dorsiflexion angles were also found in this work during the early stance phase at 10 km compared to baseline and 5 km, indicating a shifting to the relative midfoot strike pattern and may further increase

the load of the metatarsal region during running. In addition, concerning forefoot motion in the frontal plane, decreased supination angles were observed throughout the stance phase after 10 km running compared to 5 km. Moreover, since forefoot adduction is a part of foot supination during the propulsion phase [154], the significantly reduced peak forefoot adduction angle and ROM, as well as relatively smaller forefoot adduction during early (15-21%) and mid-stance (37-51%) phase at 10 km were also found in this study. Together with these above results, it was summarized that long-distance running would result in a midfoot strike pattern and more pronated foot posture, and these foot kinematics changes could further lead to a redistributed forefoot plantar load with increased pressure under medial metatarsal while decreasing under lateral metatarsals based on the findings of previous studies [14,155]. It is worth noting that the pronated foot posture after long-distance running could further lead to a reduced arch height, letting the foot move with a relatively “flat arch” pattern, consequently absorbs more impact during running and potentially increases the incidence of stress fracture in the metatarsal bones [156]. On the other hand, it is speculated that the “flat arch” pattern could also exacerbate the foot-shoe interaction and potentially increase the injury risk of BT during long-distance running [109].

Compared to previous findings, a relatively different result of hallux motion was observed in this study. Generally, rearfoot-strike runners would present great hallux dorsiflexion during the early and last stance phase of running because of the rollover mechanism [157]. However, our findings showed that, although there was no significant difference among conditions, the hallux exhibited considerably smaller dorsiflexion angle both at initial contact and toe-off when compared to previous related studies. A possible explanation for this difference may be the low and narrow forefoot part of footwear due to modern aesthetic needs. On the contrary, it is worth noting that two studies measuring the foot inter-segment kinematics while walking or running barefoot presented normal hallux dorsiflexion during the stance phase [29,158]. According to previous research, it was demonstrated that the insufficient forefoot space (width and height) may limit the ambulatory function of toes, affect its kinematic

performance during locomotion, and potentially lead to foot injuries (such as BT) because of additional repetitive friction between foot and shoes [108,159]. Meanwhile, the strike pattern could also contribute to this difference. Although all participants in this study preferred rearfoot strike at the beginning of the long-distance running test, it was demonstrated above that runners may shift to a relative midfoot landing strategy as indicated by the smaller forefoot dorsiflexion angles from early to mid-stance phases. In addition, the decreased plantarflexion angles of hallux with respect to the forefoot found during the early stance phase at 10 km when compared to baseline and 5 km further verify the above statement.

A comparison with previous data also revealed some different results in GRFs in this dissertation. Kim et al. conducted a systematic review to investigate the effect of long-distance running on lower-limb biomechanical parameters in healthy runners [110]. They summarized that lower vertical GRFs and loading rate would be presented after long-distance running due to the increased mechanical stress with decreased musculoskeletal capacities. However, no significant differences among conditions were found in this study except a lower peak propulsive force at 10 km compared to 5 km. The participants' heterogeneity between studies would be the primary explanation for these differences since the fatigue-related changes were speculated to initiate at 10 km of running according to our findings in kinematics. Investigating longer-distance running (such as 20 km) based on participants involved in this study should be performed for further verification. In terms of the reduced peak propulsive force at 10 km, together with the kinematic changes happened to the hallux, it was speculated that the toes' dynamic control function, such as gripping, gradually reduce after 10km of running, which was also in agreement with previous studies [109,110]. It should be mentioned that the toe dynamic function during the push off phase has a great implication to injury management, while the loss of toe's active control ability would further transfer load to the metatarsal regions (especially the medial metatarsal), potentially increase the MSF injury risk.

The popularity of long distance running has been reported to be accompanied by a high injury risk. In order to investigate the incidence and associated potential risk factors of RRIs, previous studies further divided the determinants into several categories, which include systemic factors (e.g., age, weight, and height), lifestyle factors (e.g., smoking and drinking alcohol), health factors (e.g., injury history), and running related factors (e.g., training frequency, distance, and shoe use), etc [78,88,101]. However, little research has considered the effects of foot shape/temperature variations on RRIs during long distance running. Therefore, in order to further validate these above speculations in terms of foot kinematics and kinetics changes, this work also investigated foot temperature and morphology alterations, perceived hallux comfort differences, and gap length changes between the hallux and toebox of the shoe after a continuous 5 and 10km of running when compared to baseline condition.

Regarding the foot morphology, the ball width of the foot was found significantly reduced after 10 km of running, which is in accordance with the previous findings [109]. In their study, Mei et al. also observed ball girth and foot volume reduction after 20 km of running and they speculated that these foot shape changes could further contribute to more space, especially for the forefoot region, and encourage greater friction between foot and shoe interface since they became less conforming to each other [109]. Despite only 10 km of running test being conducted, the reduced ball width and perceived hallux comfort while increased foot-shoe interaction observed in this study directly confirm the above-mentioned speculation, which may potentially increase the risk of BT injuries. In addition, this work also observed a decreased arch height after 10 km, partly consistent with previous studies since they only detected the significance at 20km [109,160]. This variation may be explained by the subject heterogeneity and/or different running interfaces among studies. Meanwhile, the lower arch height found in this part further confirmed the speculations of the kinematics tests that the pronated foot posture after long-distance running would reduce the arch height, increase the foot ambulation in the sagittal plane and let the toenails take more brunt of the impact with the toebox of the shoe, and consequently increases the incidence of BT and MSF injuries.

Increased contact pressure and skin friction have been shown to lead to higher skin temperature [161–163]. In this study, significantly higher skin temperatures in all forefoot regions after running were observed when compared to the baseline condition, which in turn indicates the greater contact pressure and skin friction suffered by the foot during the running test. Meanwhile, the increased skin temperature was also accompanied by sweat, creating an environment that would exacerbate the foot-shoe interaction and consequently increase the injury risk of toenails [109]. Based on the speculation of previous research, it is also worth noting that the reduced ball width observed in this study could be explained by the loss of sweat in the foot during long-distance running [109]. In addition, this study exhibited a continued increase in temperature in the medial metatarsal region after 10km of running, which further confirmed the above speculations of the redistributed forefoot plantar load caused by changed foot posture during running and was in agreement with previous research reporting running-related plantar pressure alterations [110,163–165]. To be more specific, it was found that the peak pressure at the medial metatarsal increased while the peak pressure at hallux reduced after long distance running, indicating that the stress loading would eventually be transferred to the metatarsal region, which potentially increases the injury risk of the MSF. Similarly, based on the above information, it is reasonable to deduce that the increased temperature at the UH region could be a precursor to the onset of the BT injury.

This work also measured the gap length between the hallux and toebox within one stance phase. Specifically, after the initial contact with the ground, the shoe has come to a brief-moment stop while the foot has not, as shown in the findings of the significantly reduced gap length at midstance instant compared to initial contact throughout the running test. It is supposed that this is the moment when the toenails would take impact stress with the toebox of the shoe. To make matters worse, it was found in our study that the 10km of running contributes to more gap length reduction at midstance instant, which consequently increases the potential injury risk. Afterward, the foot slid backward by a small amount in order to prepare for the push-off. However,

additional stress may be applied to the toenails since the toes need to grip the ground for propulsion during this phase. However, it has been proposed that the toes' dynamic functions would gradually lose during long distance running, as indicated by the shift of the loading and plantar temperature from the hallux to the medial metatarsal regions [163–165]. Thus, it is hard to determine which step is more important or if it is a combination. Future studies concerning the hallux biomechanics during long-distance running using more localized devices could add help. Nevertheless, to the author knowledge, this study for the first time revealed the pattern of foot-shoe interaction and also the time point that BT may occur to happen during running from a quantitative research perspective.

In summary, the key implication of this session was that for the first time the potential mechanism of BT injury development during long-distance running have been quantitatively investigated. Based on the results of this dissertation, it was found that the reduced ball width and arch height while increased skin temperature of the foot (increase in sweat) after long distance running were accompanied by the hallux discomfort and excessive foot-shoe interaction, which indicates an increased risk of BT injury during this process. In addition, the insufficient toebox space (width and height) of the shoe limits the ambulatory function of toes, potentially causing additional repetitive friction between foot and shoes and further increasing the BT injury risk. Meanwhile, the previously proposed injury mechanism of MSF during long-distance running have also been further confirmed. Long-distance running resulted in a midfoot strike pattern, more pronated foot posture, reduced arch height and the loss of toe dynamic function, which further redistribute the forefoot plantar load with increased pressure under medial metatarsal while decreasing under lateral metatarsals, causing an increased incidence of stress fracture in the metatarsal bones (especially for the medial metatarsal region). Together with all these findings, we could provide important practical advice for running and running shoe design. It is suggested that runners should consider making appropriate adjustments to the feet at least at 10km of running, which may be the starting point for foot injuries to occur, such as changing their athletic socks

and adjusting the laces to secure their feet, thereby potentially help to reduce the injury risk. In terms of running shoes design, improving the toebox space and the midsole cushioning effect on metatarsals shall add benefit.

4.2 FE modelling and footwear design optimization

Digital techniques are a strategic tool to design new products, reducing time and waste [166]. Based on the above findings regarding the underlying mechanism of forefoot injury development (BT and MSF) during long distance running, this part further integrated experimental measurements and computational simulation to propose two FE models with the aims to provide fast approach for running shoe design optimization and forefoot injury prevention.

4.2.1 Finite element analysis of the foot-shoe model

Both foot and shoe shapes would undergo deformation during locomotion, thus incorporating footwear with the foot in the model is a prerequisite to further reveal the realistic biomechanical foot responses under different movement scenarios [113]. Accordingly, in this part, a 3D, subject-specific coupled FE model of the foot and ankle together with the sports shoe was introduced.

Several previous publications have also developed the coupled foot-shoe FE model intending to observe the internal changes within bony structures under different foot motions. For example, a foot-boot model was constructed by Qiu et al. and validated through published data during balanced standing, and it would be further used for the simulation of the military parachute landing [167]. Cho et al. developed a 3D coupled foot-sports shoe model to analyze the mutual interaction between foot and footwear during landing and further assess its reliability through comparison between predicted results and experimental data [131]. Similarly, a recent paper by Li et al. constructed a coupled FE model of the foot and barefoot running footwear to investigate the plantar pressure differences between the barefoot model and the coupled model during the weight-bearing moment of running [148]. Nevertheless, all these previous shoe models were built based on the contour profile of the ankle and foot model rather than the real

structure. On the other hand, some foot models were over-simplified to one bone assembly. Although some details were also simplified in our model (e.g., shoelace and insole), the most prominent characteristic of this computational model is that it realizes the simulation of the complex biomechanical interactions between the foot and sports shoe based on their actual characteristics, which can be applied to accurately determine the gap length between the hallux and toebox without destroying the upper structure of the shoe and contribute to optimize the footwear structure to reduce BT injury risk. Improvement of other sports shoe geometry designs could also be made to the coupled model based on the specific purposes of future simulations.

The validation of a FE model is a crucial issue after it was developed since it is highly associated with model accuracy and practicality. The rearfoot pressure-based approach was commonly used in most previous works [148,167]. In the current study, both the plantar and shoe sole areas were further divided into several regions for validation. The results showed that the predicted plantar and shoe sole pressure distributions in general exhibited good consistency with the experimental balanced standing pressure data (Figure 3, 4). Moreover, all the relative errors for peak pressures were lower than 10% with two exceptions. Specifically, both the simulated peak pressures in MFF and LFF regions were lower than the volunteer measurements, which consequently increases the relative error level. This discrepancy is perhaps due to the following several reasons. First, only muscle force applied on the AT was considered in this FE model since it plays an important role during balanced standing, while other extrinsic and intrinsic foot muscle forces were neglected. Yu et al. also speculated that the lower predicted pressures found at the first and fifth metatarsal heads would be associated with the above force setting [168]. Second, a larger deformation of the forefoot was detected during the simulation, which may further offset part of the pressure effect from the GRF applied on the ground plate. On the contrary, the foot, footwear, and ground were all in a relatively static state during the balanced standing test. Nevertheless, the results of rearfoot pressure comparison and Bland-Altman analysis between two methods demonstrated the validity of the current foot-shoe model. Meanwhile, it is worth noting

that, with the accessibility of dual-plane fluoroscopy and high-resolution MRI, FE models could be further validated against in vivo joint motion and soft tissue deformation data recorded by the two techniques, respectively [150,169].

Sensitivity analysis was also performed in this study to determine the effects of shoe sole material property on pressure. The peak pressure greatly increased with hardened shoe sole and vice versa with softened one, and it was found that shoe sole with Young's modulus of 2.739MPa, which is between Young's modulus of EVA(1.000MPa) and TPU(3.000MPa), was the most suitable setting in this simulation [131]. In some of the previous studies, nonlinear hyperplastic material defined by the five-term Moonley-Rivlin model was used for the outsole model to simulate the rubber-like material behavior [131,148]. Although it is much closer to the actual outsole material property, some challenges of utilizing hyperplastic material for shoe soles still need to be overcome. First, the coefficients of Moonley-Rivlin model for the outsole are currently relatively fixed, which makes it difficult to model all various kinds of the outsole. Moreover, it is challenging to define the outsole using hyperplastic material if the whole shoe sole was fused into one assembly. Last, both the soft tissue and shoe sole were defined by linear elastic material to reduce the computational demands especially incurred by the intensive sensitivity tests. The model run time would become excessive when shifting the material to a nonlinear one and consequently reduce the efficiency. Nevertheless, recent technological advances in medical imaging demonstrated the possibility to obtain personalized nonlinear material property data, which indicates promising directions for future research [170,171].

To ensure the validity of the proposed foot-shoe model under dynamic movement condition, especially for BT injury prevention, the gap length difference between midstance and toe off phase during running was further predicted. The results demonstrated a good agreement between the experimentally measured and numerically predicted gap length difference, except for 10km of running, in which the relative errors reached 29.13% high. This difference can be credited to the changed frictional contact coefficient between foot and shoe before and after 10km of running, while the value for

FE simulation was not changed accordingly. On the other hand, as it is stated in part 4.1, the shoe briefly comes to a stop after its initial contact with the ground during running. However, the FE simulation did not consider this as a boundary condition, which could also contribute to the larger relative error observed, particularly after prolonged periods of running. Nevertheless, the proposed foot-shoe model offers an alternative tool for fast evaluation and optimization of footwear with a simultaneous reduction of the production batches and costs.

4.2.2 Finite element analysis of the feline paw model

As a typical digitigrade mammal, the uniquely designed morphological structure of feline's distal limbs can support two to three times of its BW during daily movements. On the contrary, as the main support segment during human running, the MTP joint is often exposed to instability, pain, and injury [134,135]. Accordingly, in this part, a 3D, feline fore-left paw FE model was constructed.

To the best of my knowledge, this is the first complete FE model of a paw bone structure in felines. The most prominent characteristic of this computational model is the predicted internal stress distribution in the distal limb. The findings will enhance our understanding of the force transmission mechanism occurs in relation to the distal joint in a feline limb and offer information for footwear optimization and MSF prevention.

In this study, the numerically predicted paw pressure distribution was compared to experimental measurements, as outlined previously in the human foot or in animal related research [25,172]. It can be concluded that the numerical results of paw pressure were consistent with the experimental test, which demonstrates the validity of the current feline paw model. Based on the results of the balanced standing and landing simulations, it was found that only minimal stress was presented in the phalanges portion (including proximal, middle, distal) although the phalanges segment is the main supporter of the body. According to the anatomical structure of the cat's paw, the distal joint is wrapped in the thick substrate tissue comprising the paw pad. The paw pad

consists of the digital pad and MP pad, which are placed beneath the distal interphalangeal and MCP joint respectively [28]. This structure plays a critical role in decreasing and transmitting impact effectively to protect the distal limb joints from musculoskeletal damage, which may be caused by impact forces during movements [172,173]. In addition, the pad could help to optimize force distribution in the internal bony structures. It is noteworthy to mention that the excellent cushioning performance of animal claw pads has attracted the attention of many researchers. It has been shown that the MP pad presents a peculiar columnar structure with a larger surface area compared to the digital pad, therefore it has a dominant role in distributing or absorbing mechanical forces [173]. Previous histological analysis of cats has indicated that the MP pads consist of adipose tissue compartments, surrounded by dense collagen and elastic fibers that impart a cushioning effect [174]. Recently, it was highlighted, based on elaborated FE analysis, that viscoelastic properties and multiple layers in the paw pad help to disperse impact forces [27]. Despite the inherent complex structural characteristics of the pad were not considered, this study defined the material properties of the paw pad using hyperelastic material model according to a recent research paper [27], which could to some extent reflect the cushioning effect of the pad. Nevertheless, future research should refine the model structure and further validate these predicated results. Above all, given the feature of digitigrade mammals, it is not surprising that the paw pad as a basic supportive element under the distal joint plays a significant function in attenuating impacts and even helps to minimize stress in the internal bone structure.

Figure 37 shows that the greatest internal stresses were distributed at the MP segment and the corresponding stress growth rate increased with landing height. The MP is the longest bony structure in the distal limb that is elevated off the ground, connecting two important distal joints, the MCP and wrist joint. Published research has noted that the motion of the wrist joint is limited during walking [175]. However, the carpal bones as part of the wrist joint showed more degrees of freedom than a hinge joint [176]. To counteract the multi-dimensional motion of the carpal joints during movement, the MCP joint movements may also be limited to maintain the stability of the upright

posture in the lower limbs. Therefore, a stiff junction may be created in the MCP and wrist joint by the MP segment to maintain stability. The MCP joint kinematic variation is rare and difficult to detect because of its small size and complex construction, but its strong supportive function deserves further experimental investigation. Previously published research has indicated that typical cursorial animals have less mobile forelimb joints or move in a single plane [177]. Additionally, the limited mobility in the distal joint such as the wrist and MCP joint may prevent the possibility of transitioning from digitigrade to palmigrade and allow cats to walk or run in digitigrade postures without joint collapse risk. When forelimbs experience a higher impact force such as landing from high jumps or falling, the cats' forelimbs would be forced into a palmigrade option [178]. Under these conditions, the wrist joint serves as more of a support mechanism and increases the contact area with the ground to attenuate GRF [179]. Creating stabilization in the distal joints must facilitate cooperation with muscles, ligaments, and tendons crossing the distal joints. The complex activation patterns of muscles on distal joints have been extensively studied. EMG signals showed that the long palmar flexors were active throughout the standing phase via the MCP joint into the base of the distal phalanx, as well as the extensor carpi ulnaris [180]. Also, the flexor digitorum superficialis tendons respectively extend in digits 2, 3, and 4, which connect with the forelimb muscles providing support for distal joints [174]. However, the muscles and tendons in this FE model of distal joint limbs were not investigated, this is also a limitation in the research findings presented here.

Above all, this session examined the internal stress distribution of the distal joint limb in detail. Higher stress levels were noted in the MP segment, with smaller stresses observed in the phalanges portion including the proximal, middle, and distal segments in all conditions. The raised MP segment plays an important role in creating a stiff junction between the MCP and wrist joint, stabilizing the distal limb. The paw pads help to optimize stress distribution in phalanx region. Together all these findings, it could provide fundamental information for footwear optimization and MSF prevention.

4.3 Limitations

There are some limitations of this dissertation that should be considered both for the experimental and simulation parts. The first limitation relates to the relatively small sample size and only male runners were involved in the biomechanical experiment. Further large sample size studies with both genders on this topic would reveal more profound knowledge. The second limitation is that all runners completed the 10km of running on a treadmill rather than on the trail or asphalt road. The advantage is that the running distance can be precisely controlled and the timeliness of the test (immediately after 5 and 10km run) can be guaranteed [109]. However, the findings of this work cannot be generalized to other running situations. Long distance running under other situations such as trail running and road running should be further verified. Thirdly, the muscular fatigue after 10 km of running was only speculated based on previous research results, further investigation about muscle activity before and after running is warranted for verification. Lastly, in terms of FE simulation, it should be noted that there are some simplifications for both the foot-shoe model and the feline paw model, including reliable data information for geometry reconstruction, the balance between accurate details and computational cost, accurate representations of material properties, realistic boundary and loading conditions, and thorough model validation. Nevertheless, the FE simulation part set a basic reference for fast evaluation and optimization of footwear aimed to reduce RRI risk with a simultaneous reduction of the production batches and costs.

5 CONCLUSIONS AND FUTURE WORKS

5.1 Conclusions

In this dissertation, a comprehensive method combining experimental tests and FE simulations were applied to reveal the potential mechanism of forefoot injury development (BT and MSF) during long-distance running and further aimed to provide an alternative approach for running shoe optimization and forefoot injury prevention.

In terms of the experimental tests, this work revealed multidimensional alterations of the foot before and immediately after 5 km and 10 km of running. Based on the results of these experiments, it was found that the reduced ball width and arch height while increased skin temperature of the foot (increase in sweat) after long distance running were accompanied by the hallux discomfort and excessive foot-shoe interaction, which indicates an increased risk of BT injury development. The insufficient toebox space (width and height) of the shoe limits the ambulatory function of toes, potentially causing additional repetitive friction between foot and shoes and further increasing the BT injury risk. This is the first time that the effects of foot multidimensional alterations during long distance running on the potential cause of BT injury has been quantitatively investigated. Meanwhile, the previously proposed injury mechanism of MSF during long-distance running have also been further confirmed. It was found that long-distance running led to a midfoot strike pattern, more pronated foot posture, reduced arch height and loss of toe dynamic function, consequently redistributing the forefoot plantar load with increased pressure under medial metatarsal, causing an increased incidence of medial MSF. The results variability with previous studies indicated that 10km of running may only be the starting point for BT and MSF injuries to develop. These findings shall provide an important basis knowledge for BT and MSF injury prevention and running shoe optimization.

In terms of foot-shoe FE simulation, a fully coupled 3D foot-sports shoe FE model has been reconstructed based on the CT technology, which realizes the simulation of the complex biomechanical interactions between the foot and sports shoe based on their actual characteristics. To ensure the validity of the proposed foot-shoe model, both the plantar and shoe sole areas were further divided into four regions for comparison and the Bland-Altman method was applied for consistency analysis between methods. In addition, the running scenario was simulated to calculate the gap length between the hallux and toebox during running, aiming to observe the foot-shoe interaction without destroying the upper structure of the shoe. The results demonstrated a good agreement between the experimentally measured and numerically predicted difference. In general,

the proposed foot-shoe model in this dissertation offers an alternative tool for fast evaluation and optimization of footwear with a simultaneous reduction of the production batches and costs.

In terms of feline paw FE simulations, a 3D feline fore-left paw FE model has been created to investigate the internal stress distribution of the distal joint limb both under static standing and landing with different height (0.6m, 0.8m, 1.0m). The results showed that the larger stress was concentrated on the metacarpus segment while the smaller stresses were found at the phalanges portion including the proximal, middle, and distal segments. The corresponding stress growth rate increased with landing height and is faster in the metacarpus segment than in the phalanges. The results indicated that the raised MP segment is the primary stress site, and it plays an important role in creating a stiff junction between the MCP and wrist joint, stabilizing the distal limb. In addition, the paw pads help to optimize stress distribution in phalanx region. In summary, this is first time to exhibit a high accurate feline paw structure, and the findings help us understand how a cat's paw absorbs and transmits large impact forces to avoid musculoskeletal injuries of the distal limbs during movement, which could be applied for footwear optimization and MSF prevention.

5.2 Recommendations for future works

The current dissertation presented a multidimensional experiment protocol, both from subjective and objective perspectives, to start research on forefoot running related injuries. Based on the results of this work, the underlying injury mechanism of BT and MSF at 5 and 10km of running has been reported. However, results from this work also revealed that 10km of running may only be the starting point for these injuries to develop. Moreover, the forefoot injury development, especially for the BT, may also be associated with the types of running interface. Therefore, future work on this topic should aim to further investigate the potential mechanism of forefoot injury development at different running distances under different running interfaces under the framework of the research methodology set in this work.

Based on the findings of the first session, this dissertation further introduced a 3D frictional-coupling foot-shoe FE model aiming to observe the foot-shoe interaction without destroying the upper structure of the shoe and could be further applied for fast evaluation and optimization of the footwear structure. The running scenario has been simulated but the corresponding frictional contact coefficient and loading conditions was not adjusted accordingly with the running distance, which would make it less realistic and limit its practical utility. Future work that takes these aspects into consideration will refine the effectiveness of the foot-shoe model. Meanwhile, as a new in vivo imaging technique for joints, dual fluoroscopic imaging technology are now widely used in clinical biomechanics to accurately and non-invasively capture human joint motion during dynamic/static activities. Thus, it is worth noting that future work could also consider using dual fluoroscopic imaging technology for the accurate real-time measurement of the foot-shoe interaction in vivo. In addition, this dissertation also created a feline paw model to understand its buffering mechanism during landing and further proposed the preliminary footwear design concept for MSF injury prevention. Specifically, adding a certain thickness pad to the metatarsal region at the front of the insole may be able to attenuate the impact from the ground during running and contribute to reduce the injury risk of MSF. On the other hand, the stiff material can be added at the medial foot of shoes or insoles, which may strengthen the support force of the foot. Future work could get insight into the effects of the material properties, thicknesses, and placements of the metatarsal pad on local plantar pressure and stress/strain states of the metatarsal region during functional movements such as running.

Lastly, the current dissertation only presented the up-to-date methodologies and generalized workflow for footwear optimization. Thus, the subsequent research should optimize the corresponding footwear structure based on the findings of this study and conduct FE simulations as well as biomechanical and epidemiologic tests to verify the effects of the upgraded footwear in preventing forefoot injuries.

NEW SCIENTIFIC THESIS POINTS

1st Thesis point

I investigated the underlying mechanisms of forefoot injury development (BT and MSF) during 10km of running from multidimensional perspectives. Based on my experimental results, the injury development mechanisms of BT have been quantitatively deduced for the first time and the mechanisms of MSF injury have been further confirmed.

The reduced ball width and arch height of the foot while increased foot skin temperature (increase in sweat) after long distance running were accompanied by hallux discomfort and excessive foot-shoe interaction (gap length between the hallux and toebox in sagittal plane), which could potentially be responsible for BT injury development (Figure 38A-D). In addition, the insufficient toebox space of the shoe limited the toe's ambulatory function and could lead to additional repetitive friction between foot and shoes (Figure 38E), which may further increase the BT injury risk.

Long-distance running led to a relative midfoot strike pattern, more pronated foot posture, reduced arch height and loss of toe dynamic function (peak propulsive force) (Figure 39A-C), which further redistributed the forefoot plantar load with increased skin temperature under medial metatarsals (Figure 39D), causing an increased incidence of MSF injury development.

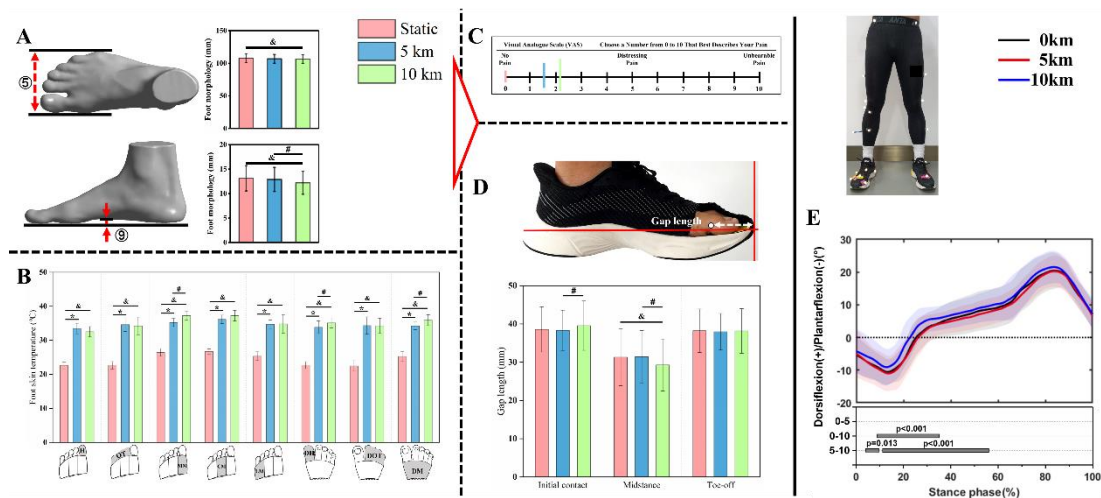


Figure 38 The injury development mechanisms of BT

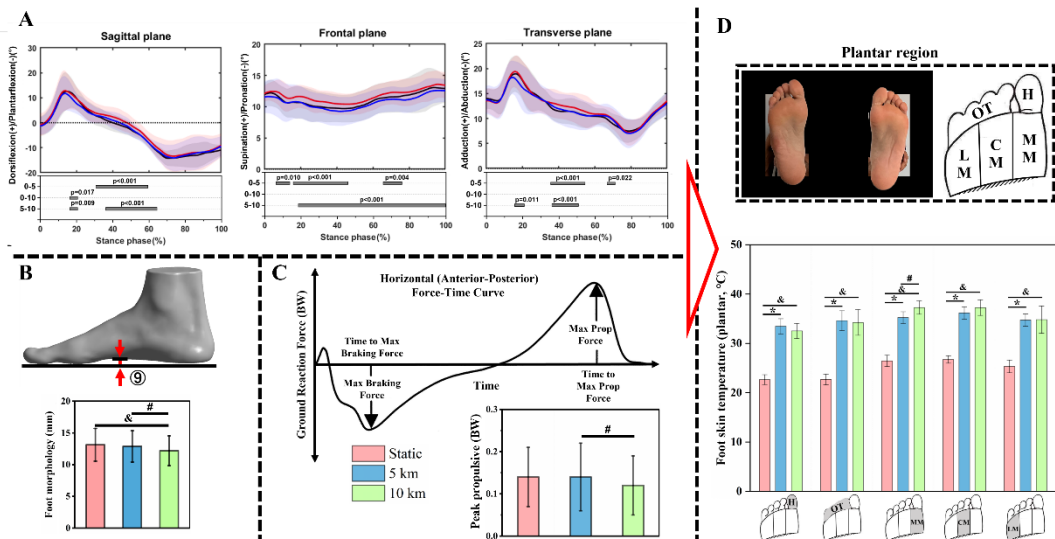


Figure 39 The injury development mechanisms of MSF

Related articles to the first thesis point:

1. Li, J., Song, Y., Xuan, R., Sun, D., Teo, E. C., Bíró, I., Gu, Y. (2022). Effect of long-distance running on inter-segment foot kinematics and ground reaction forces: A preliminary study. *Frontiers in Bioengineering and Biotechnology*, 10, 833774. **IF: 6.064, Q2**
2. Chen, H., Song, Y., Liu, Q., Ren, F., Bíró, I., Gu, Y. (2022). Gender effects on lower limb biomechanics of novice runners before and after a 5 km run. *Journal of Men's Health*. 18(8), 176. **IF: 0.789, Q3**

2nd Thesis point

Based on my experiments on the potential mechanisms of BT injury development, I proposed a high accurate 3D frictional-coupling foot-shoe FE model to provide an alternative tool for accurately observing the foot-shoe interaction without destroying the upper structure of the shoe and it could be further applied for fast evaluation and optimization of the footwear structure in order to reduce the incidence of BT injury with a simultaneous reduction of the production batches and costs(Figure 40A).

I proposed a more comprehensive approach to model validation by dividing the plantar and shoe outsole regions into four parts for pressure comparison and further applied the Bland-Altman method for consistency analysis. The results demonstrated a good agreement between the experimentally measured and numerically predicted difference (MD: 0.008MPa, 96% scattered between $\pm 1.96SD$)(Figure 40B).

I further simulated the dynamic running scenario using the boundary conditions derived from motion capture analyses of the participant's gait, which can reproduce the running motion more realistically than the foot-plate system approach. Based on the calculation, the relatively small difference (<10%) in terms of the experimental and predicted gap length between the hallux and toebox during running demonstrated the effectiveness of the model for dynamic simulations(Figure 40C).

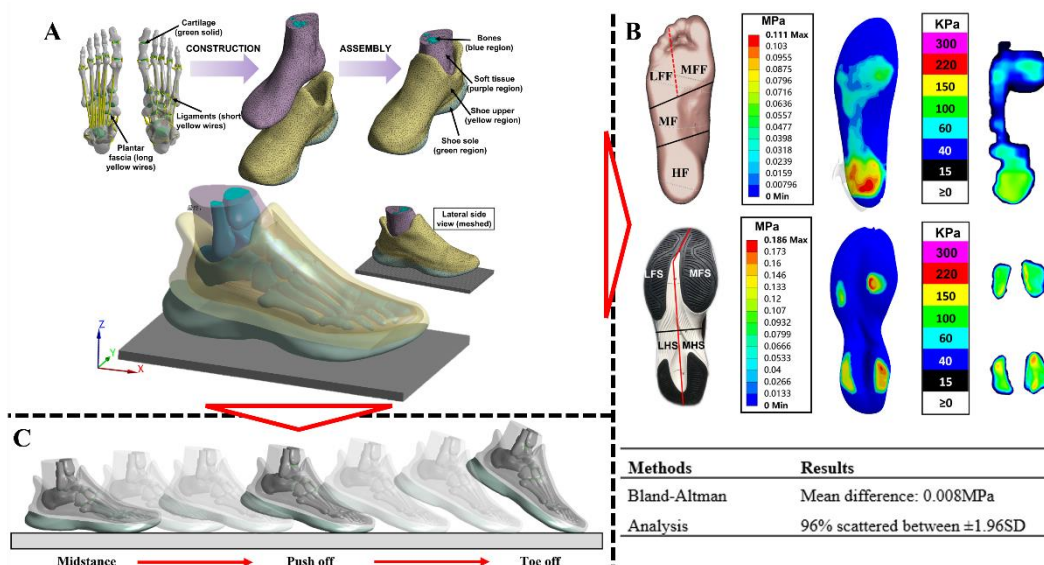


Figure 40 The proposed high accurate 3D frictional-coupling foot-shoe FE model

Related articles to the second thesis point:

1. **Song, Y.**, Shao, E., Bíró, I., Baker, J. S., Gu, Y. (2022). Finite element modelling for footwear design and evaluation: A systematic scoping review. *Heliyon*, 8(10), e10940. **IF: 3.776, Q1**
2. **Song, Y.**, Cen, X., Zhang, Y., Bíró, I., Ji, Y., & Gu, Y. (2022). Development and validation of a subject-specific coupled model for foot and sports shoe complex: A pilot computational study. *Bioengineering*, 9(10), 553. **IF: 5.046, Q2**

3rd Thesis point

I proposed a high accurate 3D feline fore-left paw FE model to investigate the GRF distribution and internal stress distribution of the distal joint limb both under static standing and landing with different height (0.6m, 0.8m, 1.0m) and reveal how a cat's paw absorbs and transmits large impact forces to avoid musculoskeletal injuries during movement (Figure 41A).

For the validation of the feline paw model, the predicted paw pressure presented a good consistency with the experimental pressure data (Figure 41B). The paw pressure concentrated mainly on the metapodial pad and minimal stress was found in phalange region even through it is the main supporter of the body, which indicated the thick substrate tissue (paw pad) under the distal joint effectively decrease the GRF and optimize its distribution.

In terms of force transmission mechanism, larger stress was concentrated on the MP segment and its growth rate increased with landing height, indicating that the raised MP segment contributes to create a stiff junction between the MCP and wrist joint, transmit impact force and stabilizing the distal joint(Figure 41C).

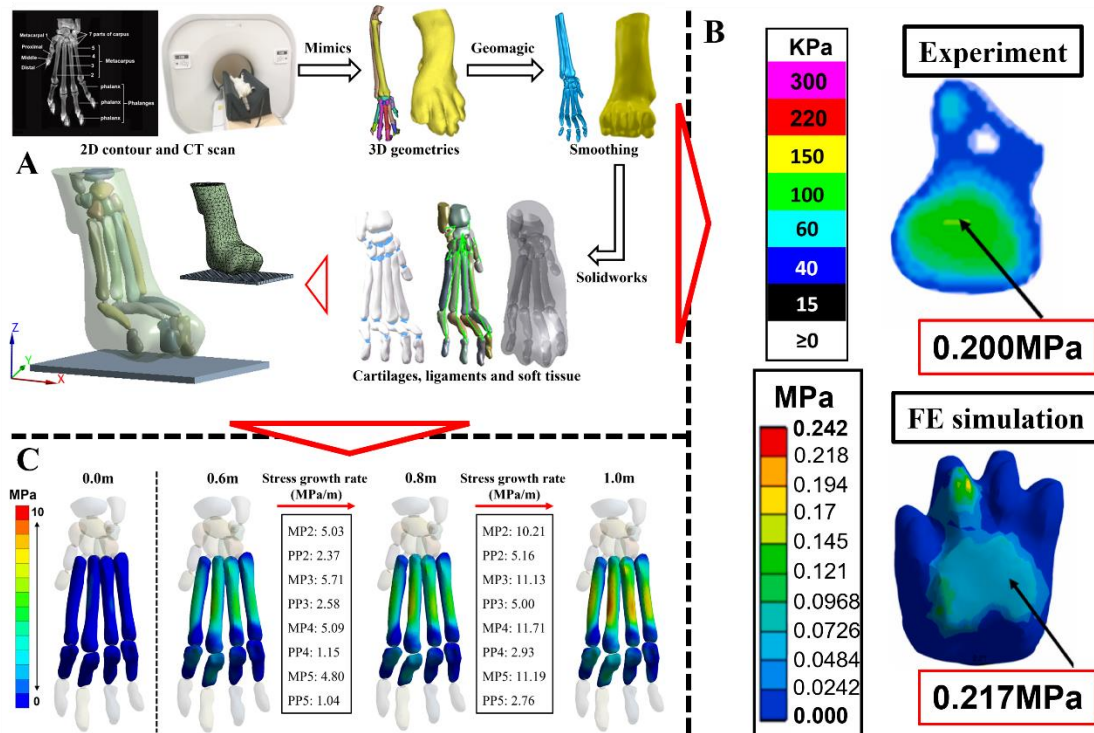


Figure 41 The proposed high accurate 3D feline fore-left paw FE model

Related articles to the third thesis point:

1. Wang, M., **Song, Y.**, Baker, J. S., Fekete, G., Ugbolue, U. C., Li, S., Gu, Y. (2021).
The biomechanical characteristics of a feline distal forelimb: a finite element
analysis study. *Computers in Biology and Medicine*, 129, 104174. **IF: 6.698, Q1**

LIST OF PUBLICATIONS

Articles related to this thesis

1. **Song, Y.**, Shao, E., Bíró, I., Baker, J. S., Gu, Y. (2022). Finite element modelling for footwear design and evaluation: A systematic scoping review. *Heliyon*, 8(10), e10940. **IF: 3.776, Q1**
2. **Song, Y.**, Cen, X., Zhang, Y., Bíró, I., Ji, Y., & Gu, Y. (2022). Development and validation of a subject-specific coupled model for foot and sports shoe complex: A pilot computational study. *Bioengineering*, 9(10), 553. **IF: 5.046, Q2**
3. Wang, M., **Song, Y.**, Baker, J. S., Fekete, G., Ugbohue, U. C., Li, S., Gu, Y. (2021). The biomechanical characteristics of a feline distal forelimb: a finite element analysis study. *Computers in Biology and Medicine*, 129, 104174. **IF: 6.698, Q1**
4. Li, J., **Song, Y.**, Xuan, R., Sun, D., Teo, E. C., Bíró, I., Gu, Y. (2022). Effect of long-distance running on inter-segment foot kinematics and ground reaction forces: A preliminary study. *Frontiers in Bioengineering and Biotechnology*, 10, 833774. **IF: 6.064, Q2**
5. Chen, H., **Song, Y.**, Liu, Q., Ren, F., Bíró, I., Gu, Y. (2022). Gender effects on lower limb biomechanics of novice runners before and after a 5 km run. *Journal of Men's Health*. 18(8), 176. **IF: 0.789, Q3**

Other publications

1. **Song, Y.**, Li, J., István, B., Xuan, R., Wei, S., Zhong, G., Gu, Y. (2021). Current evidence on traditional Chinese exercises for quality of life in patients with essential hypertension: a systematic review and meta-analysis. *Frontiers in Cardiovascular Medicine*, 7, 627518. **IF: 5.846, Q1**
2. Sun, D., **Song, Y.**, Cen, X., Wang, M., Baker, J. S., Gu, Y. (2022). Workflow assessing the effect of Achilles tendon rupture on gait function and metatarsal stress: Combined musculoskeletal modeling and finite element analysis. *Proceedings of the Institution of Mechanical Engineers, Part H: Journal of Engineering in Medicine*, 236(5), 676-685. **IF: 1.763, Q2**
3. Lin, S., **Song, Y.**, Cen, X., Bálint, K., Fekete, G., & Sun, D. (2022). The

- implications of sports biomechanics studies on the research and development of running shoes: A systematic review. *Bioengineering*, 9(10), 497. **IF: 5.046, Q2**
4. Chang, H., **Song, Y.**, Cen, X. (2022). Effectiveness of augmented reality for lower limb rehabilitation: A systematic review. *Applied Bionics and Biomechanics*, 2022, 4047845. **IF: 1.664, Q2**
 5. Lu, Z., **Song, Y.**, Chen, H., Li, S., Teo, E. C., Gu, Y. (2021). A mixed comparisons of aerobic training with different volumes and intensities of physical exercise in patients with hypertension: A systematic review and network meta-analysis. *Frontiers in Cardiovascular Medicine*, 8, 770975. **IF: 5.846, Q1**
 6. Fan, H., **Song, Y.**, Cen, X., Yu, P., Bíró, I., Gu, Y. (2021). The effect of repetitive transcranial magnetic stimulation on lower-limb motor ability in stroke patients: a systematic review. *Frontiers in Human Neuroscience*, 15, 620573. **IF: 3.473, Q2**
 7. Chen, H., **Song, Y.**, Xuan, R., Hu, Q., Baker, J. S., Gu, Y. (2021). Kinematic comparison on lower limb kicking action of fetuses in different gestational weeks: A pilot study. *Healthcare* 9(8), 1057. **IF: 3.160, Q2**
 8. Zhou, H., **Song, Y.**, Wang, M., Ugbolue, U. C., Gu, Y. (2021). Thermal imaging evaluation of the felines paw pad temperature before and after walking: A pilot study. *Veterinárni medicína*, 66(9), 393-399. **IF: 0.746, Q3**
 9. Xu, D., **Song, Y.**, Meng, Y., István, B., Gu, Y. (2020). Relationship between firefighter physical fitness and special ability performance: predictive research based on machine learning algorithms. *International Journal of Environmental Research and Public Health*, 17(20), 7689. **IF: 4.614, Q1**
 10. Xu, Y., **Song, Y.**, Sun, D., Fekete, G., Gu, Y. (2020). Effect of multi-modal therapies for kinesiophobia caused by musculoskeletal disorders: A systematic review and meta-analysis. *International Journal of Environmental Research and Public Health*, 17(24), 9439. **IF: 4.614, Q1**
 11. Liu, Q., Chen, H., **Song, Y.**, Alla, N., Fekete, G., Li, J., & Gu, Y. (2022). Running velocity and longitudinal bending stiffness influence the asymmetry of kinematic variables of the lower limb joints. *Bioengineering*, 9(11), 607. **IF: 5.046, Q2**

12. Shen, X. A., Cen, X., **Song, Y.** (2022). Investigating temporal kinematic differences caused by unexpected stimulation during gait termination through the waveform-level variance equality test. *BioMed Research International*, 2022, 4043426. **IF: 3.246, Q2**
13. Ji, Y., Zhang, Q., **Song, Y.**, Hu, Q., Fekete, G., Baker, J. S., Gu, Y. (2022). Biomechanical characteristics of two different posterior fixation methods of bilateral pedicle screws: A finite element analysis. *Medicine*. **IF: 1.889, Q2**
14. Lu, Z., Xu, Y., **Song, Y.**, Bíró, I., Gu, Y. (2021). A mixed comparisons of different intensities and types of physical exercise in patients with diseases related to oxidative stress: a systematic review and network meta-analysis. *Frontiers in Physiology*, 12, 700055. **IF: 4.755, Q2**
15. Xu, D., Fekete, G., **Song, Y.**, Zhao, L., Sun, D., Gu, Y. (2021). The application of medical imaging on disabled athletes in winter Paralympic games: A systematic review. *Journal of Medical Imaging and Health Informatics*, 11(8), 2054-2061.
16. Lu, Z., Li, X., Xuan, R., **Song, Y.**, Bíró, I., Liang, M., Gu, Y. (2022). Effect of heel lift insoles on lower extremity muscle activation and joint work during barbell squats. *Bioengineering*, 9(7), 301. **IF: 5.046, Q2**
17. Cen, X., Sun, D., Rong, M., Fekete, G., Baker, J. S., **Song, Y.**, Gu, Y. (2020). The online education mode and reopening plans for Chinese schools during the COVID-19 pandemic: a mini review. *Frontiers in Public Health*, 8, 566316. **IF: 6.461, Q2**
18. Xuan, R., Yang, M., Gao, Y., Ren, S., Li, J., Yang, Z., **Song, Y.**, Huang, X. H., Teo, E. C., Zhu, J., Gu, Y. (2021). A simulation analysis of maternal pelvic floor muscle. *International Journal of Environmental Research and Public Health*, 18(20), 10821. **IF: 4.614, Q1**

REFERENCE

- [1] N. Cejka, C.A. Rüst, R. Lepers, V. Onywera, T. Rosemann, B. Knechtle, Participation and performance trends in 100-km ultra-marathons worldwide, *J. Sports Sci.* 32 (2014) 354–366.
- [2] J. Scheerder, K. Breedveld, J. Borgers, Who is doing a run with the running boom?, in: J. Scheerder, K. Breedveld, J. Borgers (Eds.), *Run. across Eur. Rise Size One Larg. Sport Mark.*, Palgrave Macmillan UK, London, 2015: pp. 1–27.
- [3] P.T. Nikolaidis, I. Cuk, V.J. Clemente-Suárez, E. Villiger, B. Knechtle, Number of finishers and performance of age group women and men in long-distance running: comparison among 10km, half-marathon and marathon races in Oslo, *Res. Sport. Med.* 29 (2021) 56–66.
- [4] Z. Pedisic, N. Shrestha, S. Kovalchik, E. Stamatakis, N. Liangruenrom, J. Grgic, S. Titze, S.J.H. Biddle, A.E. Bauman, P. Oja, Is running associated with a lower risk of all-cause, cardiovascular and cancer mortality, and is the more the better? A systematic review and meta-analysis, *Br. J. Sports Med.* 54 (2020) 898–905.
- [5] A. Vitti, P.T. Nikolaidis, E. Villiger, V. Onywera, B. Knechtle, The “New York City Marathon”: Participation and performance trends of 1.2M runners during half-century, *Res. Sport. Med.* 28 (2020) 121–137.
- [6] W. Contributors, 2021 New York City Marathon, *Wikipedia, Free Encycl.* (2021) 1114396169.
- [7] J. Li, Y. Song, R. Xuan, D. Sun, E.-C. Teo, I. Bíró, Y. Gu, Effect of long-distance running on inter-segment foot kinematics and ground reaction forces: A preliminary study, *Front. Bioeng. Biotechnol.* 10 (2022) 833774.
- [8] D. van Poppel, M. van der Worp, A. Slabbekoorn, S.S.P. van den Heuvel, M. van Middelkoop, B.W. Koes, A.P. Verhagen, G.G.M. Scholten-Peeters, Risk factors for overuse injuries in short- and long-distance running: A systematic review, *J. Sport Heal. Sci.* 10 (2021) 14–28.

- [9] E.A. Mailler-Savage, B.B. Adams, Skin manifestations of running, *J. Am. Acad. Dermatol.* 55 (2006) 290–301.
- [10] E.A. Mailler, B.B. Adams, The wear and tear of 26.2: Dermatological injuries reported on marathon day, *Br. J. Sports Med.* 38 (2004) 498–501.
- [11] J. Dempster, F. Dutheil, U.C. Ugbohue, The prevalence of lower extremity injuries in running and associated risk factors: A systematic review, *Phys. Act. Heal.* 5 (2021) 133–145.
- [12] B.J. Krabak, B. Waite, M.A. Schiff, Study of injury and illness rates in multiday ultramarathon runners, *Med. Sci. Sports Exerc.* 43 (2011) 2314–2320.
- [13] M.F. Helm, T. N. Helm, W. F. Bergfeld, Skin problems in the long-distance runner 2500 years after the Battle of Marathon, *Int. J. Dermatol.* 51 (2012) 263–270.
- [14] Q. Mei, Y. Gu, L. Xiang, J.S. Baker, J. Fernandez, Foot pronation contributes to altered lower extremity loading after long distance running, *Front. Physiol.* 10 (2019) 573.
- [15] L.A. Carroll, S. Paulseth, R.L. Martin, Forefoot injuries in athletes: Integration of the movement system, *Int. J. Sports Phys. Ther.* 17 (2022) 81–89.
- [16] B.B. Adams, Jogger’s toenail, *J. Am. Acad. Dermatol.* 48 (2003) S58–S59.
- [17] P.R. Cohen, K.E. Schulze, B.R. Nelson, Subungual hematoma, *Dermatology Nurs.* 19 (2007) 83–84.
- [18] A.O. Istvan, P. Yvonne, J.E. Terry, B. Marco, B.Q. Timothy, V.H. Henriëtte, L.S. Gert, Common ultramarathon trail running injuries and illnesses: A review (2007-2016), *Int. J. Med. Med. Sci.* 11 (2019) 36–42.
- [19] C. Agresta, C. Giacomazzi, M. Harrast, J. Zandler, Running injury paradigms and their influence on footwear design features and runner assessment methods:

- A focused review to advance evidence-based practice for running medicine clinicians, *Front. Sport. Act. Living.* 4 (2022) 815675.
- [20] S.A. Ruiz-Alias, A. Molina-Molina, V.M. Soto-Hermoso, F. García-Pinillos, A systematic review of the effect of running shoes on running economy, performance and biomechanics: Analysis by brand and model, *Sport. Biomech.* (2022) 1–22.
- [21] E. Morales-Orcajo, J. Bayod, E. Barbosa de Las Casas, Computational foot modeling: Scope and applications, *Arch. Comput. Methods Eng.* 23 (2016) 389–416.
- [22] Y. Wang, D.W.-C. Wong, M. Zhang, Computational models of the foot and ankle for pathomechanics and clinical applications: A review, *Ann. Biomed. Eng.* 44 (2016) 213–221.
- [23] J. Zhu, J. Forman, A review of finite element models of ligaments in the foot and considerations for practical application, *J. Biomech. Eng.* 144 (2022) 080801.
- [24] P.K. Phan, A.T.N. Vo, A. Bakhtiarydavijani, R. Burch, B. Smith, J.E. Ball, H. Chander, A. Knight, R.K. Prabhu, In silico finite element analysis of the foot ankle complex biomechanics: A literature review, *J. Biomech. Eng.* 143 (2021) 090802.
- [25] S. Behforootan, P. Chatzistergos, R. Naemi, N. Chockalingam, Finite element modelling of the foot for clinical application: A systematic review, *Med. Eng. Phys.* 39 (2017) 1–11.
- [26] R. Shahar, L. Banks-Sills, R. Eliasy, Stress and strain distribution in the intact canine femur: Finite element analysis., *Med. Eng. Phys.* 25 (2003) 387–395.
- [27] X. Wu, B. Pei, Y. Pei, Y. Hao, K. Zhou, W. Wang, Comprehensive biomechanism of impact resistance in the cat's paw pad, *Biomed Res. Int.* 2019 (2019) 2183712.

- [28] H. Miao, J. Fu, Z. Qian, L. Ren, L. Ren, How does the canine paw pad attenuate ground impacts? A multi-layer cushion system, *Biol. Open.* 6 (2017) 1889–1896.
- [29] D. Sun, G. Fekete, Q. Mei, Y. Gu, The effect of walking speed on the foot inter-segment kinematics, ground reaction forces and lower limb joint moments, *PeerJ.* 2018 (2018) 1–18.
- [30] N.L. Griffin, C.E. Miller, D. Schmitt, K. D’Août, Understanding the evolution of the windlass mechanism of the human foot from comparative anatomy: Insights, obstacles, and future directions, *Am. J. Phys. Anthropol.* 156 (2015) 1–10.
- [31] E.J. McNutt, B. Zipfel, J.M. DeSilva, The evolution of the human foot, *Evol. Anthropol. Issues, News, Rev.* 27 (2018) 197–217.
- [32] C.W. Chan, A. Rudins, Foot biomechanics during walking and running, *Mayo Clin. Proc.* 69 (1994) 448–461.
- [33] G. Scott, H.B. Menz, L. Newcombe, Age-related differences in foot structure and function, *Gait Posture.* 26 (2007) 68–75.
- [34] R. Drake, A.W. Vogl, A.W. Mitchell, *Gray’s anatomy for students E-book*, Elsevier Health Science, 2009.
- [35] M. Nordin, V.H. Frankel, *Basic biomechanics of the musculoskeletal system*, Lippincott Williams & Wilkins, 2001.
- [36] M. O’Brien, Anatomy of tendons BT, in: N. Maffulli, P. Renström, W.B. Leadbetter (Eds.), *Tendon Inj. Basic Sci. Clin. Med.*, Springer London, London, 2005: pp. 3–13.
- [37] M. De Maeseneer, H. Madani, L. Lenchik, J. De Mey, S. Provyn, M. Shahabpour, Ultrasound of the distal insertions of the ankle and foot tendons with anatomical correlation: A review, *Can. Assoc. Radiol. J.* 69 (2018) 282–292.

- [38] M.N. Doral, M. Alam, M. Bozkurt, E. Turhan, O.A. Atay, G. Dönmez, N. Maffulli, Functional anatomy of the Achilles tendon, *Knee Surgery, Sport. Traumatol. Arthrosc.* 18 (2010) 638–643.
- [39] K. Winnicki, A. Ochała-Kłos, B. Rutowicz, P.A. Pękała, K.A. Tomaszewski, Functional anatomy, histology and biomechanics of the human Achilles tendon: A comprehensive review, *Ann. Anatomy-Anatomischer Anzeiger.* 229 (2020) 151461.
- [40] D.J. Farris, G. Trewartha, M.P. McGuigan, Could intra-tendinous hyperthermia during running explain chronic injury of the human Achilles tendon?, *J. Biomech.* 44 (2011) 822–826.
- [41] S. Döring, S. Probyn, S. Marcelis, M. Shahabpour, C. Boulet, J. de Mey, A. De Smet, M. De Maeseneer, Ankle and midfoot ligaments: Ultrasound with anatomical correlation: A review, *Eur. J. Radiol.* 107 (2018) 216–226.
- [42] P. Hrkal, *Fascia: The Tensional Network of the Human Body: The science and clinical applications in manual and movement therapy*, *J. Can. Chiropr. Assoc.* 59 (2015) 417–418.
- [43] J. Guo, X. Liu, X. Ding, L. Wang, Y. Fan, Biomechanical and mechanical behavior of the plantar fascia in macro and micro structures, *J. Biomech.* 76 (2018) 160–166.
- [44] A. Asghar, S. Naaz, The transverse arch in the human feet: A narrative review of its evolution, anatomy, biomechanics and clinical implications, *Morphologie.* (2021) In Press.
- [45] D. Babu, B. Bordoni, Anatomy, bony pelvis and lower limb, medial longitudinal arch of the foot, in: *StatPearls [Internet]*, Treasure Island (FL): StatPearls Publishing, 2021: pp. 1–14.

- [46] L. Welte, L.A. Kelly, G.A. Lichtwark, M.J. Rainbow, Influence of the windlass mechanism on arch-spring mechanics during dynamic foot arch deformation, *J. R. Soc. Interface.* 15 (2018) 20180270.
- [47] J. Kayano, Dynamic function of medial foot arch, *Nihon Seikeigeka Gakkai Zasshi.* 60 (1986) 1147–1156.
- [48] H.B. Kitaoka, T.K. Ahn, Z.P. Luo, K.N. An, Stability of the arch of the foot, *Foot Ankle Int.* 18 (1997) 644–648.
- [49] M. Venkadesan, A. Yawar, C.M. Eng, M.A. Dias, D.K. Singh, S.M. Tommasini, A.H. Haims, M.M. Bandi, S. Mandre, Stiffness of the human foot and evolution of the transverse arch, *Nature.* 579 (2020) 97–100.
- [50] S. Xiong, R.S. Goonetilleke, C.P. Witana, T.W. Weerasinghe, E.Y.L. Au, Foot arch characterization: a review, a new metric, and a comparison, *J. Am. Podiatr. Med. Assoc.* 100 (2010) 14–24.
- [51] D.S. Williams Iii, I.S. McClay, J. Hamill, Arch structure and injury patterns in runners, *Clin. Biomech.* 16 (2001) 341–347.
- [52] S.C. Cobb, L.L. Tis, J.T. Johnson, M.D. Geil, F.A. McCarty, The effect of low-mobile foot posture on multi-segment medial foot model gait kinematics, *Gait Posture.* 30 (2009) 334–339.
- [53] M.M. Rodgers, Dynamic biomechanics of the normal foot and ankle during walking and running, *Phys. Ther.* 68 (1988) 1822–1830.
- [54] C.L. Brockett, G.J. Chapman, Biomechanics of the ankle, *Orthop. Trauma.* 30 (2016) 232–238.
- [55] I.C. Wright, R.R. Neptune, A.J. van den Bogert, B.M. Nigg, The influence of foot positioning on ankle sprains, *J. Biomech.* 33 (2000) 513–519.
- [56] T.F. Novacheck, The biomechanics of running, *Gait Posture.* 7 (1998) 77–95.

- [57] T.L. Nicola, D.J. Jewison, The anatomy and biomechanics of running, *Clin. Sports Med.* 31 (2012) 187–201.
- [58] P. DeJong, N.S. Hatamiya, L.C. Barkley, Running gait analysis and biomechanics, *Curr. Sports Med. Rep.* 21 (2022) 107–108.
- [59] T. Hoenig, T. Rolvien, K. Hollander, Footstrike patterns in runners: Concepts, classifications, techniques, and implications for running-related injuries, *Ger. J. Sport. Med. Zeitschrift Fur Sport.* 71 (2020) 55–60.
- [60] Y. Xu, P. Yuan, R. Wang, D. Wang, J. Liu, H. Zhou, Effects of foot strike techniques on running biomechanics: A systematic review and meta-analysis, *Sports Health.* 13 (2021) 71–77.
- [61] M.O. Almeida, I.S. Davis, A.D. Lopes, Biomechanical differences of foot-strike patterns during running: A systematic review with meta-analysis, *J. Orthop. Sport. Phys. Ther.* 45 (2015) 738–755.
- [62] B. De Wit, D. De Clercq, P. Aerts, Biomechanical analysis of the stance phase during barefoot and shod running, *J. Biomech.* 33 (2000) 269–278.
- [63] B.F. LeVeau, Biomechanics: A summary of perspectives, *Phys. Ther.* 64 (1984) 1812.
- [64] B. Elliott, Biomechanics: An integral part of sport science and sport medicine, *J. Sci. Med. Sport.* 2 (1999) 299–310.
- [65] A.S. Fox, Change-of-direction biomechanics: Is what’s best for anterior cruciate ligament injury prevention also best for performance?, *Sport. Med.* 48 (2018) 1799–1807.
- [66] L.M. Anderson, J.F. Martin, C.J. Barton, D.R. Bonanno, What is the effect of changing running step rate on injury, performance and biomechanics? A systematic review and meta-analysis, *Sport. Med.* 8 (2022) 1–41.

- [67] S. Khuu, L.L. Musalem, T.A.C. Beach, Verbal instructions acutely affect drop vertical jump biomechanics—implications for athletic performance and injury risk assessments, *J. Strength Cond. Res.* 29 (2015) 2816–2826.
- [68] S.L. Colyer, M. Evans, D.P. Cosker, A.I.T. Salo, A review of the evolution of vision-based motion analysis and the integration of advanced computer vision methods towards developing a markerless system, *Sport. Med.* 4 (2018) 1–15.
- [69] P. Procter, J.P. Paul, Ankle joint biomechanics, *J. Biomech.* 15 (1982) 627–634.
- [70] J.G. Richards, The measurement of human motion: A comparison of commercially available systems, *Hum. Mov. Sci.* 18 (1999) 589–602.
- [71] E. van der Kruk, M.M. Reijne, Accuracy of human motion capture systems for sport applications; state-of-the-art review, *Eur. J. Sport Sci.* 18 (2018) 806–819.
- [72] B. Carse, B. Meadows, R. Bowers, P. Rowe, Affordable clinical gait analysis: An assessment of the marker tracking accuracy of a new low-cost optical 3D motion analysis system, *Physiotherapy.* 99 (2013) 347–351.
- [73] E. Ceseracciu, Z. Sawacha, C. Cobelli, Comparison of markerless and marker-based motion capture technologies through simultaneous data collection during gait: Proof of concept, *PLoS One.* 9 (2014) e87640.
- [74] S.I. Ismail, H. Nunome, F.F. Marzuki, I. Suaidi, The influence of additional surface on force platforms ground reaction force data during walking and running, *Am. J. Sport. Sci.* 6 (2018) 78–82.
- [75] A.H.A. Razak, A. Zayegh, R.K. Begg, Y. Wahab, Foot plantar pressure measurement system: A review, *Sensors.* 12 (2012) 9884–9912.
- [76] G. Bovi, M. Rabuffetti, P. Mazzoleni, M. Ferrarin, A multiple-task gait analysis approach: kinematic, kinetic and EMG reference data for healthy young and adult subjects, *Gait Posture.* 33 (2011) 6–13.

- [77] D. Lee, R.R. Pate, C.J. Lavie, X. Sui, T.S. Church, S.N. Blair, Leisure-time running reduces all-cause and cardiovascular mortality risk, *J. Am. Coll. Cardiol.* 64 (2014) 472–481.
- [78] D. van Poppel, M. van der Worp, A. Slabbekoorn, S.S.P. van den Heuvel, M. van Middelkoop, B.W. Koes, A.P. Verhagen, G.G.M. Scholten-Peeters, Risk factors for overuse injuries in short- and long-distance running: A systematic review, *J. Sport Heal. Sci.* 10 (2021) 14–28.
- [79] R.N. Van Gent, D. Siem, M. van Middelkoop, A.G. Van Os, S.M.A. Bierma-Zeinstra, B.W. Koes, Incidence and determinants of lower extremity running injuries in long distance runners: A systematic review, *Br. J. Sports Med.* 41 (2007) 469–480.
- [80] R.A. Gallo, M. Plakke, M.L. Silvis, Common leg injuries of long-distance runners: Anatomical and biomechanical approach, *Sports Health.* 4 (2012) 485–495.
- [81] J.R. Jastifer, Contemporary review: The foot and ankle in long-distance running, *Foot Ankle Orthop.* 7 (2022) 24730114221125456.
- [82] S.J. Warden, I.S. Davis, M. Fredericson, Management and prevention of bone stress injuries in long-distance runners, *J. Orthop. Sport. Phys. Ther.* 44 (2014) 749–765.
- [83] A.S. Tenforde, A. Yin, K.J. Hunt, Foot and ankle injuries in runners, *Phys. Med. Rehabil. Clin.* 27 (2016) 121–137.
- [84] A. Hulme, R.O. Nielsen, T. Timpka, E. Verhagen, C. Finch, Risk and protective factors for middle-and long-distance running-related injury, *Sport. Med.* 47 (2017) 869–886.
- [85] D.M. Begizew, J.M. Grace, H.J. van Heerden, Lower-extremity running-related injuries among 10,000-meter long distance runners in Ethiopia, *J. Hum. Sport Exerc.* 14 (2019) 358–373.

- [86] S. Videbæk, A.M. Bueno, R.O. Nielsen, S. Rasmussen, Incidence of running-related injuries per 1000 h of running in different types of runners: A systematic review and meta-analysis, *Sport. Med.* 45 (2015) 1017–1026.
- [87] W. van Mechelen, Running injuries: A review of the epidemiological literature, *Sports Med.* 14 (1992) 320–335.
- [88] M.P. Van der Worp, D.S.M. Ten Haaf, R. van Cingel, A. de Wijer, M.W.G. Nijhuis-van der Sanden, J.B. Staal, Injuries in runners: A systematic review on risk factors and sex differences, *PLoS One.* 10 (2015) e0114937.
- [89] B. Kluitenberg, M. van Middelkoop, R. Diercks, H. van der Worp, What are the differences in injury proportions between different populations of runners? A systematic review and meta-analysis, *Sport. Med.* 45 (2015) 1143–1161.
- [90] A.S. Tenforde, L.C. Sayres, M.L. McCurdy, H. Collado, K.L. Sainani, M. Fredericson, Overuse injuries in high school runners: Lifetime prevalence and prevention strategies, *Pm&r.* 3 (2011) 125–131.
- [91] L.C. Hespanhol Junior, W. Van Mechelen, E. Verhagen, Health and economic burden of running-related injuries in Dutch trailrunners: A prospective cohort study, *Sport. Med.* 47 (2017) 367–377.
- [92] M. Walther, I. Reuter, T. Leonhard, M. Engelhardt, Injuries and response to overload stress in running as a sport, *Orthopade.* 34 (2005) 399–404.
- [93] A.H. Gruber, K.A. Boyer, T.R. Derrick, J. Hamill, Impact shock frequency components and attenuation in rearfoot and forefoot running, *J. Sport Heal. Sci.* 3 (2014) 113–121.
- [94] S. Knorz, F. Kluge, K. Gelse, S. Schulz-Drost, T. Hotfiel, M. Lochmann, B. Eskofier, S. Krinner, Three-dimensional biomechanical analysis of rearfoot and forefoot running, *Orthop. J. Sport. Med.* 5 (2017) 2325967117719065.

- [95] S.M. Stearne, J.A. Alderson, B.A. Green, C.J. Donnelly, J. Rubenson, Joint kinetics in rearfoot versus forefoot running: Implications of switching technique, *Med. Sci. Sport. Exerc.* 46 (2014) 1578–1587.
- [96] S.A. Bergstra, B. Kluitenberg, R. Dekker, S.W. Bredeweg, K. Postema, E.R. Van den Heuvel, J.M. Hijmans, S. Sobhani, Running with a minimalist shoe increases plantar pressure in the forefoot region of healthy female runners, *J. Sci. Med. Sport.* 18 (2015) 463–468.
- [97] J. Kindred, C. Trubey, S.M. Simons, Foot injuries in runners, *Curr. Sports Med. Rep.* 10 (2011) 249–254.
- [98] S.W. Mayer, P.W. Joyner, L.C. Almekinders, S.G. Parekh, Stress fractures of the foot and ankle in athletes, *Sports Health.* 6 (2014) 481–491.
- [99] S.W. Donahue, N.A. Sharkey, Strains in the metatarsals during the stance phase of gait: Implications for stress fractures., *J. Bone Joint Surg. Am.* 81 (1999) 1236–1244.
- [100] Y. Gu, Biomechanical investigation of the human foot deformation under different landing conditions using finite element analysis, Liverpool John Moores University (United Kingdom), 2010.
- [101] T. Fokkema, R.-J. de Vos, J.M. van Ochten, J.A.N. Verhaar, I.S. Davis, P.J.E. Bindels, S.M.A. Bierma-Zeinstra, M. van Middelkoop, Preventing running-related injuries using evidence-based online advice: The design of a randomised-controlled trial, *BMJ Open Sport Exerc. Med.* 3 (2017) e000265.
- [102] J.E. Taunton, M.B. Ryan, D.B. Clement, D.C. McKenzie, D.R. Lloyd-Smith, B.D. Zumbo, A retrospective case-control analysis of 2002 running injuries, *Br. J. Sports Med.* 36 (2002) 95–101.
- [103] B. Kluitenberg, H. van der Worp, B.M.A. Huisstede, F. Hartgens, R. Diercks, E. Verhagen, M. van Middelkoop, The NLstart2run study: Training-related factors

- associated with running-related injuries in novice runners, *J. Sci. Med. Sport.* 19 (2016) 642–646.
- [104] B. Kluitenberg, M. van Middelkoop, D.-W. Smits, E. Verhagen, F. Hartgens, R. Diercks, H. van der Worp, The NL start2run study: Incidence and risk factors of running-related injuries in novice runners, *Scand. J. Med. Sci. Sports.* 25 (2015) e515–e523.
- [105] I. Buist, S.W. Bredeweg, K.A.P.M. Lemmink, W. Van Mechelen, R.L. Diercks, Predictors of running-related injuries in novice runners enrolled in a systematic training program: A prospective cohort study, *Am. J. Sports Med.* 38 (2010) 273–280.
- [106] W.-L. Chang, Y.-F. Shih, W.-Y. Chen, Running injuries and associated factors in participants of ING Taipei Marathon, *Phys. Ther. Sport.* 13 (2012) 170–174.
- [107] M.P. van der Worp, A. de Wijer, R. van Cingel, A.L.M. Verbeek, M.W.G. Nijhuis-van der Sanden, J.B. Staal, The 5-or 10-km Marikenloop Run: A prospective study of the etiology of running-related injuries in women, *J. Orthop. Sport. Phys. Ther.* 46 (2016) 462–470.
- [108] L. Xiang, Q. Mei, J. Fernandez, Y. Gu, Minimalist shoes running intervention can alter the plantar loading distribution and deformation of hallux valgus: A pilot study, *Gait Posture.* 65 (2018) 65–71.
- [109] Q. Mey, Y. Gu, D. Sun, J. Fernandez, How foot morphology changes influence shoe comfort and plantar pressure before and after long distance running?, *Acta Bioeng. Biomech.* 20 (2018) 179–186.
- [110] H.K. Kim, S.A. Mirjalili, J. Fernandez, Gait kinetics, kinematics, spatiotemporal and foot plantar pressure alteration in response to long-distance running: Systematic review, *Hum. Mov. Sci.* 57 (2018) 342–356.

- [111] C.E. Milner, R.A. Brindle, Reliability and minimal detectable difference in multisegment foot kinematics during shod walking and running, *Gait Posture*. 43 (2016) 192–197.
- [112] M.E.R. Balsdon, C.E. Dombroski, Reliability of a multi-segment foot model in a neutral cushioning shoe during treadmill walking, *J. Foot Ankle Res.* 11 (2018) 1–10.
- [113] J. Yu, J.T.-M. Cheung, D.W.-C. Wong, Y. Cong, M. Zhang, Biomechanical simulation of high-heeled shoe donning and walking, *J. Biomech.* 46 (2013) 2067–2074.
- [114] F. Hoitz, M. Mohr, M. Asmussen, W.-K. Lam, S. Nigg, B. Nigg, The effects of systematically altered footwear features on biomechanics, injury, performance, and preference in runners of different skill level: A systematic review, *Footwear Sci.* 12 (2020) 193–215.
- [115] X. Sun, W.K. Lam, X. Zhang, J. Wang, W. Fu, Systematic review of the role of footwear constructions in running biomechanics: Implications for running-related injury and performance, *J. Sport. Sci. Med.* 19 (2020) 20–37.
- [116] B.M. Nigg, S. Cigoja, S.R. Nigg, Teeter-totter effect: A new mechanism to understand shoe-related improvements in long-distance running, *Br. J. Sports Med.* 55 (2021) 462–463.
- [117] B.M. Nigg, S. Cigoja, S.R. Nigg, Effects of running shoe construction on performance in long distance running, *Footwear Sci.* 12 (2020) 133–138.
- [118] B.M. Nigg, The role of impact forces and foot pronation: A new paradigm, *Clin. J. Sport Med.* 11 (2001) 2–9.
- [119] M. Hagen, E.M. Hennig, Effects of different shoe-lacing patterns on the biomechanics of running shoes, *J. Sports Sci.* 27 (2009) 267–275.

- [120] A.N. Onodera, M.I. Roveri, W.R. Oliveira, I.C.N. Sacco, The influence of shoe upper construction on the plantar pressure distribution during running, *Footwear Sci.* 7 (2015) S81–S82.
- [121] V. Rodrigo-Carranza, F. González-Mohíno, J. Santos-Concejero, J.M. González-Ravé, The effects of footwear midsole longitudinal bending stiffness on running economy and ground contact biomechanics: A systematic review and meta-analysis, *Eur. J. Sport Sci.* 22 (2022) 1508–1521.
- [122] L.A. Healey, W. Hoogkamer, Longitudinal bending stiffness does not affect running economy in Nike Vaporfly Shoes, *J. Sport Heal. Sci.* 11 (2022) 285–292.
- [123] S.A. Bus, J.S. Ulbrecht, P.R. Cavanagh, Pressure relief and load redistribution by custom-made insoles in diabetic patients with neuropathy and foot deformity, *Clin. Biomech.* 19 (2004) 629–638.
- [124] T.J.R. Hughes, *The finite element method: Linear static and dynamic finite element analysis*, Courier Corporation, 2012.
- [125] J.T.-M. Cheung, J. Yu, D.W.-C. Wong, M. Zhang, Current methods in computer-aided engineering for footwear design, *Footwear Sci.* 1 (2009) 31–46.
- [126] Y. Song, E. Shao, I. Bíró, J.S. Baker, Y. Gu, Finite element modelling for footwear design and evaluation: A systematic scoping review, *Heliyon.* 8 (2022) e10940.
- [127] T.L.-W. Chen, D.W.-C. Wong, Y. Peng, M. Zhang, Prediction on the plantar fascia strain offload upon Fascia taping and Low-Dye taping during running, *J. Orthop. Transl.* 20 (2020) 113–121.
- [128] T.L.-W. Chen, D.W.-C. Wong, Y. Wang, J. Lin, M. Zhang, Foot arch deformation and plantar fascia loading during running with rearfoot strike and forefoot strike: A dynamic finite element analysis, *J. Biomech.* 83 (2019) 260–272.

- [129] H. Ishii, Y. Sakurai, T. Maruyama, Effect of soccer shoe upper on ball behaviour in curve kicks, *Sci. Rep.* 4 (2014) 1–8.
- [130] A. Karimi, R. Razaghi, A. Sumikura, A 3-dimensional finite element model of a newly designed adjustable high-heeled shoe, *Int. J. Ind. Ergon.* 68 (2018) 304–310.
- [131] J.R. Cho, S.B. Park, S.H. Ryu, S.H. Kim, S.B. Lee, Landing impact analysis of sports shoes using 3-D coupled foot-shoe finite element model, *J. Mech. Sci. Technol.* 23 (2009) 2583–2591.
- [132] S.H. Kim, J.R. Cho, J.H. Choi, S.H. Ryu, W.B. Jeong, Coupled foot-shoe-ground interaction model to assess landing impact transfer characteristics to ground condition, *Interact. Multiscale Mech.* 5 (2012) 75–90.
- [133] B.R. Stein, A. Casinos, What is a cursorial mammal?, *J. Zool.* 242 (1997) 185–192.
- [134] F. Caliebe, J. Häubetaler, P. Hoffmann, M. Illert, J. Schirmacher, E. Wiedemann, Cat distal forelimb joints and locomotion: An X-ray study, *Eur. J. Neurosci.* 3 (1991) 18–31.
- [135] M. Elmajee, Z. Shen, J. A’Court, A. Pillai, A systematic review of plantar plate repair in the management of lesser metatarsophalangeal joint instability, *J. Foot Ankle Surg.* 56 (2017) 1244–1248.
- [136] Q. Liu, S. Mo, V.C.K. Cheung, B.M.F. Cheung, S. Wang, P.P.K. Chan, A. Malhotra, R.T.H. Cheung, R.H.M. Chan, Classification of runners’ performance levels with concurrent prediction of biomechanical parameters using data from inertial measurement units, *J. Biomech.* 112 (2020) 110072.
- [137] Y. Song, M. Wang, J.S. Baker, Y. Gu, The effect of voluntary head movements on postural kinetics in the standing cat, *PeerJ.* 2019 (2019) 1–9.

- [138] Y. Song, M. Wang, J.S. Baker, Y. Gu, The loading characteristics of landing in cats with different body weights, *Vet. Med. (Praha)*. 64 (2019) 497–504.
- [139] Y. Song, M. Liang, W. Lian, A comparison of foot kinematics between pregnant and non-pregnant women using the Oxford foot model during walking, *Int. J. Biomed. Eng. Technol.* 34 (2020) 20–30.
- [140] L. Yu, Q. Mei, L. Xiang, W. Liu, N.I. Mohamad, B. István, J. Fernandez, Y. Gu, Principal component analysis of the running ground reaction forces with different speeds, *Front. Bioeng. Biotechnol.* 9 (2021) 629809.
- [141] C.P. Witana, S. Xiong, J. Zhao, R.S. Goonetilleke, Foot measurements from three-dimensional scans: A comparison and evaluation of different methods, *Int. J. Ind. Ergon.* 36 (2006) 789–807.
- [142] L. Requena-Bueno, J.I. Priego-Quesada, I. Jimenez-Perez, M. Gil-Calvo, P. Pérez-Soriano, Validation of ThermoHuman automatic thermographic software for assessing foot temperature before and after running, *J. Therm. Biol.* 92 (2020) 102639.
- [143] M.Z. Wang, Y. Song, G. Fekete, Y.D. Gu, The variation of plantar temperature and plantar pressure during shod running with socks or not, in: *J. Biomimetics, Biomater. Biomed. Eng., Trans Tech Publ*, 2018: pp. 1–8.
- [144] G.Z. Heller, M. Manuguerra, R. Chow, How to analyze the Visual Analogue Scale: Myths, truths and clinical relevance, *Scand. J. Pain.* 13 (2016) 67–75.
- [145] A. Pipkin, K. Kotecki, S. Hetzel, B. Heiderscheit, Reliability of a qualitative video analysis for running, *J. Orthop. Sport. Phys. Ther.* 46 (2016) 556–561.
- [146] H.E. Field, M.E. Taylor, *An atlas of cat anatomy*, University of Chicago Press, 2018.
- [147] Y. Zhang, J. Awrejcewicz, O. Szymanowska, S. Shen, X. Zhao, J.S. Baker, Y. Gu, Effects of severe hallux valgus on metatarsal stress and the

- metatarsophalangeal loading during balanced standing: A finite element analysis, *Comput. Biol. Med.* 97 (2018) 1–7.
- [148] Y. Li, K.F. Leong, Y. Gu, Construction and finite element analysis of a coupled finite element model of foot and barefoot running footwear, *Proc. Inst. Mech. Eng. Part P J. Sport. Eng. Technol.* 233 (2019) 101–109.
- [149] L. Yu, Q. Mei, N.I. Mohamad, Y. Gu, J. Fernandez, An exploratory investigation of patellofemoral joint loadings during directional lunges in badminton, *Comput. Biol. Med.* 132 (2021) 104302.
- [150] M. Akrami, Z. Qian, Z. Zou, D. Howard, C.J. Nester, L. Ren, Subject-specific finite element modelling of the human foot complex during walking: Sensitivity analysis of material properties, boundary and loading conditions, *Biomech. Model. Mechanobiol.* 17 (2018) 559–576.
- [151] R. Chang, P.A. Rodrigues, R.E.A. Van Emmerik, J. Hamill, Multi-segment foot kinematics and ground reaction forces during gait of individuals with plantar fasciitis, *J. Biomech.* 47 (2014) 2571–2577.
- [152] M.E. Graham, N.T. Jawrani, V.K. Goel, Evaluating plantar fascia strain in hyperpronating cadaveric feet following an extra-osseous talotarsal stabilization procedure, *J. Foot Ankle Surg.* 50 (2011) 682–686.
- [153] R. Ferber, B. Benson, Changes in multi-segment foot biomechanics with a heat-mouldable semi-custom foot orthotic device, *J. Foot Ankle Res.* 4 (2011) 1–8.
- [154] P. Levinger, G.S. Murley, C.J. Barton, M.P. Cotchett, S.R. McSweeney, H.B. Menz, A comparison of foot kinematics in people with normal-and flat-arched feet using the Oxford Foot Model, *Gait Posture.* 32 (2010) 519–523.
- [155] M. Bisiaux, P. Moretto, The effects of fatigue on plantar pressure distribution in walking, *Gait Posture.* 28 (2008) 693–698.

- [156] M. Fukano, T. Inami, K. Nakagawa, T. Narita, S. Iso, Foot posture alteration and recovery following a full marathon run, *Eur. J. Sport Sci.* 18 (2018) 1338–1345.
- [157] W. Samson, A. Van Hamme, S. Sanchez, L. Chèze, S.V.S. Jan, V. Feipel, Foot roll-over evaluation based on 3D dynamic foot scan, *Gait Posture.* 39 (2014) 577–582.
- [158] L. Xiang, Q. Mei, J. Fernandez, Y. Gu, A biomechanical assessment of the acute hallux abduction manipulation intervention, *Gait Posture.* 76 (2020) 210–217.
- [159] M. Wallden, Toe-tal recall—What on Earth are our toes actually for?, *J. Bodyw. Mov. Ther.* 20 (2016) 418–431.
- [160] E. Cowley, J. Marsden, The effects of prolonged running on foot posture: A repeated measures study of half marathon runners using the foot posture index and navicular height, *J. Foot Ankle Res.* 6 (2013) 1–7.
- [161] M. Yavuz, R.W. Brem, B.L. Davis, J. Patel, A. Osbourne, M.R. Matassini, D.A. Wood, I.O. Nwokolo, Temperature as a predictive tool for plantar triaxial loading, *J. Biomech.* 47 (2014) 3767–3770.
- [162] Y. Shimazaki, M. Murata, Effect of gait on formation of thermal environment inside footwear, *Appl. Ergon.* 49 (2015) 55–62.
- [163] T.M. Willems, R. De Ridder, P. Roosen, The effect of a long-distance run on plantar pressure distribution during running, *Gait Posture.* 35 (2012) 405–409.
- [164] Q. Mei, Y. Gu, Z. Zheng, L. Yang, J. Fernandez, Foot shape, perceived comfort, and plantar pressure characteristics during long-distance running, *Footwear Sci.* 9 (2017) S20–S22.
- [165] G. Schlee, T. Milani, K. Roemer, Plantar pressure distribution, rearfoot motion and ground reaction force after long distance running, *Footwear Sci.* 1 (2009) 129–134.

- [166] M. Milazzo, A. Spezzaneve, A. Persichetti, M. Tomasi, V. Peselli, A. Messina, F. Gambineri, G. Aringhieri, S. Roccella, Digital and experimental synergies to design high-heeled shoes, *Int. J. Adv. Manuf. Technol.* 109 (2020) 385–395.
- [167] T.-X. Qiu, E.-C. Teo, Y.-B. Yan, W. Lei, Finite element modeling of a 3D coupled foot-boot model, *Med. Eng. Phys.* 33 (2011) 1228–1233.
- [168] J. Yu, J.T.-M. Cheung, Y. Fan, Y. Zhang, A.K.-L. Leung, M. Zhang, Development of a finite element model of female foot for high-heeled shoe design, *Clin. Biomech.* 23 (2008) S31–S38.
- [169] J.C.K. Chow, S.K. Boyd, D.D. Lichti, J.L. Ronsky, Robust self-supervised learning of deterministic errors in single-plane (Monoplanar) and dual-plane (Biplanar) X-Ray fluoroscopy, *IEEE Trans. Med. Imaging.* 39 (2020) 2051–2060.
- [170] E. Passmore, A. Lai, M. Sangeux, A.G. Schache, M.G. Pandy, Application of ultrasound imaging to subject-specific modelling of the human musculoskeletal system, *Meccanica.* 52 (2017) 665–676.
- [171] J.E. Brandenburg, S.F. Eby, P. Song, H. Zhao, J.S. Brault, S. Chen, K.-N. An, Ultrasound elastography: The new frontier in direct measurement of muscle stiffness, *Arch. Phys. Med. Rehabil.* 95 (2014) 2207–2219.
- [172] C.A. McCarty, J.J. Thomason, K.D. Gordon, T.A. Burkhart, J.S. Milner, D.W. Holdsworth, Finite-element analysis of bone stresses on primary impact in a large-animal model: the distal end of the equine third metacarpal, *PLoS One.* 11 (2016) e0159541.
- [173] H. Miao, J. Fu, Z. Qian, L. Ren, L. Ren, How does paw pad of Canine attenuate ground impacts: A micromechanical finite element study, *PeerJ Prepr.* 4 (2016) e2340v1.
- [174] C. Hubbard, V. Naples, E. Ross, B. Carlon, Comparative analysis of paw pad structure in the clouded leopard (*Neofelis nebulosa*) and domestic cat (*Felis*

- catus), *Anat. Rec. Adv. Integr. Anat. Evol. Biol. Adv. Integr. Anat. Evol. Biol.* 292 (2009) 1213–1228.
- [175] K. Knight, How cheetahs outpace greyhounds, *J. Exp. Biol.* 215 (2012) 2425–2434.
- [176] G.H. Jaeger, D.J. Marcellin-Little, V. DePuy, B.D.X. Lascelles, Validity of goniometric joint measurements in cats, *Am. J. Vet. Res.* 68 (2007) 822–826.
- [177] L. Godfrey, M. Sutherland, D. Boy, N. Gomberg, Scaling of limb joint surface areas in anthropoid primates and other mammals, *J. Zool.* 223 (1991) 603–625.
- [178] X. Wu, B. Pei, Y. Pei, W. Wang, Y. Hao, K. Zhou, How do cats resist landing injury: Insights into the multi-level buffering mechanism, *J. Bionic Eng.* 17 (2020) 600–610.
- [179] X. Wu, B. Pei, Y. Pei, N. Wu, K. Zhou, Y. Hao, W. Wang, Contributions of limb joints to energy absorption during landing in cats, *Appl. Bionics Biomech.* 2019 (2019) 3815612.
- [180] C.F. Honeycutt, T.R. Nichols, The mechanical actions of muscles predict the direction of muscle activation during postural perturbations in the cat hindlimb, *J. Neurophysiol.* 111 (2014) 900–907.

ABBREVIATION

2D: two-dimensional	LHS: lateral hind-sole
3D: three-dimensional	LM: lateral metatarsal
ANOVA: analysis of variance	LOA: limits of agreement
AT: Achilles tendon	MCP: metacarpophalangeal
BT: bruised toenail	MF: midfoot
BW: body weight	MFF: medial forefoot
CAD: computer aided design	MFS: medial fore-sole
CM: central metatarsal	MHS: medial hind-sole
CT: computed tomography	MM: medial metatarsal
DH: dorsal hallux	MP: metacarpal
DM: dorsal metatarsal	MRI: magnetic resonance images
DOT: dorsal other toes	MSF: metatarsal stress fracture
EMG: electromyography	MTP: metatarsophalangeal
FFHFA: forefoot with respect to hindfoot angle	OT: other toes
FE: finite element	ROM: range of motion
GRF: ground reaction force	RRI: running-related injury
H: hallux	PP: proximal phalanx
HF: hindfoot	SD: standard deviation
HXFFA: hallux with respect to forefoot angle	SPM1d: one-dimensional statistical parametric mapping
LBS: longitudinal bending stiffness	VALR: vertical average loading rate
LFF: lateral forefoot	VAS: visual analogue scale
LFS: lateral fore-sole	

LIST OF TABLES

Table 1 Foot morphology definitions [141].....	42
Table 2 Material properties assigned to each component in the FE model	51
Table 3 Forefoot with respect to hindfoot motion kinematics under static condition and after 5km and 10km of running	57
Table 4 Hallux with respect to forefoot motion kinematics under static condition and after 5km and 10km of running	58
Table 5 GRF under static condition and after 5km and 10km of running	58
Table 6 Foot morphology under static condition and after 5km and 10km of running	59
Table 7 Foot temperature under static condition and after 5km and 10km of running	61
Table 8 Perceived VAS scores under static condition and after 5km and 10km of running.....	62
Table 9 Gap length analysis under static condition and after 5km and 10km of running.....	62
Table 10 Comparison of predicted peak plantar pressures and experimental pressure insole data in 4 plantar regions during balanced standing	64
Table 11 Comparison of predicted peak sole pressures and experimental pressure plate data in 4 sole regions during balanced standing	66
Table 12 Comparison of predicted gap length difference and experimental data between midstance and toe off phase during running	67
Table 13 The von Mises stresses in MP and PP segment under different landing height	69

LIST OF FIGURES

Figure 1 The bone structure of the foot	6
Figure 2 The tendons and ligaments of the foot, A: Overview; B: Achilles tendon; C: Plantar fascia.....	8
Figure 3 The arches of the foot.....	9
Figure 4 The foot movement in three planes	11
Figure 5 Functional divisions of a running stride [32]	12
Figure 6 The basic structure of a running shoe.....	22
Figure 7 Basic of the FE method	25
Figure 8 The main components of the coupled foot-shoe FE model and basic modelling methods	27
Figure 9 A: Human informed consent form; B: Animal informed consent form .	35
Figure 10 Illustration of basic information of the running shoe.....	36
Figure 11 Illustration of basic information of the cat	36
Figure 12 Illustration of cat landing procedure	38
Figure 13 Illustration of experimental setup for foot kinematics and kinetics.....	39
Figure 14 Illustration of Oxford foot model marker placement	39
Figure 15 Illustration of foot morphology measurement.....	41
Figure 16 Illustration of foot skin temperature measurement	44
Figure 17 Illustration of VAS	44
Figure 18 Illustration of gap length measurement.....	45
Figure 19 Illustration of CT imaging for the participant	47
Figure 20 Illustration of CT imaging and 3D geometries of the bone (A) and soft tissue (B).....	47
Figure 21 Illustration of CT imaging and 3D geometry of the foot and shoe and smoothing process	47
Figure 22 Illustration of 3D FE model of the foot and sports shoe complex	48
Figure 23 Illustration of the process of reconstructing the paw model	49
Figure 24 Illustration of markers setting and foot heading angles (A) and boundary	

and loading conditions for balanced standing (B).....	52
Figure 25 Illustration of boundary and loading conditions for running	53
Figure 26 Illustration of boundary and loading conditions for standing and landing	54
Figure 27 Illustration of pressure measurement for foot-shoe model validation (A) for paw model validation (B).....	55
Figure 28 The time-series data and SPM1d analysis of foot inter-segment kinematics during stance phase under static condition and after 5km and 10km of running, A: forefoot with respect to hindfoot motion in sagittal plane; B: forefoot with respect to hindfoot motion in frontal plane; C: forefoot with respect to hindfoot motion in transverse plane; D: hallux with respect to forefoot motion in sagittal plane.....	56
Figure 29 Column chart of the Bonferroni comparisons for foot morphology under static condition and after 5km and 10km of running.....	60
Figure 30 Column chart of the Bonferroni comparisons for foot temperature under static condition and after 5km and 10km of running.....	61
Figure 31 Column chart of the Bonferroni comparisons for gap length under static condition and after 5km and 10km of running, gap length comparisons in one stance phase (A), and gap length comparisons throughout the running test (B)	63
Figure 32 The subdivided plantar regions and comparison between predicted pressure distribution and experimental pressure data.....	64
Figure 33 The subdivided sole regions and comparison between predicted pressure distribution and experimental pressure data	65
Figure 34 Bland-Altman plot of experimental and simulated pressure data	66
Figure 35 Dynamic simulation of running from the midstance to toe-off phase..	67
Figure 36 The comparison between predicted pressure distribution and experimental pressure data of the feline paw model	68
Figure 37 Illustration of the maximum values of MP and PP stress growth rate and	

stress distribution of cat during landing from different height	69
Figure 38 The injury development mechanisms of BT	86
Figure 39 The injury development mechanisms of MSF	87
Figure 40 The proposed high accurate 3D frictional-coupling foot-shoe FE model	88
Figure 41 The proposed high accurate 3D feline fore-left paw FE model	90

ACKNOWLEDGEMENTS

As I write this final part of my dissertation, I am about to the end of my student career. Standing on the threshold of graduation, looking back, everything seems to be vivid in my mind and I can't help but moisten my eyes with emotion. Three years of doctoral career is hard but full of laughter and joy. At this moment when it is coming to an end, my heart is full of reluctance for the student life and deep nostalgia for Óbuda University. Looking back on these three years of doctoral study, there are too many people who have helped me and too many people to thank.

I would like to express my deep gratitude to my supervisors Prof. Dr. István Bíró and Prof. Dr. Yaodong Gu for the continuous support of my PhD study and related research, for your patience, motivation, and immense knowledge. I am truly glad to have the opportunity to be your student and have the benefit of all your knowledge. Your guidance helped me in all the time of research and writing of this dissertation. I could not have imagined having a better advisor and mentor for my PhD dissertation, thank you so much!

I'm very fortunate to work in a group full of talented people who have not only helped me with my research, but also given me invaluable advice and support. Thanks to all the professors, colleagues, and PhD students for their helpful assistance, comments, and suggestions during my research work. Thanks to everyone who took part in the studies of this dissertation, your time was much appreciated. Many other administrative, academic, secretarial and technical members of staff have facilitated the realization of this dissertation and I express them all my sincere gratitude.

I sincerely acknowledge the Doctoral School on Safety and Security Sciences, Óbuda University, Faculty of Engineering, University of Szeged, Research Academy of Grand Health & Faculty of Sports Science, Ningbo University, Stipendium Hungaricum Programme, Tempus Public Foundation, and China Scholarship Council (CSC) for the facilities and financial support provided.

Finally, I want to dedicate my PhD dissertation to my family, my father, Mr. Zhongping Song, my mother, Mrs. Lihua Mo, my little brother Haoxuan Song, and my beloved Fiancée, Ms. Jialin Li, thank you so much for supporting me to pursue what I loved, and thank you so much for your endless motivation and your unconditional love!